



1 **Review Article**

2 **Antarctica's internal architecture:**

3 **Towards a radiostratigraphically-informed age–depth model of the**

4 **Antarctic ice sheets**

5
6 Robert G. Bingham^{1*}, Julien A. Bodart^{2,3*}, Marie G. P. Cavitte^{4*}, Ailsa Chung^{5*}, Rebecca J. Sanderson^{6*},
7 Johannes C. R. Sutter^{2,3*}, Olaf Eisen^{7,8}, Nanna B. Karlsson⁹, Joseph A. MacGregor¹⁰, Neil Ross⁶, Duncan A.
8 Young¹¹, David W. Ashmore¹², Andreas Born^{13,14}, Winnie Chu¹⁵, Xiangbin Cui¹⁶, Reinhard Drews¹⁷, Steven
9 Franke^{8,17}, Vikram Goel¹⁸, John W. Goodge^{19,20}, A. Clara J. Henry²¹, Antoine Hermant^{2,3}, Benjamin H. Hills²²,
10 Nicholas Holschuh²³, Michelle R. Koutnik²⁴, Gwendolyn J.-M. C. Leysinger Vieli²⁵, Emma J. MacKie²⁶, Elisa
11 Mantelli^{7,27}, Carlos Martín²⁸, Felix S. L. Ng²⁹, Falk M. Oraschewski¹⁷, Felipe Napoleoni¹, Frédéric Parrenin⁵,
12 Sergey V. Popov^{30,31}, Therese Rieckh^{13,14}, Rebecca Schlegel¹⁷, Dustin M. Schroeder^{32,33}, Martin J. Siegert³⁴,
13 Xueyuan Tang^{16,35}, Thomas O. Teisberg³³, Kate Winter³⁶, Shuai Yan¹¹, Harry Davis¹, Christine F. Dow^{37,38}, Tyler
14 J. Fudge²³, Tom A. Jordan²⁷, Bernd Kulesa³⁹, Kenichi Matsuoka⁴⁰, Clara J. Nyqvist¹, Maryam
15 Rahnemoonfar^{41,42}, Matthew R. Siegfried²¹, Shivangini Singh^{11,43}, Vjerran Višnjević^{2,3}, Rodrigo Zamora⁴⁴,
16 Alexandra Zuhr¹⁶

17 * These authors contributed equally to this work.

18 *Correspondence to:* Robert G. Bingham (r.bingham@ed.ac.uk)

19 **Affiliations**

20 ¹ School of GeoSciences, University of Edinburgh, UK

21 ² Climate and Environmental Physics, Physics Institute, University of Bern, Switzerland

22 ³ Oeschger Centre for Climate Change Research, University of Bern, Switzerland

23 ⁴ Earth and Life Institute, Université catholique de Louvain (UCLouvain), Belgium

24 ⁵ Univ. Grenoble Alpes, CNRS, INRAE, IRD, Grenoble INP, IGE, 38000 Grenoble, France

25 ⁶ School of Geography, Politics and Sociology, Newcastle University, UK

26 ⁷ Alfred Wegener Institute Helmholtz Centre for Polar and Marine Research, Bremerhaven, Germany

27 ⁸ Department of Geosciences, University of Bremen, Germany

28 ⁹ Department of Glaciology and Climate, Geological Survey of Denmark and Greenland (GEUS), Copenhagen,
29 Denmark

30 ¹⁰ Cryospheric Sciences Laboratory, NASA Goddard Space Flight Centre, Greenbelt, Maryland, USA



- 31 ¹¹ University of Texas Institute for Geophysics, Jackson School of Geosciences, University of Texas at Austin,
32 Texas, USA
- 33 ¹² Met Office, FitzRoy Road, Exeter, UK
- 34 ¹³ Department of Earth Science, University of Bergen, Norway
- 35 ¹⁴ Bjerknes Centre for Climate Research, University of Bergen, Norway
- 36 ¹⁵ School of Earth and Atmospheric Science, Georgia Institute of Technology, Atlanta, Georgia, USA
- 37 ¹⁶ Polar Research Institute of China, Shanghai, China
- 38 ¹⁷ Department of Geosciences, University of Tübingen, Germany
- 39 ¹⁸ National Centre for Polar and Ocean Research (NCPOR), Ministry of Earth Sciences, Vasco da Gama, Goa,
40 India
- 41 ¹⁹ Department of Earth and Environmental Sciences, University of Minnesota Duluth, Duluth, Minnesota, USA
- 42 ²⁰ Planetary Science Institute, Tucson, Arizona, USA
- 43 ²¹ Department of Mathematics, Stockholm University, Sweden
- 44 ²² Department of Geophysics, Colorado School of Mines, Golden, Colorado, USA
- 45 ²³ Department of Geology, Amherst College, Massachusetts, USA
- 46 ²⁴ Department of Earth and Space Sciences, University of Washington, Seattle, Washington, USA
- 47 ²⁵ Department of Geography, University of Zurich, Switzerland
- 48 ²⁶ Department of Geological Sciences, University of Florida, Gainesville, Florida, USA
- 49 ²⁷ Department of Earth and Environmental Sciences, Ludwig-Maximilians-Universität, Munich, Germany
- 50 ²⁸ British Antarctic Survey, Cambridge, UK
- 51 ²⁹ Department of Geography, University of Sheffield, Sheffield, UK
- 52 ³⁰ St Petersburg State University, Russia
- 53 ³¹ Polar Marine Geosurvey Expedition, St. Petersburg, Russia
- 54 ³² Department of Geophysics, Stanford University, California, USA
- 55 ³³ Department of Electrical Engineering, Stanford University, California, USA
- 56 ³⁴ Tremough House, Penryn Campus, University of Exeter, Cornwall, UK
- 57 ³⁵ School of Oceanography, Shanghai Jiao Tong University, China
- 58 ³⁶ Department of Geography and Environmental Sciences, Northumbria University, Newcastle, UK



59 ³⁷ Department of Geography and Environmental Management, University of Waterloo, Ontario, Canada

60 ³⁸ Department of Applied Mathematics, University of Waterloo, Ontario, Canada

61 ³⁹ School of Biosciences, Geography and Physics, Swansea University, UK

62 ⁴⁰ Norwegian Polar Institute, Tromsø, Norway

63 ⁴¹ Department of Computer Science and Engineering, Lehigh University, Pennsylvania, USA

64 ⁴² Department of Civil and Environmental Engineering, Lehigh University, Pennsylvania, USA

65 ⁴³ Department of Earth and Planetary Sciences, University of Texas at Austin, Austin, Texas, USA

66 ⁴⁴ Centro de Estudios Científicos, Valdivia, Chile



67 **Abstract.** Radio-echo sounding (RES) has revealed an internal architecture within Antarctica’s ice sheets that
68 records their depositional, deformational and melting histories. Crucially, spatially-widespread RES-imaged
69 internal-reflecting horizons, tied to ice-core age-depth profiles, can be treated as isochrones that record the
70 age-depth structure across the Antarctic ice sheets. These enable the reconstruction of past climate and ice-
71 dynamical processes on large scales, which are complementary to but more spatially-extensive than
72 commonly used proxy records across Antarctica. We review progress towards building a pan-Antarctic age-
73 depth model from these data by first introducing the relevant RES datasets that have been acquired across
74 Antarctica over the last six decades (focussing specifically on those that detected internal-reflecting horizons),
75 and outlining the processing steps typically undertaken to visualise, trace and date (by intersection with ice
76 cores, or modelling) the RES-imaged isochrones. We summarise the scientific applications to which
77 Antarctica’s internal architecture has been applied to date and present a pathway to expanding Antarctic
78 radiostratigraphy across the continent to provide a benchmark for a wider range of investigations: (1)
79 Identification of optimal sites for retrieving new ice-core palaeoclimate records targeting different periods;
80 (2) Reconstruction of surface mass balance on millennial or historical timescales; (3) Estimates of basal
81 melting and geothermal heat flux from radiostratigraphy and comprehensively mapping basal-ice units, to
82 complement inferences from other geophysical and geological methods; (4) Advancing knowledge of volcanic
83 activity and fallout across Antarctica; (5) The refinement of numerical models that leverage radiostratigraphy
84 to tune time-varying accumulation, basal melting and ice flow, firstly to reconstruct past behaviour, and then
85 to reduce uncertainties in projecting future ice-sheet behaviour.



86 **1 Introduction**

87 Throughout the Quaternary (2.58 Ma to present), Antarctica’s ice cover has waxed and waned, inducing
88 concomitant rises and falls in global sea level on the order of several tens of metres (e.g., Drewry, 1983;
89 Pollard and DeConto, 2009; Dutton et al., 2015). It is critical to understand the rates and drivers of these past
90 oscillations in order to contextualise current observations of persistent and accelerating losses from the
91 contemporary Antarctic ice sheets (e.g., Fox-Kemper et al., 2021; Otosaka et al., 2023) and thereby project
92 as accurately as possible the rates at which future global sea-level rise fuelled by ice melt will occur (e.g.,
93 Scambos et al., 2017; Oppenheimer et al., 2019). The evidence for past Antarctic ice-sheet fluctuations has
94 been derived predominantly from sampling sediments deposited offshore around the continent (Escutia et
95 al., 2009; Naish et al., 2009; Cook et al., 2013; Bentley et al., 2014; Gulick et al., 2017; Hillenbrand et al., 2017),
96 dating the exposure history of onshore bedrock and moraine boulders (Brook and Kurz, 1993; Mackintosh et
97 al., 2014; Hillebrand et al., 2021), and by analysing the ice itself recovered from ice-core sites (e.g., EPICA
98 Community Members, 2004; Jouzel et al., 2007; Higgins et al., 2015; WAIS Divide Project Members, 2015;
99 Dome Fuji Ice Core Project Members, 2017; Yan et al., 2021) (see Brook and Buizert, 2018 for an overview).
100 Together, these form the palaeoclimate records that underpin numerical-modelling reconstructions of past
101 and present ice-sheet extents and inform projections of how these may evolve into the future and affect sea-
102 level change (e.g., Gasson et al., 2016; Golledge et al., 2019; DeConto et al., 2021; Pittard et al., 2022).
103 Recovery of further sediment and ice cores around Antarctica to refine these records and projections remains
104 a scientific imperative – and yet these records are intrinsically spatially limited. Radio-echo sounding across
105 Antarctica complements these records by providing *spatially continuous* data that record past and present
106 ice conditions and, by extension, past and present climate conditions, across the ice sheets.

107 Radio-echo sounding (RES) describes the investigation of the subsurface of ice sheets using electromagnetic
108 waves, and has been conducted from both airborne and ground-based platforms across the Antarctic ice
109 sheets for over 60 years (see reviews by Dowdeswell and Evans, 2004; Bingham and Siegert, 2007; Allen,
110 2008; Schroeder et al., 2020). Primarily deployed for mapping the ice-sheet bed and thereby measuring ice
111 thickness and thus ice volume, the majority of RES surveys have also imaged numerous englacial features,
112 predominantly internal-reflection horizons (a.k.a. internal or englacial layers), crevasses and rheologically-
113 distinct “basal units” of ice that occur between the more obvious reflections of the ice surface and bed (Fig.
114 1). For this review, we collectively term all of the Antarctic ice sheets’ RES-imaged englacial features its
115 *internal architecture*. We will demonstrate that although great progress has already been made in using some
116 of this resource to elucidate ice and climate history, Antarctica’s internal architecture has yet to be exploited
117 to its full potential in refining our understanding of past, present and future ice-sheet behaviour.

118 In Greenland, a comprehensive archive of internal architecture has already been assembled (see MacGregor
119 et al., 2015a), facilitating the ice-sheet-wide reconstruction of past accumulation and dynamics, to improve

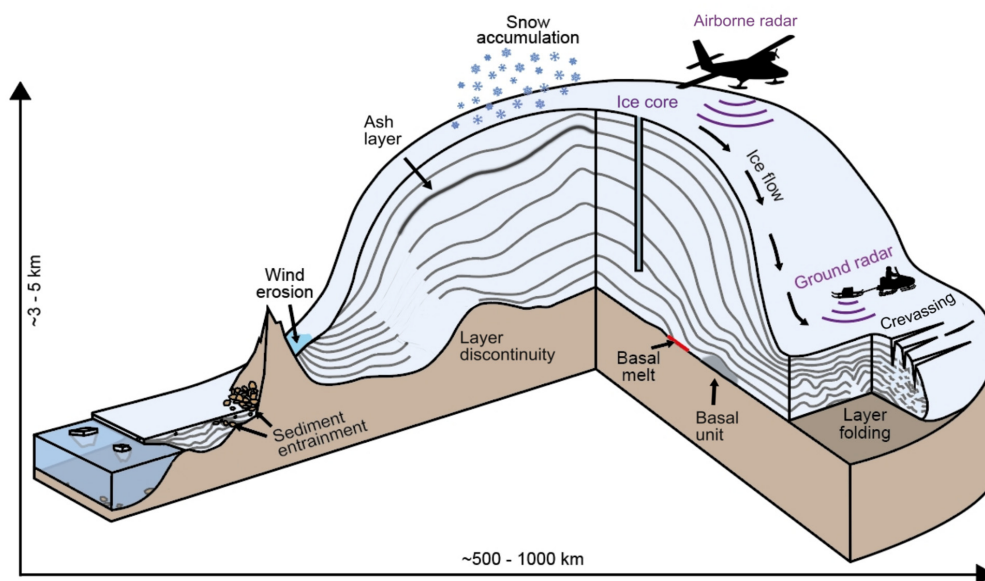


Figure 1. Schematic illustration of Antarctica's internal architecture and the key processes governing its structure. Internal-reflection horizons - the ice sheet's "radiostratigraphy" - are represented by grey lines between the surface and bed.

120

121 past and future sea-level estimates (MacGregor et al., 2016; Born and Robinson, 2021). However, several
122 major issues have confounded parallel progress in capturing and applying internal architecture across
123 Antarctica, including:

124 1) The Antarctic ice sheets together cover eight times the area of the Greenland Ice Sheet.

125 2) RES data have been collected, processed and archived by multiple international groups across the Antarctic
126 ice sheets, and hence are not available in a standardised form across Antarctica.

127 3) A comprehensive suite of strategies for using internal architecture in numerical ice-sheet models has not
128 been developed.

129 4) Much internal architecture in RES data is highly challenging to identify and map with automated methods.

130 To address these challenges and work collectively towards consistently capturing and utilising Antarctica's
131 internal architecture, an international community called *AntArchitecture* was formed in 2018. This
132 community, coordinated via the *Scientific Committee for Antarctic Research* (SCAR), aspires to the ultimate
133 scientific aim of using Antarctica's internal architecture to deconvolve its ice sheets' histories and thereby
134 facilitate improved projections of their future behaviour in the face of global climate warming. A first step in
135 this process, and one of the aims of this review, collectively written by the *AntArchitecture* community, is to
136 compile the international community's understanding of the present state of the field in terms of available



137 RES data across the Antarctic ice sheets and their potential applications. Additionally, we seek here to relay
138 community aspirations to address the aforementioned challenges and position Antarctica's internal
139 architecture as a valuable resource for improving our understanding of its ice/climate interactions.

140 We begin with a brief overview of what gives rise to internal architecture in ice, especially the internal-
141 reflection horizons (hereafter IRHs) that are measured by RES (Sect. 2). We continue by summarising the key
142 RES datasets acquired across Antarctica that image internal architecture, to contextualise in a single place
143 the type and quality of information recorded by each institute and survey in the past six decades (Sect. 3). In
144 Sect. 4, we turn to how RES data have been, and can be, processed to optimise the extraction of internal
145 architecture and its visualisation; discuss the common methods currently used to characterise and date IRHs;
146 and finally build an inventory of existing IRH datasets. In Sect. 5, we review how internal architecture has
147 been used to reconcile ice-core records, calculate changes to past surface mass balance, explore basal
148 melting in association with subglacial lakes and areas of enhanced geothermal heat flux, and investigate ice-
149 sheet dynamics and other glaciological questions; and outline how the internal architecture has begun to be
150 used in numerical-modelling applications to date. In Sect. 6, we outline a recommended pathway to
151 building a pan-Antarctic database of Antarctica's internal architecture, and discuss key science deliverables
152 that can be facilitated by this activity.

153 **2 Internal architecture in ice sheets**

154 The most common way in which internal architecture is viewed and assessed is as radargrams, which are
155 two-dimensional profiles of echo power arrayed in the along-track direction (e.g., Fig. 2). Antarctic
156 radargrams commonly display clear *radiostratigraphy*, the collective term for the multiple sub-parallel and
157 closely-spaced IRHs that are seen in radargrams and often, although do not always, broadly follow the shape
158 of the ice-bed interface (e.g., Fig. 2). IRHs occur as radio-waves propagate down through the ice column and
159 reflect off any boundary where there is a contrast in the dielectric properties within the ice. The propagation
160 of radio-waves through snow, firn and ice is controlled by the complex relative permittivities of these
161 materials, which are functions of density, electrical conductivity, and/or the development of ice-fabric
162 anisotropy where ice crystals align into a preferential orientation as a result of large englacial stress. Where
163 contrasts in any of these properties are sufficiently strong and sharp, the incident energy will partition and a
164 small fraction of it will be reflected back to the RES receiver at or above the ice surface.

165 In the upper and middle part of the ice column, radiostratigraphy typically arises from (a) density variations,
166 as snow compacts into ice (as explained in pioneering work by Robin et al. (1969) and Clough (1977)) and (b)
167 variations in electrical conductivity, as volcanic aerosols present in the air during snow deposition are
168 incorporated into the firn (Hammer, 1980; Millar, 1981; Millar, 1982). These density- and electrical-
169 conductivity-derived IRHs are related to snow and ice layers of a specific age buried under subsequent snow

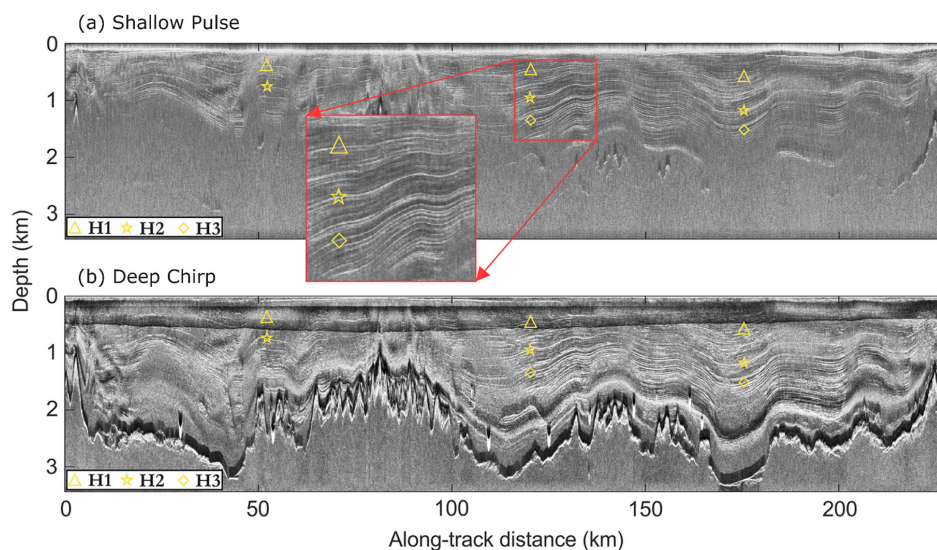


Figure 2. Radargrams from Institute Ice Stream, West Antarctica, obtained by the British Antarctic Survey PASIN RES system in (a) pulse (shallow-sounding) and (b) chirp (deep-sounding) radar modes (Frémant et al., 2022), vertically differentiated to accentuate fine detail. Symbols highlight three IRHs found widely across West Antarctica in airborne radar data. The bed reflection (black-white interface) is partially visible in (a) and clearly visible in (b). Figure modified from Ashmore et al. (2020).

170

171 accumulation, and thus may be considered isochronous (Hempel et al., 2000; Eisen et al., 2006). Such RES-
 172 imaged isochrones may often represent composites of multiple real horizons in the ice, and their thickness
 173 is dependent on RES-system resolution (Harrison, 1973; Winter et al., 2017). They are often traceable for
 174 considerable distances on RES profiles: some IRHs in the Antarctic and Greenland ice sheets are continuous
 175 for hundreds or even thousands of kilometres (e.g., MacGregor et al., 2015a; Winter et al., 2019a; Ashmore
 176 et al., 2020). For the focus of this review, isochronous reflections arising from density and electrical
 177 conductivity are of significant interest, and IRHs that can be dated at ice cores and traced continuously over
 178 long distances to form a “dated radiostratigraphy” are particularly valuable (as explored in-depth in Sect. 4
 179 and 5). There are, however, some cases, especially in the lower part of the ice column, where diachronous
 180 IRHs (i.e. IRHs that cannot be treated as single time markers) may be visualised in radargrams. The most
 181 common such examples are IRHs that are thought to manifest sudden changes in ice-crystal-orientation
 182 fabric that cause anisotropic radio-wave propagation, or cold-warm ice transitions where the pore space on
 183 the warm side is filled with meltwater instead of air (Harrison, 1973; Fujita et al., 1999; Eisen et al., 2007).
 184 Over ice shelves, pervasive IRHs can mark the boundary between atmospherically-derived (meteoric) and
 185 subglacially/submarine-accreted (marine) ice (Holland et al., 2009; Das et al., 2020).

186 The specular behaviour of IRHs also positions them as ideal targets for repeated observations of vertical
 187 velocity over time, directly tracking the deformation of the ice sheet, via static phase-sensitive repeat



188 measurements at a point (autonomous phase-sensitive radio-echo sounder, or ApRES; Nicholls et al., 2015)
189 or from airborne re-flights of transects with coherent RES systems (Castelletti et al., 2021). Although these
190 methods have been practiced in recent field campaigns (e.g., Hills et al., 2022; Chung et al., 2023; Fudge et
191 al., 2023), we do not discuss this aspect of radiostratigraphy further in this review, beyond noting that
192 establishing the distribution of appropriate IRHs could be a valuable component in expedition planning. A
193 review of static techniques is found in Kingslake et al. (2014), while repeat-pass airborne interferometry of
194 IRH is an active field of research.

195 While the imaging and analysis of radiostratigraphy and its application to assessing ice-sheet stability forms
196 the main focus of this paper, other significant features of internal architecture also convey information that
197 can be used to help understand current and past ice-sheet processes (as depicted in Fig. 1). These include
198 basal units which exhibit different dielectric properties to the surrounding ice and may result from ice-folding
199 due to contrasts in material properties, to accretion, melting due to high rates of geothermal heat flux or
200 overburden pressure from the ice above, or freeze-on processes taking place at the base of the ice sheet (Bell
201 et al., 2011; Bell et al., 2014; Bons et al., 2016; Leysinger Vieli et al., 2018; Wrona et al., 2018; Ross et al.,
202 2020; Franke et al., 2023). Additionally, buried near-surface and basal crevassing imaged by RES systems may
203 be indicative of past grounding-line evolution or ice-stream stagnation events (Retzlaff et al., 1993; Matsuoka
204 et al., 2009; Catania et al., 2010; Kingslake et al., 2018; Wearing and Kingslake, 2019). We elaborate further
205 on these other significant features of internal architecture in Sect. 5.5.

206 **3 Radio-echo sounding datasets for characterising Antarctica's internal architecture**

207 Antarctic ice-penetrating RES data have been collected in a series of regional surveys for over six decades. A
208 broad overview of the history can be gained from the periodic release of maps of subglacial topography, the
209 first by Drewry (1975) and Drewry (1983; Antarctica Glaciological and Geophysical Folio Sheet 9), and then
210 through the Bedmap series, now in its third iteration (Frémand et al., 2023; their Fig. 1). However, those
211 maps outline only where RES data have been used to pick an echo at the ice bed, and crucially do not provide
212 any information on whether the constituent surveys also captured or recorded any information on internal
213 architecture. Therefore, we review here specifically which of the RES datasets acquired over Antarctica do
214 contain, or are likely to contain, useable internal architecture.

215 The most relevant datasets for characterising internal architecture across Antarctica derive from airborne
216 RES surveys, as they are the most spatially extensive (extending over thousands of kilometres; Fig. 3), typically
217 deploy more advanced and more powerful sounders relative to most contemporaneous ground-based
218 systems, and now commonly employ state-of-the-art processing methods. These qualities favour the
219 detection of multiple IRHs over wide-ranging regions, resolving IRHs at higher resolution and to greater
220 depths in the ice sheet. Accordingly, we focus mainly on airborne RES surveys below, in Sect. 3.1 to 3.8



221 progressing chronologically by order of first Antarctic operations by each main airborne provider, and then
222 in Sect. 3.9 outlining briefly some additional airborne RES datasets acquired by other groups since airborne
223 surveying began in the 1960s. Our focus in this review, and hence throughout Sect. 3, is on “deep” RES
224 datasets, i.e. those that sound the full ice column to several kilometres’ depth. Also acquired across many
225 regions of Antarctica are several additional datasets of “shallow” RES - i.e. that image IRHs in finer detail
226 down to a few 100 m below the ice surface – which provide complementary resources for work typically
227 focussed on ice-climate interactions during more recent periods (i.e., the past few hundred years; e.g.,
228 Medley et al., 2014). To give shallow RES data and applications equal attention to their deeper counterparts
229 throughout this review would have made the paper unwieldy, but shallow IRHs imaged in RES data certainly
230 represent another hugely important and rich resource for palaeoclimate modelling and we return to this in
231 Sect. 6.2.3 when laying out future scientific aspirations.

232 Complementing the wide-ranging information acquired by airborne RES, several groups have acquired RES
233 data from vehicles driven along the snow surface. Ground-based RES (described as ground-penetrating radar,
234 GPR, in some glaciological literature) has typically been deployed to conduct dense surveys around sites of
235 particular glaciological and geophysical interest, but long exploratory traverses of several hundreds of
236 kilometres have also been undertaken. Ground-based RES surveys, usually operated with lower frequencies,
237 benefit from direct coupling to the ice (or snow/firn) surface, so are often particularly effective at mapping
238 local radiostratigraphy at fine vertical resolution or for deciphering the processes that influence the larger-
239 scale radiostratigraphy. Perhaps most notably for the purposes of building a pan-Antarctic age-depth model
240 are those ground-based surveys that can link between two or more large regions, and so in Sect. 3.10 we
241 outline where such far-ranging surveys have occurred. In parallel with the approach described for airborne
242 RES data above, here we introduce only the ground-based RES datasets that penetrate through the full ice
243 thickness.

244 Two important considerations to introduce before we proceed with introducing where RES data have been
245 obtained over Antarctica are whether the data were acquired digitally and/or coherently. While the majority
246 of the datasets discussed here were recorded digitally, RES data acquired before the 1990s were typically
247 recorded onto analogue tape recorders or film. Very few of these analogue RES datasets have been digitised,
248 with Schroeder et al. (2019) being a notable exception that has made automated digital interpretation of the
249 data possible and greatly increased their value for modern analyses. (Karlsson et al. (2024) provides an
250 equivalent legacy dataset for Greenland.) The use of pre-1990s RES datasets is also challenged by navigational
251 uncertainties occasioned by their acquisition from before digital navigation systems supported by Global
252 Navigation Satellite System (GNSS) were fully integrated into survey platforms. By their nature, the analogue
253 datasets were acquired incoherently, meaning that the RES systems only recorded signal amplitude and not
254 phase. Until the 2000s, when most airborne RES systems were equipped with GNSS and acquiring data
255 digitally, most RES systems remained incoherent. Despite this limitation, such systems have successfully



256 imaged internal architecture, and indeed many ground-based RES systems presently deployed in Antarctica
257 remain incoherent. The advantage of incoherent ground-based systems is the relative simplicity of operating
258 and maintaining such RES systems in challenging field conditions. However, with improvements in technology
259 through the late 1990s/early 2000s, all of the airborne RES operators gradually transitioned to operating
260 coherent RES systems that detect both returned power and phase, permitting synthetic aperture radar (SAR)
261 processing of the data (see Sect. 4). This has been crucial for imaging finer details such as low-amplitude
262 englacial reflections lower in the ice column and across complex terrain that previously was shrouded by
263 scattering and frequently characterised as echo-free (Hélière et al., 2007; Peters et al., 2007). The overall
264 progression of RES systems from analogue to digital, from not having digital navigation to navigating with
265 high-precision GNSS, and from incoherent to coherent RES systems, is depicted in Fig. 3, and introduced in
266 further selected details below.

267 **3.1 Scott Polar Research Institute / National Science Foundation / Technical University of Denmark**

268 From the mid-1960s the UK-based Scott Polar Research Institute (SPRI) began airborne RES surveying across
269 parts of Antarctica, initially supported logistically by a combination of the British Antarctic Survey (BAS) and
270 the USA's National Science Foundation (NSF) in reconnaissance flights in the Antarctic Peninsula, and out of
271 McMurdo and South Pole stations (Swithinbank, 1969; Evans and Smith, 1970; Drewry, 2023). From 1971,
272 engineers from the Technical University of Denmark (DTU) added antennas designed to operate at 60 MHz
273 centre frequency for improved reflection of IRHs (Gudmandsen et al., 1975) and thus commenced the earliest
274 extensive airborne RES campaigns across Antarctica which continued throughout the 1970s (Turchetti et al.,
275 2008). The SPRI-NSF-DTU surveys profiled >400,000 km across nearly half of the continent, contributing much
276 of the first iteration of Bedmap (Lythe et al., 2001) across West Antarctica and over East Antarctica between
277 Wilkes Land, the South Pole and Domes A and C (Fig. 3b). The clarity of IRHs in the 1970s SPRI-NSF-DTU
278 datasets rivals that sounded in many modern RES surveys, but use of the data is challenging because (1) they
279 were recorded onto 35-mm optical film and (2) navigation techniques before the use of GNSS were less
280 precise, leading to several kilometres of positional uncertainties (Schroeder et al., 2019). In the early 2000s,
281 many of the films were scanned as non-georectified digital images, from which a first archive of
282 radiostratigraphy across West Antarctica was constructed (Siegert et al., 2005). This seeded many early
283 applications of radiostratigraphy to glaciological problems across both ice sheets (e.g., Hodgkins et al., 2000;
284 Siegert and Hodgkins, 2000; Rippin et al., 2003b; Leysinger Vieli et al., 2004; Siegert and Payne, 2004; Siegert
285 et al., 2004; Bingham et al., 2007; Leysinger Vieli et al., 2011). All those studies acknowledged the inherent
286 limitations of using analogue data with low positional accuracy. Recently, the SPRI-NSF-DTU data have been
287 revived by a new finer-resolution digitisation and distribution programme (Schroeder et al., 2019; Schroeder
288 et al., 2022), which has substantially improved the visibility and accessibility of this wide-ranging
289 radiostratigraphy. Navigational uncertainties remain, but the radiometric digitisation process offers the

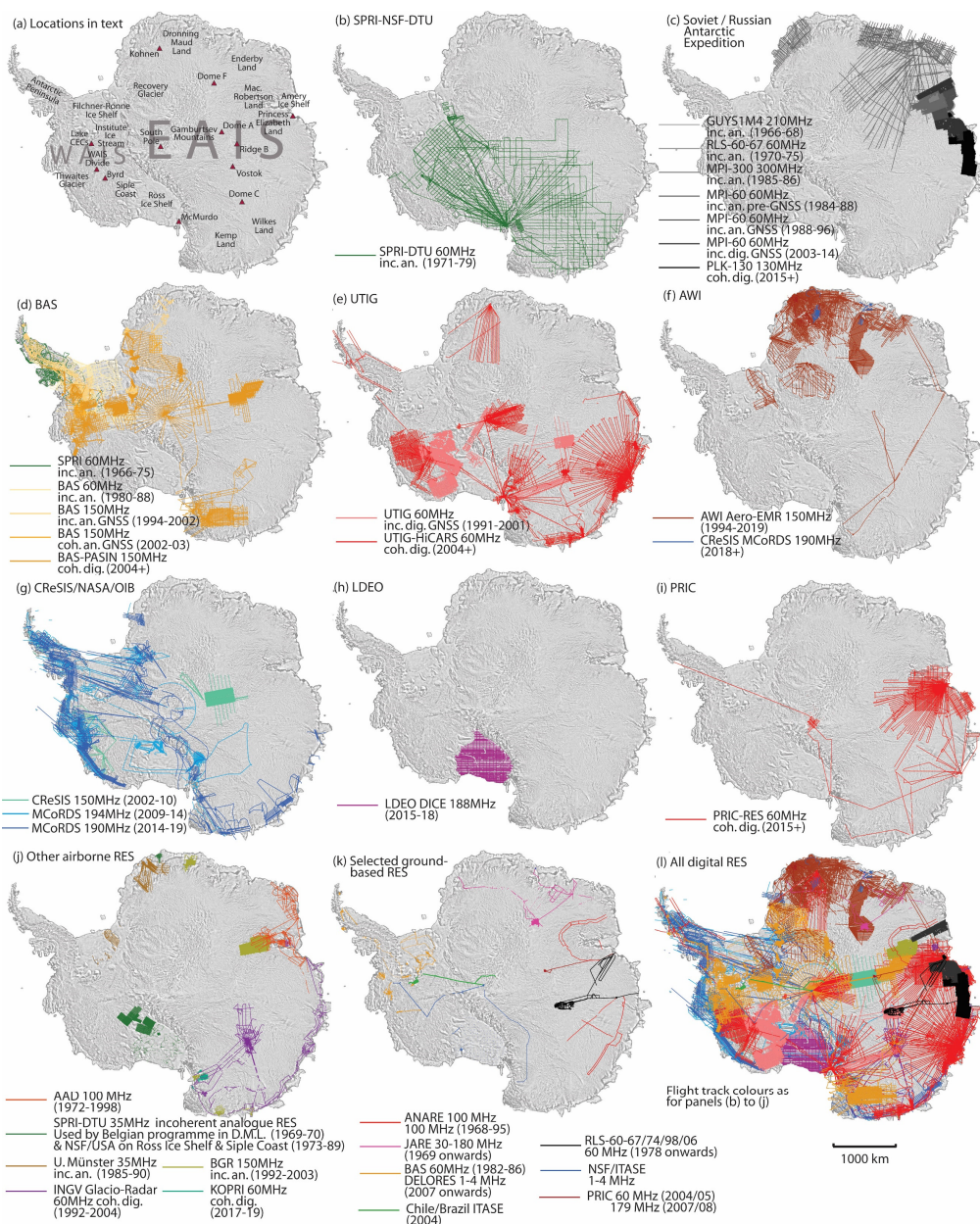


Figure 3. (a) Reference map of main Antarctic locations mentioned in this review. (b) to (j) Airborne RES coverage by data provider as discussed through Sect 3.1 to 3.9. Each legend outlines basic details of the provider's RES system by system-name, typical centre frequency, whether the system was incoherent (inc.) or coherent (coh.), whether the acquisition was analogue (an.) or digital (dig.), whether flight navigation used GNSS (assumed not for data collection before 1990), and the date ranges over which a system was used. (k) Coverage of long-range ground-based RES data across Antarctica with potential for extraction of deep internal-reflecting horizons. (l) Combined coverage of all digital RES datasets across Antarctica with potential for contributing to *AntArchitecture*.



291 prospect of using crossovers with more modern datasets to reconstruct the navigation with improved
292 accuracy (Teisberg and Schroeder, 2023).

293 **3.2 Soviet / Russian Antarctic Expedition**

294 Airborne RES surveying of Antarctica coordinated by the Soviet (later Russian) Antarctic Expedition began in
295 the mid-1960s. Surveys undertaken with a 60 MHz system, designed primarily to sound the bed but also
296 capable of imaging IRHs, were conducted between 1967 and 2014, after which all data acquisition was
297 conducted with a new 130 MHz RES system (Popov, 2020). Throughout the 1980s, systematic surveying was
298 conducted across large swathes of East Antarctica, extending across Enderby Land and to Vostok Station and
299 Domes A and F (Popov, 2020). For the early decades of these RES surveys, as for the SPRI-NSF-DTU surveys,
300 the data were recorded onto film and have a spatial accuracy of several kilometres due to not benefitting
301 from GNSS navigation; however, they likely contain a rich resource of radiostratigraphy which could be
302 particularly important because a number of these surveys span approximately one-fifth of East Antarctica
303 that is otherwise mostly unsurveyed (compare Fig. 3c and 3l). From the 1990s onwards, Russian airborne RES
304 surveying continued systematically around coastal East Antarctica between $\sim 20^{\circ}\text{E}$ and 95°E , generally
305 extending at most 500 km inland to 75°S (Fig. 3c; Popov, 2020; Popov, 2022). A key development for the
306 ready recovery and future utilisation of radiostratigraphy from these datasets was the switch from analogue
307 to digital data acquisition that took place in the early 2000s.

308 **3.3 British Antarctic Survey**

309 The British Antarctic Survey (BAS) has performed large-scale airborne RES surveys of Antarctica since the
310 1960s. Until the late 1970s, before which BAS field logistics were run centrally but BAS science was led out
311 of university research groups, the RES system-development and data analysis were the responsibility of SPRI,
312 and the RES systems that were deployed were as described in Sect. 3.1. As BAS became more autonomous
313 from the mid-1970s it transitioned to developing and running its own in-house RES systems, which
314 progressed in the early 2000s from incoherent to coherent systems (Robin et al., 1977; Corr et al., 2007;
315 Frémand et al., 2022). Prior to the early 2000s, BAS surveys focused on the Antarctic Peninsula and Filchner-
316 Ronne Ice Shelf and data were recorded only in analogue form (Fig. 3d). From 2004 onwards, BAS transitioned
317 to digital data acquisition (Rippin et al., 2003a; Ferraccioli et al., 2005) by developing the 150 MHz, higher-
318 power, coherent Polarimetric Radar Airborne Science Instrument (PASIN; Corr et al., 2007; Hélière et al., 2007;
319 Frémand et al., 2022). PASIN was upgraded in the mid-2010s to enable the acquisition of swathes (i.e. wide
320 strips) of RES data to map the ice-sheet bed (Arenas-Pingarrón et al., 2023). PASIN transmits two waveforms,
321 a narrow pulse ($0.1\ \mu\text{s}$) for detecting shallow radiostratigraphy in the upper 2 km of the ice column, and a
322 deep-sounding chirp ($4\ \mu\text{s}$) for detecting deeper radiostratigraphy and the bed (see Fig. 2 for examples of
323 each). It has been deployed widely across Antarctica (Fig. 3d) and has detected radiostratigraphy across both
324 West and East Antarctica (Karlsson et al., 2009; Karlsson et al., 2014; Bingham et al., 2015; Winter et al., 2015;



325 Ashmore et al., 2020; Ross et al., 2020; Bodart et al., 2021; Bodart et al., 2023; Sanderson et al., 2023).
326 Recently, >450,000 km of PASIN radargrams acquired between 2004 and 2020 were made accessible in open-
327 access format (Frémand et al., 2022).

328 **3.4 University of Texas Institute for Geophysics**

329 The USA-based University of Texas Institute of Geophysics (UTIG) has conducted airborne RES surveys of
330 Antarctica since the early 1990s, using several generations of systems of increasing sophistication, all with a
331 centre frequency of 60 MHz (Young et al., 2016). Their earliest surveys, principally of West Antarctica, used
332 adapted versions of the system used for the SPRI-NSF-DTU surveys and were recorded digitally but
333 incoherently (Blankenship et al., 2001; Carter et al., 2007). In the early 2000s, UTIG integrated a coherent
334 RES system (Moussessian et al., 2000) with the DTU radio-frequency hardware to allow high-power coherent
335 recording, which enabled synthetic-aperture-radar (SAR) processing of acquired data (Peters et al., 2005;
336 Peters et al., 2007; SAR processing is described in Sect. 4.1). This initial High-Capability Radar Sounder (HiCARS)
337 system (Blankenship et al., 2017a) was translated to commercially available components (HiCARSII,
338 Blankenship et al., 2017b) which were incorporated into the subsequent Multifrequency Airborne Radar-
339 sounder for Full-phase Assessment (MARFA), capable of cross-track interferometry for clutter discrimination
340 (Castelletti et al., 2017; Scanlan et al., 2020). These systems have successfully detected detailed
341 radiostratigraphy throughout the Antarctic ice sheets (Fig. 3e) as part of large-scale multi-national campaigns
342 (e.g., Morse et al., 2002; Carter et al., 2007; Muldoon et al., 2018; Beem et al., 2021) including, from 2008,
343 across large regions of East Antarctica as part of the ICECAP (Investigating the Cryospheric Evolution of the
344 Central Antarctic Plate) international consortium (e.g., Young et al., 2011; Wright et al., 2012; Cavitte et al.,
345 2016; Cavitte et al., 2018) and integrated into NASA's Operation IceBridge (OIB; other airborne RES surveys
346 by OIB are introduced in Sect. 3.6). RES systems based on the commercial HiCARSII design have been
347 integrated into the Chinese (Sect. 3.8) and Korean Antarctic programmes, and UTIG is collaborating with
348 CReSIS (Sect. 3.6) on the mapping of Dome A as part of the US National Science Foundation's Center for
349 Oldest Ice Exploration (COLDEX).

350 **3.5 Alfred-Wegener Institute**

351 The Germany-based Alfred-Wegener Institute (AWI) has performed airborne RES surveys since the mid-1990s
352 (Steinhage et al., 2001), recording digitally and acquiring a total of ~420,000 km of RES data (Fig. 3f), often as
353 part of multinational projects. Its primary system until the mid-2010s – the Aero-EMR (Electro-Magnetic
354 Reflection) instrument – operated around a centre frequency of 150 MHz in a toggle mode that allowed for
355 short (60 ns; high resolution but low-penetration depth) and long (600 ns; low-resolution but high-
356 penetration depth) pulses to be transmitted simultaneously (Nixdorf et al., 1999; Eisen et al., 2007). Following
357 progressive upgrades to the flexibility and sensitivity of its Aero-EMR, AWI began using an improved version
358 (MCoRDS5) of the CReSIS ultra-wideband RES system (Hale et al., 2016; see Sect. 3.6 below). Antarctic



359 operations of this newer system have so far operated across Dronning Maud Land using frequencies ranging
360 from 180-210 and 150-520 MHz, respectively (Franke et al., 2021; Koch et al., 2023; Franke et al., 2024). AWI
361 RES data (Fig. 3f) have been used extensively to recover radiostratigraphy across East Antarctica with a
362 particular focus around the EPICA (European Project for Ice Coring in Antarctica) Dome C, Kohnen and Dome
363 F ice-core sites, Recovery Glacier (Humbert et al., 2018) and Dronning Maud Land (e.g., Steinhage et al., 2001;
364 Steinhage et al., 2013; Karlsson et al., 2018; Winter et al., 2019b; Wang et al., 2023). Additional significant
365 AWI RES surveys also span the Lambert and Recovery glacier catchments (Fig. 3f).

366 **3.6 Centre for the Remote Sensing of Ice Sheets / Operation IceBridge**

367 The USA-based University of Kansas began developing coherent RES systems in the 1980s but primarily
368 focussed on Greenland. A Kansas RES system with 150 MHz centre frequency was first deployed over
369 Antarctica in 2002 on a joint USA (NASA; National Aeronautics and Space Administration) / Chile (CECs;
370 Centro de Estudios Científicos) mission to survey fast-changing regions of West Antarctica (Rignot et al., 2004).
371 In 2005, Kansas became host to the USA's Center for Remote Sensing of Ice Sheets (CReSIS), an NSF-
372 designated national Science and Technology Centre with a focus on ice-sheet sounding¹; and began to
373 operate an upgraded series of deep-looking RES systems named Multichannel Coherent Radar Depth
374 Sounders (MCoRDS). An early application of these RES systems was a wide-ranging survey of the Gamburtsev
375 Subglacial Mountains region of central East Antarctica in 2008/09 (Fig. 3g) that notably imaged multiple
376 basal-ice units disrupting the radiostratigraphy (Bell et al., 2011; and Sect. 5.4; Wolovick et al., 2014; Wrona
377 et al., 2018; and Sect. 5.4).

378 From 2009 to 2019, MCoRDS was frequently deployed onboard NASA's Operation IceBridge (OIB) programme,
379 which performed ten Antarctic RES campaigns collecting ~350,000 km of RES data (Fig. 3g; MacGregor et al.,
380 2021). Most surveys detected widespread radiostratigraphy using centre frequencies of ~190-194 MHz, but
381 for the 2009 to 2011 campaigns MCoRDS Version 1 the radiostratigraphic continuity is relatively poor
382 (MacGregor et al., 2021). From 2012, MCoRDS Versions 2 to 7 were introduced with progressively greater
383 power and bandwidth, significantly improving the detection of radiostratigraphy using frequencies in the
384 range of 150-450 MHz (Rodriguez-Morales et al., 2013; MacGregor et al., 2021). NASA OIB / CReSIS data have
385 been used to assess and track radiostratigraphy within the central East Antarctic Ice Sheet (Cavitte et al.,
386 2016; Winter et al., 2017), and across West Antarctica's central divide and Thwaites Glacier (Holschuh et al.,
387 2014; Koutnik et al., 2016; Bodart et al., 2021). Significantly, CReSIS pioneered early open access to processing
388 routines and radargrams (Liu et al., 2016), and continues to do so as part of the Open Polar Radar project
389 (Paden et al., 2021; and Sect. 6).

¹ From 2022 CReSIS, reflecting an expanding remit, was renamed the Center for Remote Sensing of *Integrated Systems*.



390 **3.7 Lamont-Doherty Earth Observatory**

391 From 2010, the Lamont-Doherty Earth Observatory (LDEO) of the USA's Columbia University developed an
392 in-house Deep ICE Radar (DICE) RES system as part of an aerogeophysical suite ("IcePod") designed to be
393 operated from LC-130 aircraft typically deployed by the US Antarctic Programme. DICE, with 188 MHz centre
394 frequency and 60 MHz bandwidth, was operated between 2015 and 2017 to systematically survey the
395 500,000 km² Ross Ice Shelf (Fig. 3h; Tinto et al., 2019; Das et al., 2020).

396 **3.8 Polar Research Institute of China**

397 The Polar Research Institute of China (PRIC) has undertaken considerable airborne RES surveying across East
398 Antarctica since 2015 (Fig. 3i). Deploying a 60 MHz centre-frequency RES system, which has heritage in the
399 UTIG HiCARSII system (Sect. 3.4), configured in the "Snow Eagle 601" airborne platform, PRIC has
400 systematically and extensively surveyed the Princess Elizabeth Land sector of East Antarctica (Cui et al.,
401 2020b). Further profiling has also covered much of Mac. Robertson Land including Amery Ice Shelf (Cui et al.,
402 2020a; Cui et al., 2020c). Several long profiles across Dome A, Ridge B, Vostok, Dome C and Wilkes Land (Cui
403 et al., 2020a) could also be used to link radiostratigraphy with other RES campaigns across key sectors of East
404 Antarctica. Recent efforts applying machine learning methods to the extraction of radiostratigraphy from
405 these airborne RES data (Dong et al., 2021) show rich promise.

406 **3.9 Additional airborne RES datasets**

407 The RES providers discussed in the preceding sections have acquired >90% of the airborne RES data suitable
408 for extracting internal architecture across the Antarctic ice sheets. Of the remainder (Fig. 3j), airborne RES
409 data have been acquired, primarily with analogue systems, around parts of coastal East Antarctica by
410 Antarctic programmes, institutions and universities from Australia (e.g., Morgan et al., 1982), Belgium (Van
411 Autenboer and Declair, 1975; using a SPRI RES system), Germany (by groups led from University of Münster,
412 e.g., Thyssen and Grosfeld (1988) and the Federal Institute for Geosciences and Natural Resources (BGR), e.g.,
413 and the Federal Institute for Geosciences and Natural Resources (BGR), e.g., Damaske and McLean (2005))
414 and Italy (e.g., Frezzotti et al., 2004; Urbini et al., 2010). In West Antarctica, airborne RES data were acquired
415 by the NSF in the 1970s across Ross Ice Shelf (Bentley, 1990) and in the 1980s across West Antarctica's Siple
416 Coast region (Retzlaff et al., 1993) using a SPRI RES system; after which USA-led airborne RES surveys were
417 arranged through the institutions already introduced above (Sect. 3.4 [UTIG], 3.6 [NASA/CREsIS] and 3.7
418 [LDEO]). More recently, the Korean Polar Research Institute has conducted airborne RES surveys around
419 coastal East and West Antarctica with a system based on the UTIG MARFA RES system (e.g., Lindzey et al.,
420 2020; Lee et al., 2021). Almost all of these campaigns, although we have broadly labelled them by national
421 programmes or institutions, have relied on, and fundamentally been supported by, international
422 collaboration in some or all of their component funding, logistical or scientific aspects. In most cases, because



423 they are now some decades old or not digitally rendered, the contemporary utility of these additional
424 airborne RES datasets for providing useful information on internal architecture remains largely to be
425 investigated, but some of them may yet prove instrumental in linking between two or more wider-ranging
426 surveys across parts of the ice sheet. The most promising, because they comprise several links between
427 coastal regions and the deep interior of East Antarctica at Dome C, were acquired by the Italian programme
428 under the auspices of EPICA (e.g., Tabacco et al. (1999) and Tabacco et al. (2008); plus see Siegert et al.
429 (2001b), for an example of a combined use of these data and those from the SPRI-NSF-DTU surveys of the
430 1970s).

431 **3.10 Ground-based RES datasets**

432 Since the 1960s, groups from at least twelve institutions have acquired ground-based RES datasets focussed
433 on sounding Antarctica's subglacial bed and have also typically imaged internal architecture in the process.
434 Typically, these ground-based surveys have been confined to smaller regions or shorter profiles than covered
435 by the airborne RES surveys, befitting the more common application of ground-based RES to detailed site
436 surveys in preparation for retrieving ice cores, or for accessing the ice bed or subglacial lakes (e.g., Frezzotti
437 et al., 2004; Laird et al., 2010; Christianson et al., 2012; Ross et al., 2020). From these surveys, several local
438 radiostratigraphies have been published (e.g., Eisen et al., 2005; Jacobel and Welch, 2005; Koutnik et al.,
439 2016; Cavitte et al., 2023; Chung et al., 2023; Koch et al., 2023). These detailed studies provide invaluable
440 seeding points for extending radiostratigraphies much more widely across the ice sheets (e.g., Winter et al.,
441 2019a) and for understanding better ice-sheet history and glaciological processes.

442 Supplementing the more local surveys, some ground-based profiles have been acquired over traverses of
443 multiple 100s of km over the Antarctic ice sheets, and these traverses, marked on Fig. 3k, merit special
444 attention as potential resources for analysing pan-continental radiostratigraphy. A particularly extensive
445 programme of ground-based surveys has been conducted since 1969 by the Japanese Antarctic Research
446 Expedition (JARE) connecting coastal East Antarctica in Dronning Maud and Enderby Land to Dome F, with
447 data from some of these traverses conducted in the 1990s underpinning seminal work on the origins of IRHs
448 (Fujita et al., 1999; Matsuoka et al., 2003). Today, data from JARE represent some of the most spatially
449 extensive of Antarctica's ground-based RES datasets and a rich repository of internal architecture (Fujita et
450 al., 2011; Van Liefferinge et al., 2021; Tsutaki et al., 2022). Further long ground-based RES traverses were
451 acquired by several national and international teams in the 2000s under the auspices of the International
452 Trans-Antarctic Scientific Expedition (ITASE). RES profiles containing particularly rich internal architecture
453 were acquired by the USA-NSF's ITASE traverses across both West (Welch and Jacobel, 2003; Jacobel and
454 Welch, 2005) and East Antarctica (Welch et al., 2009), with findings from Arcone et al. (2012a) suggesting
455 that in some parts of East Antarctica the radiostratigraphy is unconformable and may present significant
456 challenges to tracking radiostratigraphy.



457 Other institutes/consortia who have acquired wide-ranging and deep-looking ground-based RES profiles
458 extending 100s of km across the Antarctic ice sheets include the Australian National Antarctic Research
459 Expedition (ANARE; over Mac. Robertson and Princess Elizabeth Lands, traversing around ice feeding Amery
460 Ice Shelf - Craven et al. (2001); Wilkes Land - Jones and Hendy (1985); Medhurst (1985)); BAS (e.g., surveys
461 across West Antarctic catchments by King (2009); King (2011); Ross et al. (2011); Bingham et al. (2012);
462 Bingham et al. (2017); and Filchner-Ronne Ice Shelf; (Kingslake et al., 2016)); the Chilean Antarctic Institute
463 (Instituto Antártico Chileno, INACH, surveys around Institute Ice Stream including Subglacial Lake CECs; Rivera
464 et al. (2015); Napoleoni et al. (2020) - and connecting Institute Ice Stream to South Pole in a joint enterprise
465 with the Brazilian Antarctic Programme; Zamora et al. (2007)); the Russian Antarctic Expedition (traverses
466 connecting coastal stations to Vostok and Ridge B; (Popov, 2015; Popov, 2020)); PRIC (traverses connecting
467 coastal Zhongshan Station with Dome A; Luo et al. (2022)); and the International Thwaites Glacier
468 Collaboration (WAIS Divide to lower Thwaites Glacier between 2022 and 2024 using BAS and CReSIS ground-
469 based RES systems) (Fig. 3k). Especially for ice-core-related imaging of radiostratigraphy, deep-looking
470 ground-based surveys are still essential because of their high horizontal resolution.

471 **3.11 Summary**

472 Figure 3l collates the coverage of those RES datasets which were digitally acquired with GNSS navigation and,
473 in principle, represent the present coverage of existing RES data that could be used to develop a pan-Antarctic
474 radiostratigraphy. In practice, as the following section explores, only a small subset of these data have so far
475 been exploited, in part due to challenges in accessing data and working with them consistently, but mainly
476 because tracing and dating radiostratigraphy using existing methods is a highly time- and resource-intensive
477 process.

478 **4 Extracting and dating internal architecture from RES data**

479 The information available from radargrams (e.g. Fig. 2), and the degree to which the internal architecture can
480 be used for different applications, depend firstly on the settings of the RES system acquiring the data and
481 secondly on choices made in processing the data. Below we summarise the typical processing workflow for
482 radargram generation and highlight key decisions that influence interpretation of the resulting
483 radiostratigraphy. Figure 4 presents a conceptual support to this discussion. We then discuss the different
484 methods used to trace radiostratigraphy through radargrams, and to date key IRHs, and provide an inventory
485 of existing traced radiostratigraphy across Antarctica.

486 **4.1 Pulse compression, filtering, and image focussing for optimising IRH tracing**

487 RES can be categorised broadly based on two criteria: (a) Phase control of the transmitter or phase sampling
488 by the receiver (i.e., coherent vs. incoherent); and (b) the nature of the transmitted wave (pulsed versus

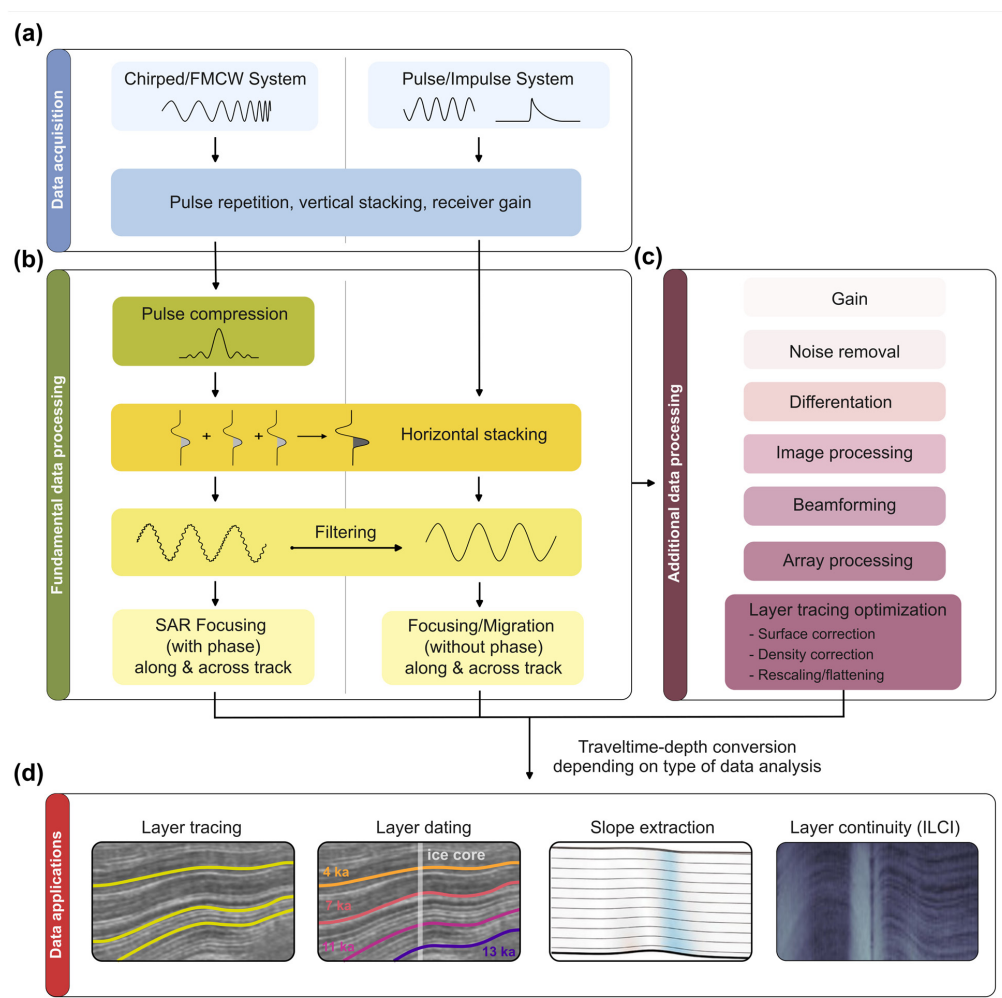


Figure 4. Flowchart illustrating key steps for the processing of RES data from chirp and pulse systems for subsequent radiostratigraphic analysis. (a) Basic configurations and parameters defined on data acquisition. (b) Fundamental and (c) additional steps commonly taken when processing data to visualise IRHs. (d) Depiction of some common ways of tracing or otherwise quantifying IRH geometry.

489

490 chirped; Gogineni et al. (1998); Peters et al. (2005)) (Fig. 4a). Processing is similar for all systems, so here we
 491 highlight differences that affect radargram quality. Direct measurements of the dielectric properties of ice cores
 492 show that ice conductivity varies on much smaller length scales than can be imaged by RES (Harrison,
 493 1973; Eisen et al., 2003). Therefore, each RES system represents subsurface reflectors differently, and data
 494 acquired from the same area but by different RES systems may show different IRHs on intersecting
 495 radargrams due to the differences in RES imaging capabilities (see Fig. 5, after Winter et al. (2017), for an
 496 example of a comparison between different RES systems). For pulsed systems, processing cannot improve

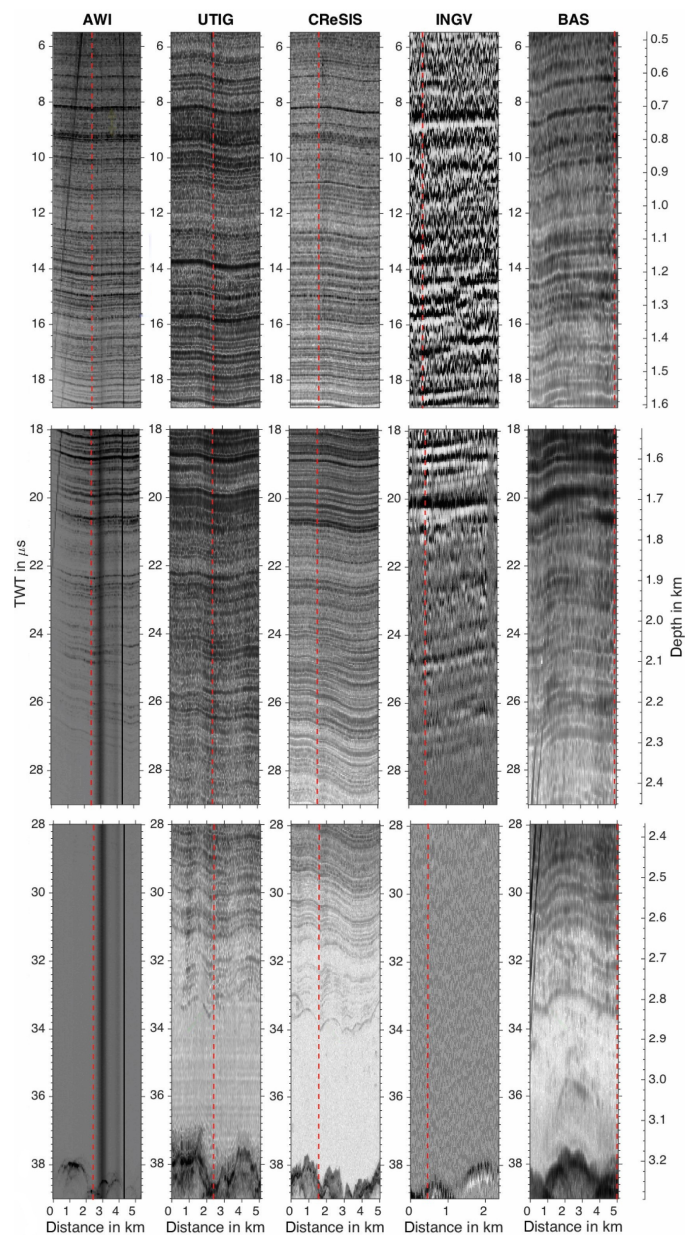


Figure 5. RES profiles of a few km length for five RES systems, that have profiled across or near EPICA Dome C. The vertical red line in each profile marks the position of the trace closest to Dome C. The surface reflections are shifted to time zero and the length of the RES profiles is indicated on the horizontal axes. For the bottom UTIG and CreSIS panels a 2-D-focused processing is applied. The RES data were acquired with: 1. AWI 150 MHz Aero-EMR; 2. UTIG 60 MHz HiCARS; 3. CreSIS 194 MHz MCoRDS; 4. Italian National Institute of Geophysics and Volcanology (INGV) 150 MHz RES system; and 5. BAS 150 MHz PASIN; for full details and original figure from which this is modified, see Winter et al. (2017).



498 the vertical resolution, which is controlled by the bandwidth and the rate of sampling of the received
499 waveform. For chirped systems, the waveform must be fully sampled first and then match-filtered,
500 integrating the received power while also finely resolving radiostratigraphy targets based on the chirp's
501 bandwidth (Hélière et al., 2007; Peters et al., 2007). This “pulse compression” is the first step in producing a
502 radargram from a chirped system.

503 Following initial data acquisition, RES data are typically processed using geophysical techniques of varying
504 sophistication (Fig. 4b). For example, incoherent noise is typically reduced by various forms of horizontal
505 averaging, and bandpass-filtering can remove irrelevant components of the measured signal. Finally, if
506 possible the data should be focused or migrated to reposition the received signal energy as precisely as
507 possible to their true subsurface locations. This can be done via several methods: (a) Incoherent echo
508 summation, often termed *migration* as in reflection seismology (Yilmaz, 2001); (b) SAR-focusing for point
509 scatterers, common in satellite applications (Ulaby and Lang, 2015); or (c) algorithms designed specifically
510 for RES of specular reflections (Heister and Scheiber, 2018; Castelletti et al., 2019; Xu et al., 2022). SAR-
511 focusing has a proven ability to reduce image artefacts and improve along-track resolution, especially in areas
512 with steeply-sloping radiostratigraphy (Holschuh et al., 2014; Castelletti et al., 2019). Multiple SAR-processing
513 techniques currently exist for coherent RES systems, including: (a) unfocused SAR (short apertures without
514 phase correction and equivalent in name to Doppler filtering or coherent echo summation; Hélière et al.
515 (2007)); or (b) more advanced focused SAR, using either 1-D correlations resulting in intermediate apertures,
516 or 2-D correlations resulting in longer apertures (Peters et al., 2005; Peters et al., 2007). The latter is the
517 processing of choice for modern coherent systems for the detection of IRHs in areas with steeply dipping
518 reflections. Unfocused and 1-D SAR approaches will emphasise flat specular reflectors and reduce clutter, at
519 a cost of dipping specular horizons. Large SAR apertures are critical for tracking steeply dipping IRHs, but
520 present greater computational costs and an overall reduction of signal to noise ratio. Cross-track antenna
521 arrays can allow for determination of cross-track IRH slopes.

522 A series of additional corrections and image-processing steps can also be taken to optimise RES data for
523 tracing radiostratigraphy (Fig. 4c). For radar data acquired by airborne platforms, the aircraft-to-ice surface
524 space on the radargram must be removed to obtain true depths below the ice surface; this is often conducted
525 by shifting the vertical axis of the radargram to time zero for each RES trace and flattening the surface based
526 on the location of the surface reflection on the radargram. This can be done using data from the altimeter
527 and/or LIDAR onboard the aircraft, high-resolution surface DEMs, or using the picked surface reflection from
528 the radargram itself (e.g., MacGregor et al., 2015a). Localised density corrections, based on ground-truthing
529 measurements in the upper section of ice cores or other geophysical measurements (e.g., radar data acquired
530 by airborne platforms; Eisen et al., 2002), may also be applied to convert the two-way-travel time from the
531 RES data to ice-equivalent depths. Alternatively, for depth-correcting RES below the pore close-off depth, a
532 spatially uniform density value that is typically of the order of several metres may be used to obtain ice-



533 equivalent depths (e.g., Ashmore et al., 2020), although this assumption may only be valid in dry and stable
534 parts of the ice sheet and not in highly dynamic regions (Dowdeswell and Evans, 2004). Others have also
535 vertically rescaled (or flattened) RES data to facilitate the tracing of continuous reflections by semi-automatic
536 pickers (e.g., Fahnestock et al., 2001a; Sect. 4.2; MacGregor et al., 2015a). Finally, specific image-processing
537 filters can also be applied to enhance the gain and reduce incoherent noise, which can facilitate IRH tracing
538 on RES data (Ashmore et al., 2020; Bodart et al., 2021; Wang et al., 2023).

539 Importantly for users interested in tracing IRHs, and especially the deepest IRHs, most RES data over
540 Antarctica, including those available from open-access repositories, are not optimised for detecting
541 radiostratigraphy. Typically the data have been acquired and processed to optimise retrieval of the bed echo,
542 and some datasets require considerable reprocessing from the raw data to improve the clarity of the
543 radiostratigraphy between the ice surface and the bed (Castelletti et al., 2019). In particular, for thick or
544 unusually heterogenous ice, the best strategy is often to experiment with filtering data differently at different
545 depths until the IRHs at selected depths are most clearly visualised.

546 **4.2 Tracing radiostratigraphy**

547 The primary method for extracting internal architecture from radargrams has been to trace or “pick” IRHs,
548 typically using semi-automated techniques (e.g., Cavitte et al., 2016; Koch et al., 2023). Where radargram
549 quality is high, IRHs are easily traced and continuous, and automated methods may also perform well (e.g.,
550 Panton, 2014; Xiong et al., 2018; Delf et al., 2020). Machine-learning methods show promise for more rapidly
551 tracing radiostratigraphy in new datasets; but so far successful applications have been limited to shallow IRHs
552 in the upper few tens of metres of the ice column (e.g., Dong et al., 2021; Rahnemoonfar et al., 2021; Yari et
553 al., 2021). Thus, for most radargrams and deep-ice applications, semi-automated tracing of IRHs is presently
554 required. This relies on algorithms that typically follow the local maxima in return power between adjacent
555 traces within a predetermined vertical window, using either open-source or commercial and bespoke
556 software from the seismic industry (e.g., Winter et al., 2019a; Ashmore et al., 2020; Sanderson et al., 2024).
557 A comprehensive overview of IRH-tracing methods is provided by Moqadam and Eisen (2024).

558 The process of tracing IRHs can be categorised into two main approaches: (a) tracing as many IRHs as possible
559 regardless of their amplitudes or continuity (MacGregor et al., 2015a); or (b; more commonly) by identifying
560 IRHs that have a high echo-power, appear distinguishably brighter than adjacent IRHs on radargrams and are
561 continuous for long distances (>100 km), using crossovers between intersecting RES profiles to ensure
562 reliability in the tracing process (e.g., Cavitte et al., 2016; Winter et al., 2019a; Ashmore et al., 2020; Bodart
563 et al., 2021; Wang et al., 2023).

564 Importantly, the thickness of a given IRH in a radargram is dependent on the range resolution of the RES
565 system used to image it, such that RES systems with high pulse-width, and thus finer vertical resolution, may



566 detect several thinner IRHs that would otherwise appear as a single, broader reflection in coarser-resolution
567 systems (see Fig. 5 and Harrison, 1973; Millar, 1982; Karlsson et al., 2014; Winter et al., 2017; Bodart et al.,
568 2021; Cavitte et al., 2021). This must be accounted for when comparing the position and aspect of IRHs traced
569 in data from RES systems operating with different frequencies and system characteristics (Winter et al., 2017).

570 **4.3 Complementary approaches to tracing IRHs for characterising radiostratigraphy**

571 Even having applied all possible data processing strategies described above, radiostratigraphy may remain
572 challenging or impossible to trace over some regions due to the innate physical properties of ice in such areas.
573 For example, IRHs may become warped/buckled or disrupted by differential ice flow or flow over steep
574 topography (e.g., Siegert et al., 2003b; Ross et al., 2011; Bingham et al., 2015; Franke et al., 2023; Jansen et
575 al., 2024), while unconformities can be introduced by significant wind scouring of the ice surface (e.g., Welch
576 and Jacobel, 2005; Luo et al., 2022). This variability in itself provides important information about past and
577 present ice behaviour (as we explore further in Sect. 5), and hence warrants alternate methods to
578 characterise the radiostratigraphy where IRHs cannot readily be traced.

579 One method for assessing the general variability of radiostratigraphy across large regions of ice sheets is the
580 Internal Layering Continuity Index (ILCI) developed by Karlsson et al. (2012). This tool maps the variability in
581 vertical signal strength for individual RES traces, acting as a relative measure of the number of dielectric
582 contrasts compared to signal-to-noise ratio. High ILCI values typically indicate regions of an ice sheet
583 characterised by multiple, traceable IRHs, while low ILCI values tend to indicate regions of ice sheet with
584 disrupted or discontinuous IRHs or regions with very few or no IRHs detected by the RES system. Although
585 the method is not easily transferable between different RES systems due to acquisition and processing
586 differences, ILCI has been extensively applied to several regions both in Antarctica (Fig. 6) and Greenland as
587 a mechanism for identifying rapidly the specific sub-regions in which IRHs are likely to be traceable (e.g., Sime
588 et al., 2014; Bingham et al., 2015; Karlsson et al., 2018; Frémand et al., 2022; Tang et al., 2022; Sanderson et
589 al., 2023).

590 Alternative methods have focussed on the extraction of IRH slopes. This avenue acknowledges the challenges
591 of tracing and dating radiostratigraphy in areas of fast or complex ice flow, or where the acquisition or
592 processing methods that have been used were not tailored to the recovery of radiostratigraphy. For
593 discontinuous radiostratigraphy, local slope information is valuable, because radiostratigraphic slope is
594 closely related to particle trajectories within the ice sheet (Hindmarsh et al., 2006; Parrenin and Hindmarsh,
595 2007; Ng and King, 2011; Holschuh et al., 2017). Several methods have therefore been developed to extract
596 slope information, such as incoherent averaging methods (Sime et al., 2011; Holschuh et al., 2017; Delf et al.,
597 2020) and methods that use along-track phase information during SAR processing to estimate IRH slope
598 (MacGregor et al., 2015a; Castelletti et al., 2019; Oraschewski et al., 2023).

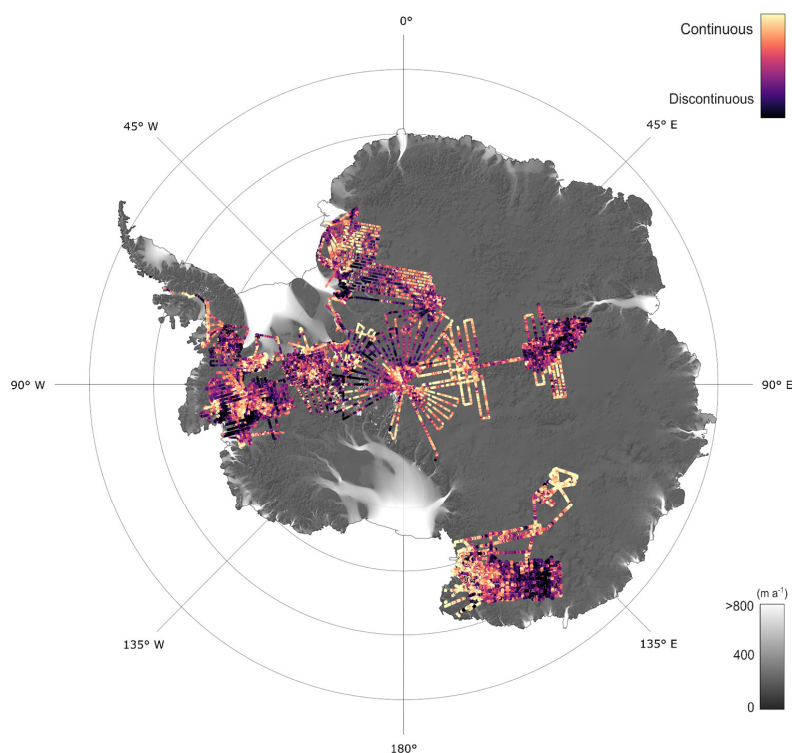


Figure 6. Radiostatigraphic continuity (ILCI) calculated over 10 airborne RES datasets acquired by BAS. Continuous and readily traceable IRHs are indicated in the slow-flowing regions of the ice sheet (high ILCI; bright yellow) whereas disrupted or absent IRHs are likely in the faster-flowing sections of ice streams or where subglacial topography is highly variable (low ILCI; dark purple). The background maps show ice-flow velocities from MEaSUREs (Rignot et al., 2017) and a hillshade of the bedrock from BedMachine (Morlighem, 2020). Figure modified from Frémand et al. (2022).

599

600 **4.4 Dating internal-reflection horizons (isochrones)**

601 As introduced in Sect. 2, most RES-imaged IRHs have been shown to be isochronous, and the majority of
602 those we treat in this review (i.e. that are imaged in between the first and last few hundreds of metres of the
603 ice column) arise due to the RES systems imaging variations in the electrical conductivity (i.e. acidic content)
604 of the ice with depth. Hereafter in this paper, reiterating that most IRHs are isochrones, we will use the term
605 isochrones to refer to IRHs, and will only re-use the term IRH where it may be ambiguous concerning whether
606 IRHs are isochronous.

607 Ages can be assigned to isochrones at intersections with deep ice cores where age-depth models have already
608 been derived from chemistry analyses (e.g., McConnell et al., 2017; Cole-Dai et al., 2021; Bouchet et al., 2023),
609 but also using modelling techniques where this is not possible. Before any age can be assigned, the age



610 uncertainty that arises from the RES system itself must first be assessed. Uncertainty in reflector depth arises
611 from several sources: (a) proximity of the RES profile to the ice-core site, otherwise a specific reflector
612 geometry (typically flat) must be assumed between the point of closest approach and the ice-core site
613 (MacGregor et al., 2015a); (b) the radio-wave speed, which varies based on permittivity variations as a
614 function of englacial density and anisotropy (e.g., Kovacs et al., 1995; Fujita et al., 2000); (c) the range
615 resolution of the RES system and the signal-to-noise ratio of each traced reflection at (or near) the ice-core
616 site, which enable an estimate of the depth precision to which each traced reflection can be known (e.g.,
617 Cavitte et al., 2016); and (d) the picking accuracy of both the ice surface and the isochrones themselves,
618 which can add several metres of uncertainty. This latter point may include the uncertainty arising from the
619 source of the surface product (i.e. either from cm-resolution onboard altimeter/LIDAR), or directly from the
620 RES data which have much lower resolution of the order of several metres); and whether the picking
621 algorithm is tailored to extract the onset of the reflection, the half-amplitude, or the peak value.

622 The ideal scenario for assigning ages to isochrones is that a RES profile intersects or passes sufficiently close
623 (~500 m vicinity) to the location of an ice-core site for the ice core's depth-age scale (from chemical profiling
624 or layer counting) to be useable for directly assigning ages to the RES-imaged isochrones. In such cases, the
625 isochrone-depth uncertainty can then be combined with the ice-core age uncertainty to assign a total age
626 uncertainty to the mapped reflections; in these cases, uncertainty is generally dominated by the ice-core-
627 derived age uncertainty in the upper third of the ice column, while the RES-derived depth uncertainty
628 increasingly dominates at larger depth (e.g., MacGregor et al., 2015a; Cavitte et al., 2016; Muldoon et al.,
629 2018; Winter et al., 2019a; Wang et al., 2023). More recently, some isochrones have been dated not by their
630 direct intersection with an ice core, but rather by intersecting other RES datasets that in turn have already
631 been dated by their intersection with a distant ice core. In these cases, the age-depth profile is transferred
632 to the new dataset at the crossover(s) between the intersecting RES datasets (e.g., Ashmore et al., 2020;
633 Bodart et al., 2021). In these cases, the relative uncertainties of the different RES systems at the intersections
634 between RES datasets additionally need be factored into the final age estimation, and the final age estimates
635 are commonly checked using the modelling techniques introduced next (e.g., Bodart et al., 2021; Sanderson
636 et al., 2024).

637 Where isochrones cannot be directly correlated to an ice-core age-depth relationship due to a lack of nearby
638 ice cores, any intersections with previously dated isochrones, or missing sections in the record (e.g., due to
639 disrupted englacial stratigraphy), age-depth modelling is required to assign ages to isochrones. This is
640 typically done using 1-D models in stable parts of the ice sheet such as at ice divides (e.g., Nye, 1957;
641 Dansgaard and Johnsen, 1969; Ashmore et al., 2020; Bodart et al., 2021; Sanderson et al., 2024); or using
642 more complex multidimensional (2D/3D) models in areas with challenging ice-flow or bed conditions (e.g.,
643 Waddington et al., 2007; MacGregor et al., 2015a; Parrenin et al., 2017; Lilien et al., 2021).



644 **4.5 Existing dated radiostratigraphy across Antarctica**

645 Before the inception of *AntArchitecture* in 2018, several studies had produced radiostratigraphies spanning
 646 the last 17.5 ka across West Antarctica and 352 ka for East Antarctica (e.g., Hodgkins et al., 2000; Siegert and
 647 Hodgkins, 2000; Siegert, 2003; Siegert and Payne, 2004; Jacobel and Welch, 2005; Leysinger Vieli et al., 2011;
 648 Steinhage et al., 2013; Karlsson et al., 2014; Wang et al., 2016). However, the spatial extents of these
 649 radiostratigraphies were relatively limited. Through *AntArchitecture*, a more coordinated and focused
 650 approach to characterising Antarctic radiostratigraphy has been conducted, as depicted in Figure 7 and
 651 detailed in Table 1. This programme has facilitated the recovery and characterisation of several isochrones
 652 with ages up to 25 ka across much of the Amundsen and Weddell Sea sectors of West Antarctica (Muldoon
 653 et al., 2018; Ashmore et al., 2020; Bodart et al., 2021; Bodart et al., 2023). Over East Antarctica, a much older
 654 record has been extracted, owing to the more stable and slow-flowing ice conditions in the area, including
 655 isochrones dating back to the last 705 ka (Cavitte et al., 2016; Winter et al., 2019a; Beem et al., 2021; Cavitte
 656 et al., 2021; Chung et al., 2023; Wang et al., 2023; Sanderson et al., 2024).

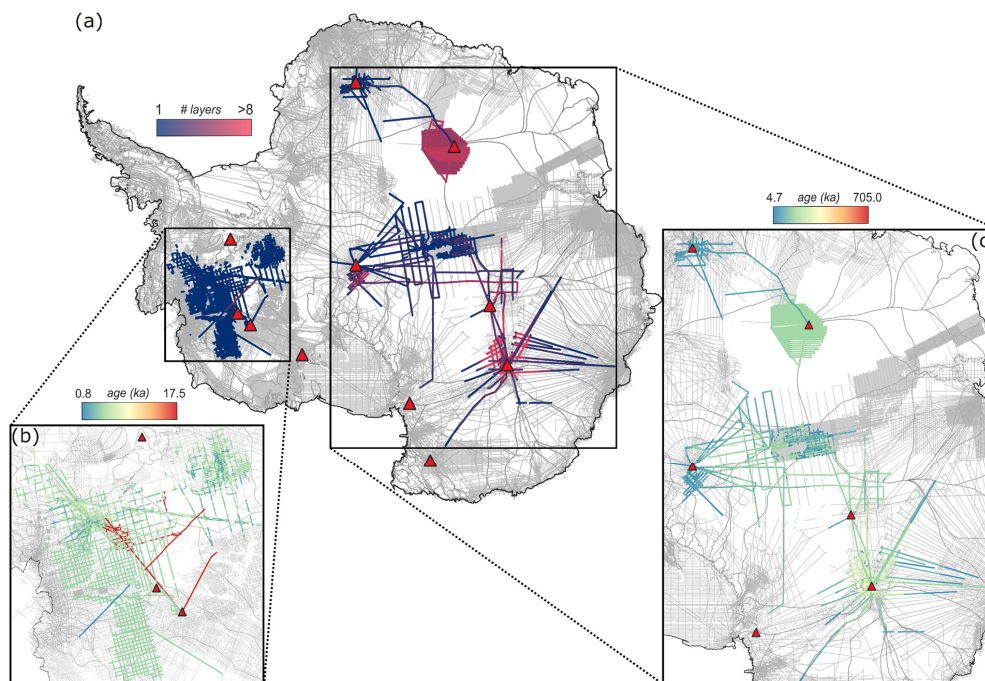


Figure 7. Existing open-access dated stratigraphies across Antarctica obtained from the Digital Object Identifiers (DOIs) provided in Table 1, with RES profiles for Bedmap-2 and Bedmap-3 products shown in the background (grey; Frémand et al., 2023). Existing deep ice cores (defined here as ice cores that have been drilled to near the ice-bed interface and that provide a multi-millennial record) are shown as red triangles. (a) Maximum number of layers traced through each dataset (from 1 to >8). (b-c) age of the deepest (oldest) layer across each dataset for the WAIS (b) and EAIS (c) regions respectively.



658 **Table 1.** Inventory of expansive radiostratigraphic datasets for the Antarctic ice sheets, ordered by region
 659 and length (km of RES profiles) of dataset. The data are mapped in Figure 7; locations of ice cores are marked
 660 on Fig. 3a. DOIs are provided where the underlying isochronal data are available in open-access format. Data-
 661 provider acronyms are expanded in Sect. 3 of the text; in most cases we also list here a specific project
 662 acronym for each survey which can be cross-referenced through the reference and/or dataset listed in each
 663 row.

664 (For EGU sphere formatting, this 10-column table is presented across two pages.)

Region	Survey dates	Data provider (cf. Sect. 3)	Survey name / acronym	Ice-core intersection(s)	No. of traced isochrones
EAIS	1998 - 2008	AWI / CReSIS	DoCo / EPICA / AGAP	Kohnen / Vostok / Dome C	5
EAIS	2016 - 2017	AWI	Beyond EPICA Dome Fuji	Kohnen / Dome F	7
EAIS	2008 - 2018	UTIG	ICECAP	Dome C	26
EAIS	2007 - 2016	BAS	AGAP / PolarGap	South Pole	3
EAIS	1974 – 1979	SPRI-NSF-DTU	-	Vostok / Dome C	12
EAIS	1974 – 1979	SPRI-NSF-DTU	-	Vostok / Dome C	>32
EAIS	2016 – 2017	PRIC	South Pole Corridor	South Pole	8
EAIS	2016 – 2018	BAS	Beyond EPICA Little Dome C	Dome C	20
EAIS	2002 – 2003	AWI	-	Dome F	8
EAIS	1974 – 1979	SPRI-NSF-DTU	-	Vostok	15
EAIS	2004 – 2005	PRIC	Dome A (CHINARE-21)	Vostok	6
WAIS	1991 – 2014	UTIG	CASERTZ / SOAR / AGASEA / GIMBLE	Byrd / WAIS Divide	1
WAIS	2004 – 2018	BAS / CReSIS	BBAS / OIB	WAIS Divide	4
WAIS	2010 – 2011	BAS	IMAFI	-	3
WAIS	2000 – 2001	NSF	ITASE	Byrd	1
WAIS	1977 – 1978	SPRI-NSF-DTU	-	Byrd	5

665



666 **Table 1** continued: Columns 6-10.

Isochrone age range (ka)	Length of traced IRHs (km)	Reference	Dataset DOI
38.0 – 161.0	40 000	Winter et al. (2019a)	10.1594/PANGAEA.895528
31.4 – 232.7	20 000	Wang et al. (2023)	10.1594/PANGAEA.958462
10.0 – 705.0	15 500	Cavitte et al. (2021)	10.15784/601411
38.0 – 162.0	13 000	Sanderson et al. (2024)	10.5285/cfafb639-991a-422f-9caa-7793c195d316
17.5 – 352.4	8 000	Leysinger Vieli et al. (2011)	10.1029/2010JF001785
45.9 – 169.7	4 000	Siegert (2003)	-
4.7 – 93.9	2 000	Beem et al. (2021)	10.15784/601437
10.5 – 414.6	1 280	Chung et al. (2023)	10.1594/PANGAEA.963470
4.7 – 72.4	1 200	Steinhage et al. (2013)	-
17.0 – 211.0	1 000	Leysinger Vieli et al. (2004)	-
34.3 – 161.4	215	Wang et al. (2016)	-
4.7	19 000	Muldoon et al. (2018)	10.15784/601673
2.3 – 16.5	15 000	Bodart et al. (2021)	10.5285/f2de31af-9f83-44f8-9584-f0190a2cc3eb
1.9 – 8.1	6 000	Ashmore et al. (2020)	10.5281/zenodo.4945301
17.5	1 850	Jacobel and Welch (2005)	10.7265/N5R20Z9T
0.8 – 16.0	800	Siegert and Payne (2004)	10.1002/esp.1238

667



668 A notable finding is the presence of widespread and ubiquitous isochrones that have been imaged by
669 different RES systems and are found in several ice-core records. Across West Antarctica, the most ubiquitous
670 isochrone, dated precisely and independently at Byrd and WAIS Divide ice cores to ~ 4.7 ka, has been
671 identified by several studies (Jacobel and Welch, 2005; Karlsson et al., 2014; Holschuh et al., 2018; Muldoon
672 et al., 2018; Ashmore et al., 2020; Table 1; Bodart et al., 2021; Bodart et al., 2023). There is evidence that this
673 same isochrone may also be found widely across East Antarctica, based on sulphate concentrations in ice
674 cores and findings from individual RES surveys across the region (Steinhage et al., 2013; Winski et al., 2019;
675 Beem et al., 2021; Cole-Dai et al., 2021; Sigl et al., 2022). Additionally, across much of the West Antarctic Ice
676 Sheet an isochrone dated at 17.5 ka has been observed in both ground-based and airborne RES data (Jacobel
677 and Welch, 2005; Muldoon et al., 2018; Bodart et al., 2021; Table 1). This 17.5 ka RES isochrone has been
678 identified and linked to an eruption from West Antarctica's Mount Takahe in both the Byrd (Hammer et al.,
679 1997) and WAIS Divide (McConnell et al., 2017) ice cores. Over East Antarctica, packages of closely spaced
680 isochrones of ages ~ 38 ka, ~ 73 ka, ~ 128 ka, ~ 160 ka, and ~ 170 ka have been traced from ice cores (Leysinger
681 Vieli et al., 2011; Winter et al., 2019a; Cavitte et al., 2021; Table 1; Wang et al., 2023; Sanderson et al., 2024);
682 notably, the ~ 73 ka isochrone has been linked by ice-core profiling to the Toba Eruption in Indonesia
683 (Svensson et al., 2013). Together, such distinct isochrones, imaged by and from multiple RES systems and
684 platforms, provide important regional or continental-wide time markers, equivalent to Greenland's highly
685 recognisable "three sisters" (Fahnestock et al., 2001a; MacGregor et al., 2015a) for inferring past changes at
686 specific time intervals.

687 Despite the advances discussed here, the established radiostratigraphy across the Antarctic ice sheets
688 currently represents only a small subset of the total available RES data (Fig. 7, and refer back to Sect. 3 and
689 Fig. 3). The establishment of the *AntArchitecture* community, and its commitment to establish protocols for
690 sharing and processing internal architecture across the multiple datasets, is expected to facilitate further
691 isochrone tracing, which will in turn contribute to the development of the first three-dimensional age-depth
692 model of the ice sheet.

693 **5 Applications of internal architecture to wider Antarctic science**

694 Here, we now review to what scientific purposes internal architecture has already been exploited. Sect. 5.1
695 to 5.4, supported by Figure 8, exemplify four primary applications of RES-imaged isochrones, Sect. 5.5
696 explores the scientific applications of other forms of internal architecture, and Sect. 5.6 discusses how
697 radiostratigraphic data have been incorporated into numerical modelling, and their use in calibrating ice-
698 sheet models of varying complexity. This section contextualises the following Sect. 6 which then suggests
699 priorities for future research that will be enabled as Antarctica's internal architecture, and particularly its
700 radiostratigraphy, continue to be explored and made available.

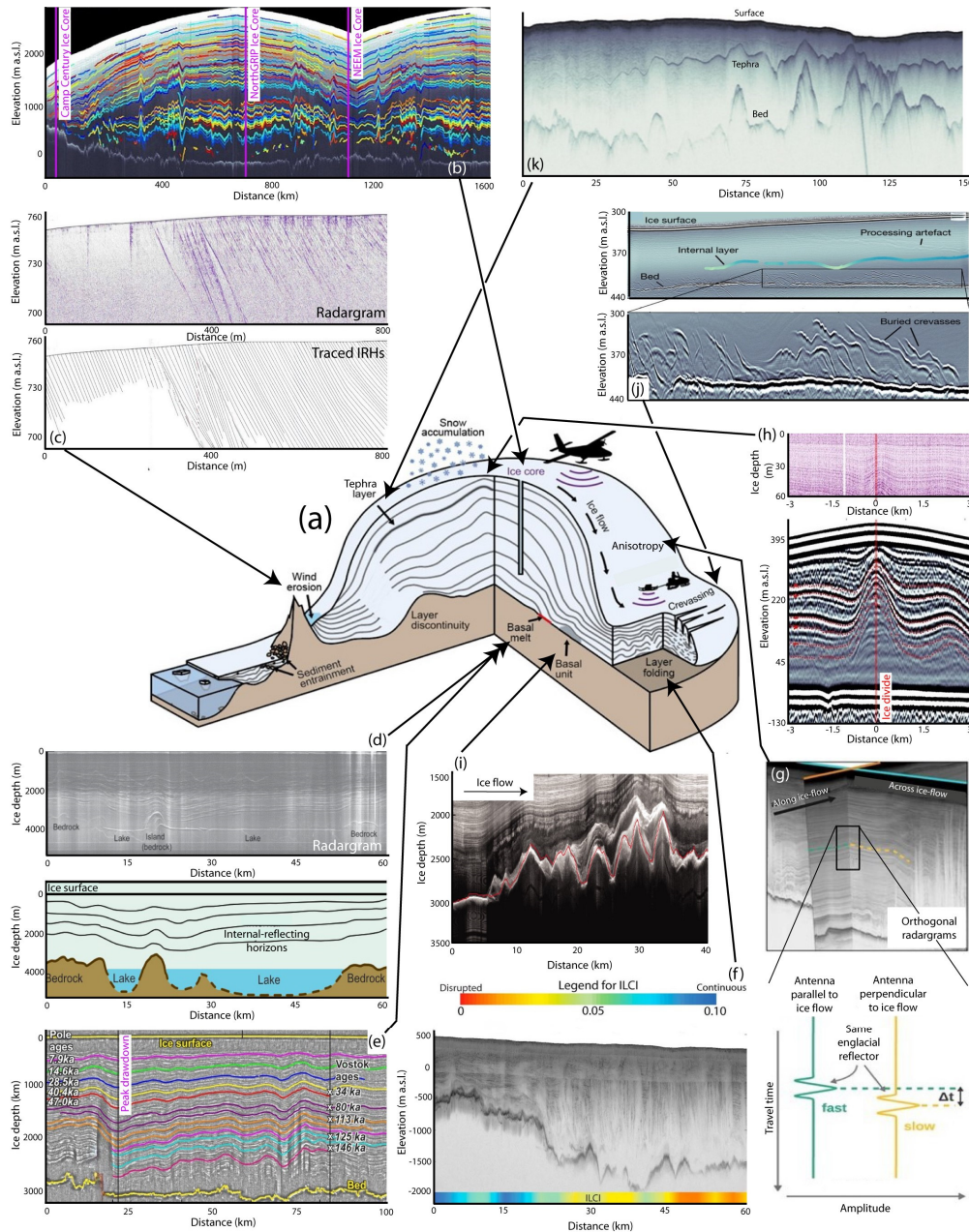


Figure 8. Schematic illustration of radiostratigraphic observations within an ice sheet and their scientific applications; (a), in the centre, depicts typical ice-sheet locations for applications shown in subsequent panels. (b) Connecting and validating ice cores in Greenland (after MacGregor et al., 2015a). (c) Imaging intersections of IRHs with ice surface in region of surface wind scouring (after Winter et al., 2016). (d) Using isochrones to calculate basal melting across Subglacial Lake Vostok (after Siegert et al., 2001a). (e) Using isochrone drawdown to locate region of elevated geothermal heat flux near South Pole (after Jordan et al., 2018). (f) Application of “Internal Layering Continuity Index” (ILCI) to quantify disruption (folding/warping) to otherwise continuous isochrones (after Bingham et al., 2015). (g) Using intersecting RES profiles to explore ice anisotropy (after Gerber et al., 2023). (h) Raymond Arch imaged in shallow (top panel) and deep RES across Derwael Ice Rise, Dronning Maud Land (after Drews et al., 2015). (i) Basal-ice units and suggested accreted basal ice in East Antarctica (after Bell et al., 2011). (j) Basal crevasses imaged in West Antarctica and used to date regrounding of previously floating ice (after Kingslake et al., 2018). (k) Prominent tephra horizon imaged by RES across Pine Island Glacier, West Antarctica (after Corr and Vaughan, 2008).



702 5.1 Radiostratigraphy and ice cores

703 Ice cores from Antarctica provide fundamental palaeoclimate records (e.g., EPICA Community Members,
704 2004; WAIS Divide Project Members, 2015), and we have already introduced the concept that RES records
705 tied to existing ice cores provide a basis for extending these “point-source” age-depth chronologies into 3-D
706 age-depth fields that extend widely across the Antarctic ice sheets (Sect. 4; especially 4.4 and 4.5). Conversely,
707 RES-imaged radiostratigraphy can be used to guide the best locations for recovering future ice cores.
708 Accumulation rate, ice dynamics and age-depth relationships extracted from isochrones have previously
709 informed the appropriateness of coring sites (e.g., Neumann et al., 2008; Parrenin et al., 2017; Beem et al.,
710 2021; Wang et al., 2023) and have been essential for pre-site survey of potential future ice coring, e.g. for
711 the *Oldest Ice* endeavour of the International Partnerships for Ice Core Sciences (IPICS; e.g., Fischer et al.,
712 2013; Van Liefferinge and Pattyn, 2013; Karlsson et al., 2018; Lilien et al., 2021; Chung et al., 2023).

713 Radiostratigraphy has also provided opportunities for synchronising and reducing uncertainties in ice-core
714 chronologies by facilitating the direct tracing of isochrones between two or more ice cores in order to
715 correlate ice-core chronologies (as achieved for the Greenland Ice Sheet by MacGregor et al., 2015a; see Fig.
716 8b). In Antarctica, previous studies that have used isochrones to correlate chronologies between ice cores
717 include Siegert et al. (1998), Steinhage et al. (2013), Cavitte et al. (2016) Le Meur et al. (2018) and Winter et
718 al. (2019a) for East Antarctica, and Muldoon et al. (2018) for West Antarctica. These studies have provided
719 confidence that ice cores obtained from locations separate by 100s of km capture analogous variations in
720 palaeoclimate at regional scales, and that the signals recorded by RES correspond to genuine physical
721 variations in the ice (typically variations in electrical conductivity, often related to fallout from past volcanic
722 eruptions; as noted in Sect. 4.5).

723 The key challenge in synchronising ice-core records between distant sites using RES has been in resolving the
724 radiostratigraphically- and ice-core-derived chronologies between each ice-core site, given the order-of-
725 magnitude difference in resolution of chronologies recoverable from RES (on the order of metres) versus ice-
726 core records (on the order of centimetres). This has typically been dealt with using forward modelling based
727 on electrical-conductivity measurements or dielectric profiling of the ice cores to provide a transfer function
728 (e.g., Miners et al., 1997; Hempel et al., 2000; Eisen et al., 2003; Eisen et al., 2006; Winter et al., 2017;
729 Mojtabavi et al., 2022), or by adopting Bayesian frameworks which provide a probability distribution of the
730 age of the isochrones (Muldoon et al., 2018). Thus, while the age-depth fields compiled from isochrones will
731 never match the precision and accuracy of ice-core age-depth relationships (MacGregor et al., 2015a; Winter
732 et al., 2017), they provide the spatial context that ‘point-source’ ice cores cannot. Through isochrone-
733 constraint modelling (see Sect. 5.6), the age of the ice and its spatial distribution can be more effectively
734 constrained in regions distant from the current drilling sites (Born and Robinson, 2021; Sutter et al., 2021).



735 In marginal locations of the ice sheets, or around nunataks, where persistent pronounced surface scouring is
736 co-located with upward ice flow over subglacial topography – i.e., in regions of so-called “blue ice” – very old
737 ice may outcrop obliquely to the ice surface and hence allow the recovery of a “horizontal ice core” along
738 the ice surface (Spaulding et al., 2013). Dated isochrones have been used to trace the age-depth model
739 recovered from horizontal ice cores back into the ice sheet (Reeh et al., 2002; Siegert et al., 2003a; Winter et
740 al., 2016; Fogwill et al., 2017; Baggenstos et al., 2018; see Fig. 8c). However, shearing and folding can disrupt
741 the stratigraphic order of the outcropping IRHs, rendering the interpretation of their radiostratigraphy more
742 complex than for most vertical ice cores.

743 **5.2 Surface mass balance**

744 In slow-flowing ice and especially around ice divides, the depth of isochrones is largely controlled by surface
745 mass balance and therefore dated radiostratigraphy has made it possible to reconstruct past surface mass
746 balance over millennial timescales across spatially extensive regions (e.g., Nereson et al., 2000; Siegert, 2003;
747 Siegert and Payne, 2004; Eisen et al., 2005; Waddington et al., 2007; Neumann et al., 2008; MacGregor et al.,
748 2009; Leysinger Vieli et al., 2011; Karlsson et al., 2014; Koutnik et al., 2016; Cavitte et al., 2018; Bodart et al.,
749 2023). Such records have fundamentally informed us about how mass balance has changed with time over
750 past millenia, for example showing that accumulation rates changed significantly over central (Siegert and
751 Payne, 2004; Neumann et al., 2008; Koutnik et al., 2016; Bodart et al., 2023) and coastal (Karlsson et al., 2014)
752 West Antarctica throughout the Holocene. Typically, vertical strain rates must be corrected for the whole ice
753 column, particularly in regions of (present or past) fast flow, or there is a need to account for basal processes
754 such as enhanced basal melting (e.g., Leysinger Vieli et al., 2011; Chung et al., 2023), because in such cases
755 the isochrone depths will be dynamically modified and therefore will not represent the surface mass balance
756 at the time of deposition (e.g., Koutnik et al., 2016). Where the radiostratigraphy has not been impacted
757 significantly by strain, the shallow-layer approximation can be applied, which allows us to ignore these strain-
758 rate corrections (Waddington et al., 2007). If horizontal advection influences the stratigraphy 2D, 2.5D or 3-
759 D modelling is required (see Sect. 5.6).

760 Regions of unconformable radiostratigraphy occurring throughout the ice column in parts of Antarctica have
761 partly limited the extent to which some surface mass balance records could be more widely extrapolated
762 (Arcone et al., 2012b; Cavitte et al., 2016). RES surveys of the upper ~100 m of the ice column in the affected
763 regions typically reveal widespread conformal, annual horizons modified by local variations in accumulation
764 or ice flow (Eisen et al., 2008), and the majority of them have been ascribed to wind scouring out surface
765 deposits and forming “megadunes” (Das et al., 2013; Traversa et al., 2023) that then become progressively
766 buried as sets of unconformable IRHs. Studies have identified such unconformities in several locations in East
767 Antarctica (Welch and Jacobel, 2005; Traversa et al., 2023) and West Antarctica (Woodward and King, 2009;
768 Holschuh et al., 2018).



769 **5.3 Basal melting and geothermal heat flux**

770 Isochrones have been used to calculate melting at the base of the ice exploiting the principle that melting
771 from the presence of a subglacial water body or enhanced geothermal heat flux draws isochrones down
772 towards the ice base. Mismatches between surface-accumulation-driven modelled isochrones and traced
773 isochrones have been used to infer regions of enhanced basal melting in Greenland (Dahl-Jensen et al., 1997;
774 Fahnestock et al., 2001b) and Antarctica (Carter et al., 2009) on the principle that removal of ice at the base
775 by basal melting thins annual layers above. However, for locating areas of enhanced geothermal heat flux (or
776 subglacial lakes, which may sometimes owe their existence to enhanced geothermal heat flux) researchers
777 now typically rely more on analysing the reflectivity or specularity of the ice-bed echo in RES data (e.g., Young
778 et al., 2016; Chu et al., 2021), and only use isochrones to guide derivations of basal melting where such more
779 direct data are lacking.

780 Isochrones have been analysed in more detail over parts of Antarctica to constrain basal melting in more
781 localised settings. For example, Siegert et al. (2000) used deviations in the dip of deep isochrones away from
782 parallelism with the ice-bed/subglacial-lake surface over Subglacial Lake Vostok to calculate basal melting
783 and water exchange between the lake and the overlying ice sheet (Fig. 8d). Jordan et al. (2018) identified
784 isochrones dipping towards the bed ~200 km from the South Pole (Fig. 8e), and used these to model how
785 much basal melt would be required to draw the isochrones down towards the bed. By assuming that minimal
786 frictional melting would be generated by the slow ice flow in this region, they showed that the most likely
787 cause of the isochrones being drawn down towards the bed must be enhanced geothermal heat flux in this
788 region. Ross and Siegert (2020) undertook a detailed survey of isochrone geometry over Subglacial Lake
789 Ellsworth, West Antarctica, and showed that the isochrones were preferentially drawn down over the NW
790 shoreline of the lake, rather than the lake itself. This conclusion was in agreement with the pattern of basal
791 mass balance derived from previous numerical modelling of water circulation in the lake and indicated very
792 high basal melting of ~16 cm a⁻¹ on its northern shoreline.

793 **5.4 Ice-flow dynamics**

794 Present-day (last ~35 years) information on ice-flow dynamics is derived from satellite monitoring of ice-
795 surface flow (Rignot et al., 2017), but to understand fully where and how ice-flow dynamics have changed
796 over the past several thousand years, and hence may be likely to do so again, researchers have interrogated
797 how changes to ice-flow dynamics have been imprinted into the RES-imaged internal architecture. The most
798 common methodology has been to explore and classify where the radiostratigraphy diverges from relatively
799 flat isochrones to profiles that show folding (a.k.a. buckling, warping or disruption) of the isochrones (Fig. 8f).
800 Wherever there is folding of isochrones, and we assume they were originally deposited as flat layers, it is an
801 indication that the ice has experienced considerable strain, often as a result of flowing around or over
802 significant bedrock obstacles (Robin and Millar, 1982; Hindmarsh et al., 2006; Tang et al., 2022) or becoming



803 variously stretched and compressed as it flows through an ice-stream onset region or through ice-stream
804 shear margins (Jacobel et al., 1993; Bell et al., 1998; Ng and Conway, 2004; King, 2011). Overall, isochrone
805 folding can indicate convergent ice flow, anisotropic rheology, basal freeze-on, basal sliding, non-negligible
806 transverse velocity gradients, or the abutting of units of contrasting rheology. Importantly, the signature
807 recorded by these processes is often advected downstream, so that where it is observed does not necessarily
808 indicate where the folding took place (Weertman, 1976; Jacobel et al., 1993; Leysinger Vieli et al., 2004;
809 NEEM Community Members, 2013; Wolovick et al., 2014; Bons et al., 2016; Leysinger Vieli et al., 2018; Ross
810 et al., 2020; Franke et al., 2021; Jennings and Hambrey, 2021; Jansen et al., 2024). In certain cases, relict folds
811 that do not correspond to the current ice-flow direction indicate a past change in ice-flow direction (Conway
812 et al., 2002; Siegert et al., 2004; Rippin et al., 2006; Franke et al., 2022).

813 While, therefore, there are multiple origins for isochrone folding, their geographical association with fast ice
814 flow has led to their presence being used as a broad diagnostic of the long-term stability (or otherwise) of ice
815 flow around Antarctica (e.g., Rippin et al., 2003b; Siegert et al., 2003b; Bingham et al., 2007; Karlsson et al.,
816 2009; Ross et al., 2011; Bingham et al., 2015; Winter et al., 2015; Sanderson et al., 2023). In areas where
817 isochrones are strongly disrupted by (past or present) enhanced flow, extracting ILCI or isochrone-slope
818 products from the radiostratigraphy (as introduced in Sect. 4.3) has helped to complement reconstructions
819 of past or present ice-flow dynamics (e.g., Karlsson et al., 2012; Bingham et al., 2015; Holschuh et al., 2017;
820 Ashmore et al., 2020; Luo et al., 2020; Sanderson et al., 2023). In some cases, sequences of folded isochrones
821 have been observed beneath sequences of conformable isochrones, indicative of a past sudden change from
822 fast to slow ice flow (e.g., Conway et al., 2002; Siegert et al., 2013; Kingslake et al., 2016). To obtain more
823 complex information on past ice-dynamic changes falls into the realm of applying numerical modelling, which
824 is taken up in Sect. 5.6.

825 An important outcome of most ice flow is that the ice crystals themselves develop a preferred orientation,
826 typically termed anisotropic crystal-orientation fabric, which may then influence the direction-dependent
827 propagation speed of radio waves through ice (Gow and Williamson, 1976; Robin and Millar, 1982; Fujita et
828 al., 1999; Matsuoka et al., 2003; Eisen et al., 2007; Drews et al., 2012; Jordan et al., 2020; Jordan et al., 2022).
829 Studies have reconstructed and constrained the mechanical anisotropy of ice and histories of ice deformation
830 by calculating the travel-time difference for IRHs across intersecting RES profiles where the radio waves have
831 been polarised in different directions (e.g., Fig. 8g; Ershadi et al., 2022; Jordan et al., 2022; Gerber et al., 2023;
832 Zeising et al., 2023). A special case of isochrone folding due to changes in ice-crystal fabric occurs at ice
833 divides, where upward-pointing folds termed Raymond Arches (Fig. 8h) form due to the interplay of the
834 strain-rate dependence of ice viscosity, which leads to stiffer ice beneath the divide, slowing isochrone
835 thinning down relative to the flanks (Raymond, 1983; Vaughan et al., 1999; Martín et al., 2009; Hindmarsh et
836 al., 2011; Matsuoka et al., 2015). The special geometry of these isochrone arches has been used to infer local
837 ice-flow history including the onset of divide flow (Conway et al., 1999; Kingslake et al., 2016), divide



838 migration (Nereson et al., 1998; Martín et al., 2009; Schannwell et al., 2019) and ice-thickness changes (Drews
839 et al., 2015). With stable ice-divide positions over extended periods of time, these arches can evolve further
840 into double-peaked Raymond Arches, as observed (Drews et al., 2013) and simulated by incorporating
841 anisotropy into the ice-flow models (Pettit et al., 2007; Martín and Gudmundsson, 2012; Martín et al., 2014).
842 In terms of efforts to trace isochrones widely across the Antarctic ice sheets, Raymond Arches have the
843 greatest relevance in how they affect site selection for deep ice cores that are ideally used to assign ages to
844 Antarctic-wide isochrones (as introduced in Sect. 4.4). The relative thinness of isochrones at the apex of
845 Raymond Arches implies that better resolution age-depth records reaching further back in time would be
846 obtained around the flanks, rather than on the apexes, of ice divides where arches are present.

847 **5.5 Applications of internal architecture complementary to radiostratigraphy**

848 The basal ice of Antarctica and Greenland is typically characterised by an echo-free or low-backscatter zone
849 lacking coherent layered reflections, termed an *echo-free zone* (EFZ) in early observations (Drewry and
850 Meldrum, 1978; Robin and Millar, 1982; Fujita et al., 1999). With modern RES systems, this zone now appears
851 as a basal unit in which IRHs are often warped, folded and winnowed out, and consequently lack coherent
852 reflections (Drews et al., 2009), but even without traceable radiostratigraphy this architecture contains useful
853 information about ice properties and origins. With the progressive enhancement of RES-system range
854 resolution, a variety of reflection sub-units distinctly standing out from the otherwise low-backscatter zone
855 have been identified (e.g., Fig 8i; Bell et al., 2011; Bell et al., 2014; Wrona et al., 2018; Ross et al., 2020; Lilien
856 et al., 2021; Franke et al., 2024). Some of these features manifest as zones with nearly continuous high
857 backscatter spanning several hundred metres in thickness. Some features drape over mountainous subglacial
858 regions (e.g., in Antarctica's Gamburtsev Mountains and Jutulstraumen drainage basin; Bell et al., 2011;
859 Wrona et al., 2018; Franke et al., 2024), while others build plume-like structures within the cores of englacial
860 folds (e.g., in northern Greenland and Antarctica's Institute Ice Stream; Bell et al., 2014; Ross et al., 2020).
861 These basal units are likely of different origins and exhibit different dielectric properties compared to their
862 low-backscatter surroundings, offering insights into potential formation mechanisms. Current hypotheses
863 include strong deformation on the micro-scale by ice dynamics (Drews et al., 2009), freeze-on of subglacial
864 water at the ice base (Bell et al., 2011; Creyts et al., 2014; Leysinger Vieli et al., 2018), and the incorporation
865 of point reflectors (e.g., basal sediment; Winter et al., 2019b; Franke et al., 2024), as well as ice flowing over
866 regions with changes in basal friction (Wolovick et al., 2014; Wolovick and Creyts, 2016) or convergent flow
867 (Bons et al., 2016; Ross et al., 2020). The presence of these basal units can influence the rheological
868 properties and fabric structure of the ice column, as well as impact the continuity of climatic records,
869 highlighting their significance for ice-core drilling projects and ice-flow-modelling endeavours (Bell et al.,
870 2014; MacGregor et al., 2015a; Panton and Karlsson, 2015).



871 Buried surface crevasses imaged in RES data have been used as key evidence for timing the shutdown of
872 Kamb Ice Stream (Retzlaff et al., 1993; Jacobel et al., 2000; Smith et al., 2002; Catania et al., 2006) and the
873 reorganisation of flow through Whillans Ice Stream (Conway et al., 2002). The locations and geometry of
874 basal crevasses formed near the grounding line (Fig. 8j) have also been used to identify previously floating
875 ice, and time the formation of ice rises and ice-flow reorganisation during the Holocene in Antarctica's
876 Weddell Sea Sector (Kingslake et al., 2018; Wearing and Kingslake, 2019).

877 Finally, some particularly bright isochrones have been used to constrain the timing of past volcanic eruptions
878 and constrain the ranges of their tephra fallout. Most such reflectors are relatively bright through chemical
879 signatures alone (e.g., Welch and Jacobel, 2003), but a particularly prominent isochrone, ~30 dB stronger
880 than other typical isochrone-reflection strengths, and thus interpreted as containing physical tephra
881 fragments in addition to chemical residues, was mapped and interpreted by Corr and Vaughan (2008) to
882 demonstrate a volcanic eruption occurred ~2000 years ago in West Antarctica and covered much of the Pine
883 Island Glacier basin (Fig 8k).

884 **5.6 Using isochrones in ice-sheet models**

885 Ice-flow models of different complexities comprise the foremost tools for projecting future ice-sheet and
886 glacier evolution (e.g., Gagliardini et al., 2013; Cornford et al., 2015; DeConto and Pollard, 2016; Seroussi et
887 al., 2020). Incorporating radiostratigraphic data into ice-sheet models provides a means for validation,
888 improves their calibration and might be essential for making more robust projections by models seeking to
889 constrain ice-sheet evolution over the past few centuries to the late Quaternary (Hindmarsh et al., 2009;
890 Leysinger Vieli et al., 2011; Holschuh et al., 2017; Born and Robinson, 2021; Sutter et al., 2021). Palaeo-proxy
891 records such as exposure-age dating (Brook and Kurz, 1993; Mackintosh et al., 2014; Hillebrand et al., 2021),
892 grounding-line reconstructions (Bentley et al., 2014; Wearing and Kingslake, 2019) or estimates of past sea-
893 level highstands (Dutton et al., 2015) provide invaluable snapshots of ice-sheet variability on local, regional
894 and continental scales (Lecavalier et al., 2023, present a state-of-the-art database), but their interpretation
895 remains challenging in terms of attribution of ice volume, and changes to the grounding zone and ice
896 elevation. Dated radiostratigraphy, on the other hand, contains detailed information on the evolution of ice
897 flow on the relevant timescales (as compiled for today in Sect. 4.5) and thus provides a much-refined
898 calibration target bridging gaps in between snapshot proxy data. Although the theoretical link between ice
899 flow and isochrone geometry has been established for steady tube flow of an ice sheet (Parrenin and
900 Hindmarsh, 2007), the general 3D and transient case remains far more challenging. In this section, we
901 overview recent developments in ice-sheet modelling that incorporate or exploit isochronal data from RES
902 surveys.

903 **5.6.1 Modelling past climate and ice-dynamic changes**



904 Radiostratigraphy is an ideal tuning target for ice-sheet models on continental, regional (catchment) and local
905 scales, because it inherently records the history of the ice flow as well as its response to changing climate
906 conditions in its geometry. As opposed to traditionally-employed tuning targets such as surface flow, ice-
907 sheet geometry or ice volume, which only represent snapshots of ice-sheet evolution, radiostratigraphy
908 provides a 3-D structure which has been formed by the transient palaeo-evolution of the ice sheet. Modelling
909 isochronal geometry and age is technically relatively straightforward, with the main challenge being
910 pervasive uncertainties in boundary conditions (e.g. climate forcing and geothermal heat flux) and the
911 intrinsic uncertainties of ice-sheet models due to their parameterisations of physical processes (Sutter et al.,
912 2021). Isochrones in RES data, age-depth profiles in ice cores and the isotopic content of ice sheets have
913 been modelled either by employing Lagrangian (Sutter et al., 2021) or semi-Lagrangian (Tarasov and Peltier,
914 2003; Clarke et al., 2005; Goelles et al., 2014) advection or isochronal models (Born, 2017; Rieckh et al., 2024).
915 Models that simulate stratigraphy can thus be used to explore the effects of palaeoclimate evolution on ice-
916 dynamic changes, such as marine ice-sheet instabilities or the evolution of ice-sheet drainage systems.

917 Continental-scale ice-sheet models employing approximations of the full-Stokes equations have allowed the
918 computation of ice flow on time scales of centuries to millions of years, albeit at the cost of resolution, which
919 is usually ~5–40 km (Pollard and DeConto, 2009; Gollledge et al., 2015; Sutter et al., 2019; Albrecht et al.,
920 2020; Seroussi et al., 2020). While these relatively coarse grid sizes (compared to applications of full-Stokes
921 models; e.g. Zhao et al., 2018) preclude a meaningful interpretation of small-scale processes that influence
922 radiostratigraphy (e.g. local freezing, melting, bedrock features etc.), large-scale models have the advantage
923 that they incorporate the whole thermomechanically-coupled ice-sheet system and its response to changing
924 climate conditions. Consequently, large-scale models are also the main tools for projections of sea-level
925 contributions from the Antarctic and Greenland ice sheets (e.g., Goelzer et al., 2020; Seroussi et al., 2020).

926 The analysis of isochrones to inform on past ice flow need not be limited to the grounded parts of an ice
927 sheet and has been extended to ice shelves (Višnjević et al., 2022; Moss et al., 2023), ice rises (Goel et al.,
928 2018; Goel et al., 2024), and the ice-rise/ice-shelf system (Henry et al., 2024). In these studies, isochrones
929 have served as valuable resources for reconstructing both the surface and/or basal mass balance of ice
930 shelves and ice rises using forward and inverse modelling along the flowline (in 2D), and for investigating
931 rheological properties of ice rise/ice shelf systems in 3D (Henry et al., 2024). Extending this approach to
932 include the past ice-shelf evolution and linking the isochronal structure to its grounded counterparts remains
933 challenging due to the lack of tie points to dated isochrones and a lack of observable isochronal structure
934 across the grounding line.

935 **5.6.2 Model integration of isochronal data**

936 A range of models has been used to calculate the age-depth relationship in ice over both large and small
937 portions of Antarctica and compare this with existing radiostratigraphies; an exercise that can offer valuable



938 insights into ice-sheet processes and how these are represented in ice-sheet models (Fig. 9). When
939 integrating isochronal data in models, multiple factors play a role in the choice of model set up, such as the
940 size of the area of interest (e.g. regional or continental) and the type of flow regime present (e.g. dome,
941 vertical shearing, extension). Various types of flow regime are found in Antarctica, ranging from vertical
942 compression at domes moving to vertical shear and finally to longitudinal extension in ice streams and ice
943 shelves. Consequently 1D, 2D or 3D models might be the optimal choice to simulate the age or stratigraphy
944 of ice, with 2.5D models, i.e. 2D models that take into account some aspects of a third dimension, providing
945 another option (Chung et al., 2024).

946 1D models typically assume negligible horizontal flow, making simplifying assumptions such as a steady-state
947 velocity field and the local layer approximation (Waddington et al., 2007, provide guidelines on its
948 applicability) and have predominantly been used at domes such as Dome C (Parrenin et al., 2017; Lilien et al.,
949 2021; Chung et al., 2023) and Dome F (Obase et al., 2023; Wang et al., 2023), where vertical compression
950 dominates. Dated isochrones have been used in multiple studies to constrain 1D age-depth models of
951 different complexity to determine millennial-scale accumulation rates in Antarctica (e.g., Leysinger Vieli et
952 al., 2004; Siegert and Payne, 2004; MacGregor et al., 2009; Karlsson et al., 2014; Koutnik et al., 2016; Cavitte
953 et al., 2018; Zhao et al., 2018; Ashmore et al., 2020; Bodart et al., 2023; Sanderson et al., 2024) and retrieve
954 horizontal flow velocity from 2D isochrone architecture (Eisen, 2008). While most such studies have been
955 restricted to using steady-state due to temporal limitations in available data, some models have allowed for
956 temporal changes in boundary conditions (Callens et al., 2016; Parrenin et al., 2017; Chung et al., 2023).

957 3D modelling of ice-rise stratigraphy (Henry et al., 2024) has provided a step towards constraining long-term
958 simulations in coastal areas. The influence of model physics on this stratigraphy was first investigated in 2D
959 idealised studies of Raymond arches (Pettit and Waddington, 2003; Pettit et al., 2007; Martín and
960 Gudmundsson, 2012), with Hindmarsh et al. (2011) extending this work in 3D idealised simulations.
961 Modelling studies have examined the influence of Glen's flow law exponent on Raymond-arch amplitude
962 (Pettit and Waddington, 2003; Martín et al., 2006; Martín and Gudmundsson, 2012). This methodology has
963 been extended to 2D simulations of real-world ice rises and domes in coastal Antarctica with the comparison
964 of modelled and observed Raymond arches at ice divides (Martín et al., 2009; Hindmarsh et al., 2011; Pettit
965 et al., 2011; Martín et al., 2014; Drews et al., 2015; Goel et al., 2018; Goel et al., 2024).

966 Isochrones have also been used to estimate ice temperature on catchment- to continent-wide scales.
967 Because the electrical conductivity of ice varies exponentially with temperature, resulting in higher dielectric
968 attenuation in warmer ice (MacGregor et al., 2007), temperature variability across the ice sheets leaves a
969 signature in the returned power of measured radio waves. To date, studies have concentrated on using
970 thermomechanical ice-sheet models to improve interpretation of RES data by using modelled temperature
971 fields to remove attenuation effects and strengthen interpretations of bed properties based on basal

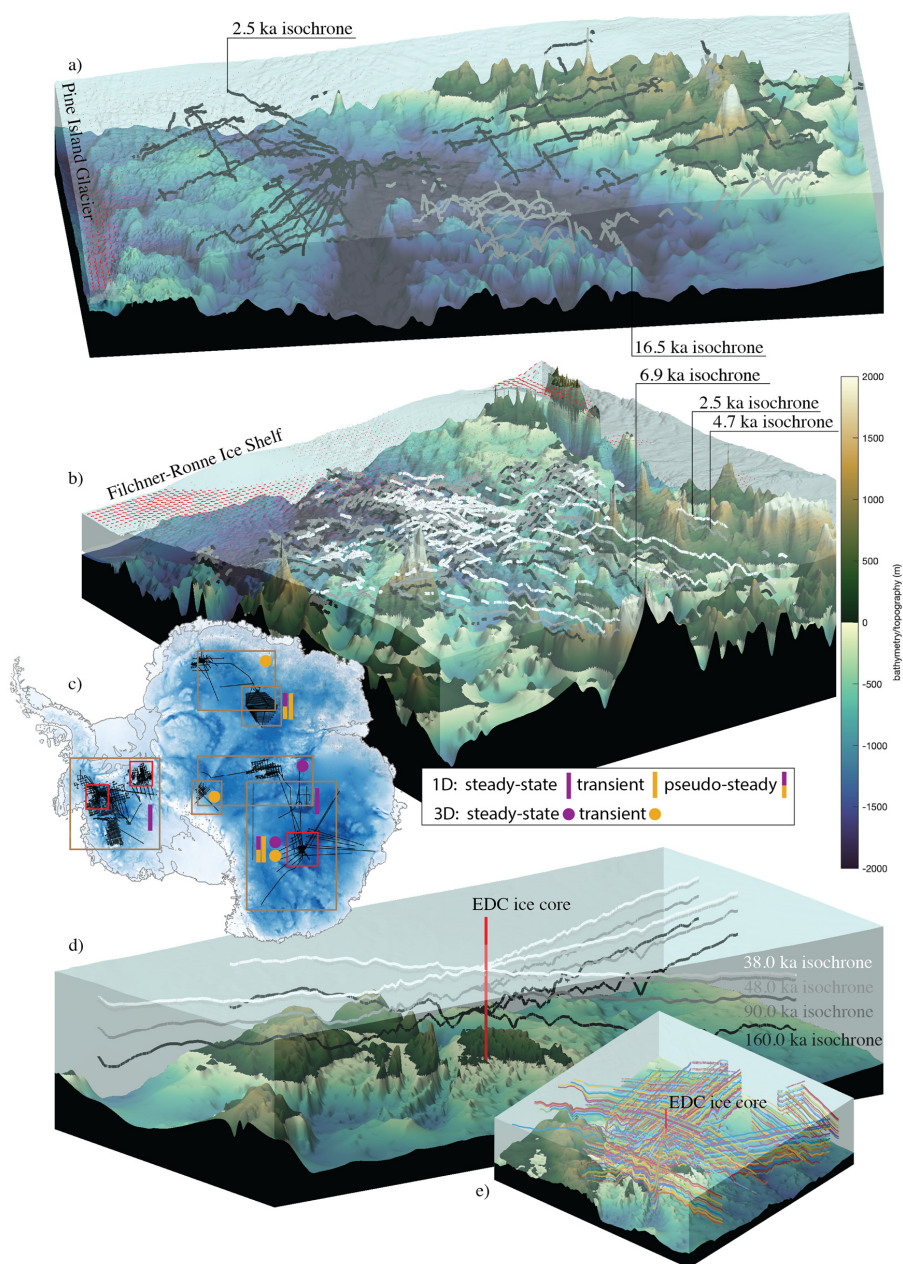


Figure 9. 3D visualisation of selected traced and dated isochrones in East And West Antarctica, and locations where different modelling applications have been conducted. (a) 2.5 ka (black lines) and 16.5 ka (grey lines) isochrones across the Pine Island/Thwaites Glacier catchment area (Bodart et al., 2021). (b) 2.5, 4.7 and 6.9 ka isochrones spanning Institute Ice Stream (Ashmore et al., 2020). (c) Map of Antarctic traced and dated isochrone transects (black lines) and areas where at least one modelling study is available (grey boxes); red boxes denote areas of the 3D visualisations. (d) Traced and dated (38, 48, 90, 160 ka) isochronal structure around Dome C from Winter et al. (2019a) and (e) Cavitte et al. (2021).



973 reflectivity (Matsuoka et al., 2012; MacGregor et al., 2015b; Chu et al., 2021; Dawson et al., 2022). This
974 approach assumes that thermomechanical models can estimate the ice temperature field to high confidence.
975 Additionally, 1D age-depth models that incorporate a thermomechanical component (Parrenin et al., 2017;
976 Passalacqua et al., 2017; Obase et al., 2023) have been used to infer basal melt rates in Antarctica close to
977 domes. Temperature modelling, however, can be challenging in fast-flowing areas where heat production by
978 viscous dissipation is substantial, such as along shear margins or ice streams. As efforts to reduce ambiguity
979 in the direct inference of temperature from RES reflection strength develop, it will become possible to
980 assimilate RES measurements of temperature to improve model performance, as has been done with other
981 direct and indirect observations of subsurface temperature (Pattyn, 2010; Van Liefferinge and Pattyn, 2013).
982 While a combined evaluation of model temperature and velocity data from RES data has been performed
983 qualitatively (Holschuh et al., 2019), there is a growing desire to incorporate *both* radiometric and structural
984 information in a formal modelling framework.

985 **6 Future directions**

986 In this review, we have considered how the internal architecture of the Antarctic ice sheets, and in particular
987 their radiostratigraphy, is increasingly being exploited to elucidate ice and climate history. The ultimate aim
988 of these endeavours is to constrain in ever finer detail the rates, locations and underlying processes of past
989 ice-sheet changes in response to climate forcing. This is crucial to inform and reduce uncertainties in models
990 projecting future ice-sheet changes and concomitant global sea-level rise. Yet, despite the progress reported
991 above, Antarctica's internal architecture remains an underutilised resource for this purpose. In this final
992 section, we set out recommendations for future research activities to be underpinned by an expanded and
993 accessible database of Antarctica's internal architecture. Firstly (Sect. 6.1), we present a pathway towards
994 expanding the volume of radiostratigraphy across Antarctica towards the goal of building a 3-D age-depth
995 model of the ice; secondly (Sect. 6.2), we set out a number of future science challenges that a comprehensive
996 database of Antarctica's englacial architecture can help to address; and finally (Sect. 6.3), we make some
997 recommendations for community actions to facilitate the delivery of these goals.

998 **6.1 Pathway to expanding Antarctic radiostratigraphy**

999 We have identified throughout this review a clear need to expand significantly the traced radiostratigraphy
1000 across the Antarctic ice sheets, covering both more area and a greater depth range through the ice. To
1001 achieve this requires the following steps:

1002 ***6.1.1 Numerical modelling to guide where radiostratigraphic constraints are most needed***

1003 We recommend that future targets for tracing radiostratigraphy across different regions of Antarctica, from
1004 existing RES data or guiding new RES surveys, are informed directly by the needs of the ice-sheet modelling



1005 community to benchmark and constrain their models. Modelling can guide location-based suggestions (e.g.
1006 to recover more radiostratigraphy away from ice divides and into more dynamic regions where simple model
1007 heuristics may misrepresent englacial conditions), or require targeting of particular time periods (e.g.
1008 targeting older isochrones that could advance understanding of glacial-interglacial transitions, amongst
1009 others).

1010 **6.1.2 Systematic assessment of the potential of existing data for tracing radiostratigraphy**

1011 For this review, we have compiled the spatial coverage of existing published RES data across Antarctica that
1012 have high-quality (GNSS) navigation and were acquired digitally, and often coherently (Figure 3I). In principle,
1013 this demonstrates the present coverage of RES data from which radiostratigraphy could be extracted and
1014 mapped, and indicates that RES datasets range and interconnect widely across both the East and West
1015 Antarctic ice sheets. While this presents a positive message of the potential for pan-Antarctic tracing of
1016 radiostratigraphy, whether and how much radiostratigraphy *can* be extracted so widely across the ice sheets
1017 from all of these profiles remains unknown. Not all of the RES tracks necessarily contain traceable
1018 radiostratigraphy, for reasons that range from inherent RES-system limitations upon data acquisition,
1019 decisions made in the processing of the data that are available (see Sect. 4), to the presence of physical
1020 phenomena in the ice that disrupt radiostratigraphy or steeply sloping basal topography that makes
1021 isochrones too steep to be traced (Sect. 5).

1022 A community effort is therefore required to investigate the full potential for mapping radiostratigraphy
1023 through these existing datasets. A useful first step, which was beyond the scope of this paper, would be to
1024 apply the ILCI to all of the modern datasets presented in Figure 3I to assess their viability for tracing
1025 isochrones across different regions, i.e., to produce a more comprehensive version of Figure 6 expanded to
1026 all the datasets discussed in Sect. 3.

1027 **6.1.3 Reprocessing of existing datasets to accentuate internal architecture**

1028 While the visibility of internal architecture is partly determined by the initial acquisition parameters and
1029 varies across Antarctica (Sect. 3), the information visible in RES data is also influenced significantly by the
1030 processing applied to the data *after* they have been acquired (Sect. 4.1). Where the raw data exist, the data
1031 can be reprocessed, which may significantly enhance the value of some existing datasets for tracing their
1032 radiostratigraphy. For much of Antarctica's RES data, the only processing that has been applied was
1033 implemented to emphasise and pick the bed echo. In some cases, the same processing accentuated
1034 radiostratigraphy in parallel but, in others, it has suppressed the imaging of isochrones or induced artefacts
1035 in the radargrams that have hampered or precluded any tracing of radiostratigraphy. Therefore, where
1036 existing data lack distinct isochrones in locations identified by numerical modelling as optimal candidates for
1037 radiostratigraphy, we recommend, where feasible, firstly reprocessing the raw data to enhance internal



1038 architecture. Such an initiative is currently being trialled as part of the Open Polar Radar project using AWI,
1039 BAS and USA-acquired RES data across Antarctica (Paden et al., 2021).

1040 **6.1.4 New data acquisition**

1041 Importantly, new RES data for radiostratigraphic constraints need only be acquired where the processes
1042 described above have highlighted that existing data cannot provide the radiostratigraphic constraints
1043 required by modelling applications. Such areas will fall into three categories:

1044 (a) Regions that are still unsurveyed or undersurveyed. Clear examples of this situation, from Figure 3I,
1045 comprise data gaps > 100 km wide in East Antarctica in Enderby Land; between South Pole and Vostok;
1046 and between Wilkes and Kemp lands; and we also note that the Filchner-Ronne Ice Shelf does not have
1047 dense survey cover.

1048 (b) Regions where RES surveys have occurred but where the existing data – even after reprocessing – do not
1049 contain any internal architecture. These regions typically comprise those last surveyed by RES several
1050 decades ago with less sophisticated RES systems. From Figure 3, we identify the Siple Coast region of West
1051 Antarctica as one such data gap. Although this region was intensively studied and surveyed during the
1052 1980s and 1990s, its last major RES surveys predate widespread use of coherent RES systems.

1053 (c) Regions where RES surveys have occurred but where the existing data – even after reprocessing – contain
1054 some internal architecture, but which does not meet modelling needs. Likely scenarios here are that age-
1055 depth information is needed at finer resolution than is retrievable in the existing data, or there is a
1056 requirement to recover radiostratigraphy deeper into the ice than has been imaged by the existing survey.
1057 This situation is common amongst existing datasets that were acquired for projects focussed on other
1058 scientific priorities. For example, where some airborne RES datasets have been acquired in combination
1059 with potential-field data (gravity and magnetics), the requirement to fly the aircraft at a stable elevation
1060 has sometimes led to poor-quality radiostratigraphy where the range from aircraft to ice surface was too
1061 large.

1062 These cases should fundamentally guide the locations, nature and platforms of any new RES data acquisition
1063 for internal architecture. As reviewed in Sect. 3, modern airborne RES systems and processing algorithms are
1064 adept at detecting multiple isochrones over large regions. In some cases, such as through regions of complex
1065 topography, complex flow dynamics or a requirement for very fine resolution of isochrones over regional
1066 scales, ground-based RES systems that can typically sound more IRHs and deeper into the underlying ice may
1067 still represent the optimal tool and justify the resources required to emplace deep-field parties. However,
1068 uncrewed aerial vehicles capable of carrying RES systems (Arnold et al., 2020; Teisberg et al., 2022), when
1069 routinely operationalised, may offer a cheaper and safer solution over remote and challenging terrains.



1070 **6.1.5 Advances in deep learning to expedite the extraction of internal architecture from RES data**

1071 As reviewed in Sect. 4, all of the present radiostratigraphy mapped across Antarctica (Fig. 7) has been
1072 generated in the absence of a fully automated isochrone-picking algorithm. Although substantial progress
1073 has been made, the need for frequent manual intervention has slowed the generation of pan-Antarctic
1074 radiostratigraphy. The greatest promise for a step-change in our ability to trace radiostratigraphy significantly
1075 faster lies in the application of deep-learning methods to the challenge. As we discussed in Sect. 4.2, deep
1076 learning has so far only been implemented to tracing shallow isochrones in the first few hundred metres of
1077 ice, which are typically more continuous over many 100s of km. Tracing isochrones deeper in the ice column
1078 is challenged by IRH fading, unconformities, and/or merging and splitting of isochrones as ice flows over or
1079 around large bedrock obstacles. However, the significant volume of traced radiostratigraphic data now
1080 assembled to date across Antarctica (Fig. 7) can now contribute training data to facilitate the advance and
1081 wider application of deep learning to tracing Antarctica's deeper isochrones.

1082 **6.2 Recommendations for future scientific deliverables using internal architecture**

1083 **6.2.1 Identification of optimal areas for retrieving new palaeoclimate records**

1084 As outlined in Sect. 5.1, Antarctica's deep ice cores have provided invaluable palaeoclimate records from
1085 both West and East Antarctica and yet there remain two outstanding directives in the quest for augmenting
1086 these existing datasets. One, presently the primary focus of the SCAR IPICS *Oldest Ice* programme, is to
1087 identify where a potential climate record extending further back in time than Antarctica's current record
1088 (back to ~800,000 k.a. from Dome C; Bouchet et al., 2023) can be sampled. This would address the substantial
1089 unknown of whether Antarctica's ice holds a direct continuous record of the mid-Pleistocene transition
1090 switch from 41-kyr to 100-kyr glacial-interglacial cycles that is inferred to have occurred between ~1.25-0.8
1091 M k.a. from marine-sediment oxygen-isotope records (Hays et al., 1976; Clark et al., 2006; Legrain et al.,
1092 2023). A second requirement is to locate sites in the Antarctic ice sheets that preserve higher-resolution
1093 palaeoclimate records of epochs than are currently represented in the already-sampled sites. In particular,
1094 regions with relatively high present or past accumulation rates can potentially preserve high-resolution
1095 climate records of the last millenia. We contend that the development of a pan-continental radiostratigraphy
1096 could form a crucial tool for identifying most future ice-core locations around Antarctica.

1097 We further recommend that attention is placed on tracing radiostratigraphy around Antarctica's blue-ice
1098 zones which, as discussed in Sect. 5.1, have and can represent sites for retrieving ice older than 800 k.a.
1099 Targeted studies on their radiostratigraphy could improve understanding of how ice deforms to produce the
1100 sampled structures, and hence better contextualise how the ice outcropping in such regions is related to ice
1101 buried at depth in interior Antarctica.



1102 These initiatives may be complemented by the strategic deployment of rapid-access drilling techniques that
1103 could be deployed, alongside intersections with ice cores (discussed in Sect. 5.1), to date and validate the
1104 radiostratigraphy. Rapid-access drilling (e.g., Goodge and Severinghaus, 2016; Rix et al., 2019; Goodge et al.,
1105 2021; Schwander et al., 2023) can provide borehole access into the ice for deploying sensors to record
1106 physical characteristics that correlate with RES isochrones (IceCube Collaboration, 2013; Goodge et al., 2021;
1107 Schwander et al., 2023). Additionally, rapid-access drilling allows direct sampling of ice that can be used for
1108 radiometric-age dating that can validate the radiostratigraphy (e.g., Bender et al., 2008; Rowell et al., 2023).
1109 A dedicated programme of rapid-access ice drilling coordinated with *AntArchitecture* could therefore both
1110 help to validate radiostratigraphic age-depth models, and provide a relatively quick and cost-effective
1111 methodology for targeting potential future sites for both vertical and horizontal ice coring.

1112 **6.2.2 Reconstruction of surface mass balance – millennial timescales**

1113 In Sect. 5.2, we discussed that tracing deep (>200 m below the ice surface) isochrones across the Antarctic
1114 ice sheets enables reconstruction of changes in surface mass balance over the past several millenia. While
1115 the few existing studies have mostly focussed at or near ice divides, where horizontal flow and its associated
1116 complexities can mostly be neglected, an expanded pan-continental radiostratigraphy that more
1117 comprehensively spans and connects all of Antarctica’s central divide regions will enable these simple
1118 applications to be expanded, and can provide a spatially widespread record of how surface mass balance has
1119 varied regionally at millennial timescales. Such a record would help us to understand the pervasiveness of
1120 synoptic snow-accumulation patterns (e.g., Le Meur et al., 2018; Pauling et al., 2023), and could inform
1121 scenarios of future plausible surface-mass-balance variability to be incorporated into model projections (see
1122 Lenaerts et al., 2019, for a review). In turn, such refined surface-mass-balance reconstructions would greatly
1123 improve the climate forcings employed by palaeo-ice-sheet-modelling studies and increase confidence in
1124 their conclusions.

1125 **6.2.3 Reconstruction of surface mass balance – historical timescales**

1126 To reduce uncertainties in near-term (i.e., ~next 200 years) projections of Antarctica’s future evolution, and
1127 thereby improve global sea-level projections, there is a critical need to constrain further the regional climate
1128 models (e.g., Pratap et al., 2022) that are fundamental to forcing ice-sheet models. Important validation for
1129 these models comes from the historical record provided primarily by ice cores, but also by radiostratigraphy
1130 sounded in the upper few 100 m of the ice sheet, hereafter termed *shallow radiostratigraphy*. Neither this
1131 review, nor the *AntArchitecture* community to date, has focussed on shallow IRHs. However, the majority of
1132 RES surveys depicted in Figure 3 also detected shallow radiostratigraphy, and many additional surveys have
1133 been undertaken over the past decades across Antarctica using a range of airborne and ground-based
1134 platforms that focussed on detecting shallow isochrones, often for local, but sometimes also for more
1135 regional, scientific applications (e.g., Medley et al., 2013; Medley et al., 2014; Konrad et al., 2019; Kowalewski



1136 et al., 2021; Cavitte et al., 2022). We therefore propose that an important future deliverable should be a
1137 “shallow” of pan-Antarctic radiostratigraphy complementary to the deeper version that has primarily formed
1138 the focus of this review. In parallel with the techniques and philosophy we have discussed for dating deep
1139 isochrones across Antarctica, shallow radiostratigraphy can be dated from intersections with shallow-ice-
1140 core records; and the product could be progressively refined by using it to identify where future shallow-ice
1141 cores should be drilled to provide finer dating control. It is likely that the overall task of tracing shallow
1142 isochrones across Antarctica could benefit from the application of machine learning to isochrone tracing
1143 sooner than for deeper isochrones, as the former are typically less disrupted by ice dynamics and are more
1144 continuous. Indeed, shallow isochrones have already been traced with deep learning with some success in
1145 several studies (e.g., Dong et al., 2021; Rahnemoonfar et al., 2021; Yari et al., 2021).

1146 **6.2.4 Estimate geothermal heat flux from radiostratigraphy**

1147 The studies mentioned in Sect. 5.3 speak to the significant potential for Antarctica’s radiostratigraphy to be
1148 used as a resource for constraining variations to the continent’s geothermal heat flux, which remains
1149 enigmatic (Burton-Johnson et al., 2020). As exemplified by Fahnestock et al. (2001b) across the Greenland
1150 Ice Sheet, and more locally in Antarctica by Jordan et al. (2018), it is possible to quantify basal melt with
1151 isochrones by calculating how much melting is required to draw isochrones down towards the base. However,
1152 the relationship between isochrone geometry and basal melting is complex, multi-dimensional and partly
1153 controversial (Leysinger Vieli et al., 2007; Carter et al., 2009; Bons et al., 2021; Wolovick et al., 2021b;
1154 Wolovick et al., 2021a). For a continental-scale application of this technique, a more detailed pan-Antarctic
1155 radiostratigraphy is needed. The optimal data product to invert for geothermal heat flux would be the most
1156 widespread tracings of the deepest undisrupted isochrones across the ice sheets, which is challenging
1157 because deeper isochrones are harder to image and significant drawdown of isochrones where basal melting
1158 is high can prohibit widespread tracing (e.g., Ross and Siegert, 2020). Nevertheless, there is significant
1159 potential to use deep isochrone geometry as further calibration for numerical models seeking to invert
1160 geothermal heat flux (Pattyn, 2010; Van Liefferinge and Pattyn, 2013; Burton-Johnson et al., 2020).

1161 **6.2.5 Comprehensive mapping of basal-ice units and deep-isochrone geometry**

1162 In Sect. 5.5, we noted that in some regions of the Antarctic ice sheets, RES data indicate that the deeper ice
1163 has distinctive physical characteristics compared with the ice above, i.e., where this deeper ice obscures or
1164 precludes imaging of IRHs, and where distinct basal-ice units exist around which the overlying IRHs have
1165 become folded or warped. An improved understanding of the distribution of these features across Antarctica
1166 is important for several reasons. Firstly, it would identify where deep-ice palaeoclimate records would be
1167 compromised by ice deformation or basal melting, thus critically informing ice-core site identification.
1168 Secondly, it would act as an observationally-informed broad-scale indicator of which areas of the ice sheet
1169 are prone to basal melting and hence inform mapping of geothermal heat flux. Thirdly, it would provide



1170 information towards a better understanding of how the rheology of Antarctica’s ice varies, what are the
1171 causes of this variation, and how these effects impact on Antarctica’s ice dynamics. Some of these issues
1172 would be informed by some specific rapid-access drilling into basal-ice units, and a comprehensive mapping
1173 exercise of basal-unit distribution would inform which targets might be most easily accessed. In addition to
1174 mapping basal units themselves, a complementary deliverable could be to map the degree to which deep-
1175 ice radiostratigraphy follows or diverges from the ice-bed interface across Antarctica. This exercise would
1176 inform modelling aimed to deconvolve how much isochrone geometry is affected by basal topography versus
1177 ice dynamics versus basal melt. This, in turn, will better inform projections of the ice sheets’ future with
1178 radiostratigraphic constraints.

1179 **6.2.6 Advance knowledge of volcanic activity and fallout across Antarctica**

1180 Given that most isochrones traced across the Antarctic ice sheets manifest changes to acidity, and that some
1181 of the brightest have been linked to precipitated fallout from volcanic eruptions within and beyond Antarctica,
1182 there is significant potential to use isochrones across Antarctica more comprehensively to trace the spatial
1183 distribution of volcanic fallout from the numerous past eruptions that have been identified by chemical
1184 analyses of Antarctica’s ice cores (Narcisi and Petit, 2021). Despite many tephra and cryptotephra
1185 (microscopic layers of volcanic ash) having been detected in Antarctica’s ice cores, few have explicitly been
1186 traced widely beyond the ice cores using radiostratigraphy, and most isochrones that have been linked to
1187 past volcanic events have been used as time markers for other purposes, e.g. calculating past accumulation,
1188 rather than having been traced to focus on the origins and properties of the volcanic events themselves (e.g.,
1189 Jacobel and Welch, 2005; Bodart et al., 2023). There is therefore significant potential, already with existing
1190 data, to use Antarctica’s radiostratigraphy to trace the geographical distribution of volcanic fallout from
1191 numerous eruptions that have been detected in ice-core records, and this information may be used to help
1192 trace further the origins and nature of past eruptions beyond that which can be gleaned solely from the ice-
1193 core chemistry. This objective would complement the ongoing activities and recent recommendations for
1194 future research on volcanism presented by the SCAR AntVolc group (Geyer et al., 2023).

1195 **6.2.7 Development of a new model benchmark for the Antarctic ice sheets**

1196 As reviewed in Sect. 5.6, the vast majority of ice-sheet models presently employed for ice-sheet
1197 reconstruction and future projections are initialised with present-day snapshots of the ice-sheet state (e.g.,
1198 surface velocity, ice thickness). An Antarctic-wide radiostratigraphy would provide a much better
1199 initialisation and tuning target for ice-sheet models, as it inherently records both ice-flow history and the ice
1200 sheet’s response to changing external forcings (e.g., atmospheric and ocean conditions) – all within a tangible
1201 set of physical horizons that can be reproduced by existing models. The development of an Antarctic-wide
1202 radiostratigraphy is therefore a primary scientific objective for SCAR’s *AntArchitecture* community.



1203 **6.3 Community actions**

1204 The greatest challenge for attaining the deliverables described above is how to foster and maintain
1205 engagement between scientists working across numerous different disciplines and operating at institutions
1206 spread across Earth. Even within the scientific community who self-describe as RES, radar, or even
1207 radioglaciology specialists, this challenge is innate. As we have reviewed, the history and ongoing practices
1208 of Antarctic RES surveying encompass multiple agencies whose foci are typically on medium-term projects of
1209 a few years' duration. The intent of this review was to communicate to a wider audience (both within and
1210 beyond the radioglaciology community) the baseline availability and potential of the present archive of
1211 existing RES data spanning both East and West Antarctica's ice sheets, and to showcase their value for
1212 tackling major science questions concerning Antarctica's ice and climate history and future.

1213 A major challenge to greater progress in the study of Antarctica's internal architecture has been the lack of
1214 a common framework for archiving RES data and metadata between different operators and potential users.
1215 The establishment of the FAIR (Findable, Accessible, Interoperable, and Reusable; Wilkinson et al., 2016)
1216 data-exchange guidelines has provided a clear framework making possible the release of RES data in open-
1217 access repositories, facilitating open-access releases of some of the datasets discussed in Sect. 3. These
1218 releases have been accompanied by interactive data portals and FAIR-compliant data standards, including
1219 rich metadata relating to the acquisition, processing and quality of the data, and provide examples for
1220 releasing further data in the future. We recommend that the next significant community data focus should
1221 be on developing common protocols for processing RES data, formatting and sharing raw data files, and in
1222 some cases reprocessing existing data to facilitate much greater interoperability of the data moving into the
1223 future. This recommendation falls into the remit of the Open Polar Radar project currently being trialled with
1224 AWI, BAS and USA-acquired RES data (Paden et al., 2021) but, specifically with regards to publishing and
1225 sharing future radiostratigraphy datasets, there remains a need to set a common standard. We suggest a
1226 standardised structure here in Appendix 1.

1227 A core principle moving forwards with our science must also be on improving sustainability, given the
1228 significant resource and carbon impact of using aircraft and establishing deep-field camps in Antarctica.
1229 When proposing new Antarctic RES acquisition, we suggest that it first be demonstrated that it is needed,
1230 following the procedures laid out in Sect. 6.1. Although crewed airborne and ground-based RES platforms
1231 currently presently continue to provide the most reliable options, where new data are clearly needed n
1232 pathways for improving the sustainability of data collection are opening up with the development of
1233 uncrewed aerial vehicles capable of hosting RES systems (Arnold et al., 2020; Teisberg et al., 2022).

1234 Finally, we call for continued efforts to build and enhance the inclusion and diversity of researchers involved
1235 in acquiring and analysing RES datasets towards understanding better Antarctica's past and future. This paper
1236 has benefitted immeasurably from including perspectives from authors spread across the world, navigating



1237 different stages of their careers, and identifying as different genders, ethnicities, nationalities and religions;
1238 and from including the expertise of field- and data-focussed scientists in the same space as the expertise of
1239 practitioners whose focus is on applying the data and integrating them into numerical models. We conclude
1240 by reiterating our core scientific ambitions for *AntArchitecture* above: to build a pan-Antarctic database of
1241 isochrones that are accessible, sustainable over the long term, and useful for multiple scientific applications
1242 across multiple users, for example ice-sheet modellers and the substantial ice-core community. Alongside
1243 this, and of equal importance, the community that is active both in acquiring and analysing Antarctica's
1244 internal architecture must continue to diversify.

1245 **Author contributions**

1246 The paper was jointly written by RGB, JAB, MGPC, AC, RJS and JCRS (the lead-writing team). All co-authors
1247 contributed ideas, perspectives and edits. The review was conceptualised by RGB, OE, NBK, JAM, NR and DAY
1248 as a deliverable for the SCAR *AntArchitecture* 2018-2022 Action Group. RGB coordinated the writing process.
1249 DWA, RGB, JAB, AB, MGPC, WC, OE, NH, NBK, MRK, GJMCLV, JAM, EJM, EM, CM, FP, NR, JCRS, KW & DAY
1250 made significant contributions to first draft compiled during the covid-19 pandemic in 2020-21, forming the
1251 framework for the current version handled by the lead-writing team since 2023. Original figures were drawn
1252 by KW, NBK & JAB (Fig. 1), DWA (Fig. 2), RGB (Fig. 3), SF (Fig. 4), JAB (Fig. 6 & 7), MGPC & RJS (Fig. 8), and JCRS
1253 (Fig. 9), and Table 1 was assembled by JAB. Prior to submission, DWA, AB, RD, JWG, MRK, CM, FN, SVP, DMS,
1254 TOT, XC & XT provided substantive edits; SF, VG, ACJC, AH, BHH, FMO, TR & SY led detailed reviews of each
1255 section of the manuscript which shaped further edits; and OE, NBK, GJMCLV, JAM, FSLN, NR, RS, MJS & DAY
1256 contributed final checks and perspectives informing the final version of the paper.

1257 **Competing interests**

1258 Nanna Karlsson is Co-Editor-in-Chief, Olaf Eisen is Advisory Editor, and Reinhard Drews, Joseph MacGregor,
1259 Elisa Mantelli, Carlos Martín and Johannes Sutter are Editors of *The Cryosphere*.

1260 **Disclaimer**

1261 The views and opinions expressed here are those of the author(s) only and do not necessarily reflect those
1262 of the European Union or the European Research Council Executive Agency. Neither the European Union nor
1263 the granting authority can be held responsible for them.

1264 **Acknowledgements**

1265 This research is a contribution to the Scientific Committee for Antarctic Research's *AntArchitecture* Action
1266 Group, and we thank members of SCAR's Physical Sciences and Geosciences Divisions for ongoing support of



1267 the group since 2018. All of the UK-based authors acknowledge research funding support from the UK Natural
1268 Environment Research Council, including Doctoral Training Scholarships to CJN (Edinburgh E4), RJS (One
1269 Planet) and HD (SENSE). JCRS, JAB, AH, and VV acknowledge funding from the Swiss National Science
1270 Foundation (grant no. 211542). MGPC is a postdoctoral researcher of the FRS-FNRS. AC, OE, EM and FP
1271 acknowledge funding from the European Union: AC, OE and FP via the Horizon 2020 Marie Skłodowska-Curie
1272 grant agreement no. 955750 (DEEPICE), EM from European Research Council Starting Grant 101076793. JAM,
1273 DAY, TOT, SY and SS acknowledge support from the US National Aeronautical and Space Administration; TOT
1274 was supported by a NASA FINESST Grant (80NSSC23K0271) and the TomKat Center for Sustainable Energy.
1275 DAY, BHH, NH, MK, EJM, DMS, SY, MR and SS acknowledge funding from the US National Science Foundation:
1276 for DAY, NH, MK, SY and SS through the Center for Oldest Ice Exploration, an NSF Science and Technology
1277 Center (NSF 2019719); for DAY, SY and SS additionally from Earthcube (NSF 2127606); for BHH from an Office
1278 of Polar Programs Postdoctoral Research Fellowship (NSF 2317927); for EJM from Geosciences Open System
1279 Ecosystem Award NSF 2324092; for DMS from Office of Polar Programs Award NSF 1745137; and for MR
1280 from BIGDATA (IIS-1838230, 2308649) and NSF Leadership Class Computing (OAC-2139536) awards. DAY, SY
1281 and SS were also supported by the G. Unger Vetlesen Foundation. This paper is University of Texas Institute
1282 for Geophysics contribution #####. AB and TR acknowledge funding from the Norwegian Research Council
1283 Grant 314614 (Simulating Ice Cores and Englacial Tracers in the Greenland Ice Sheet). RD was supported by
1284 an Emmy Noether Grant from the Deutsche Forschungsgemeinschaft (DR 822/3-1). SF was funded by the
1285 Walter Benjamin Programme of the German Research Foundation (DFG; project number 506043073). ACJH
1286 is supported by the Wallenberg Foundation (KAW 2021.0275). FMO acknowledges support from the German
1287 Academic Scholarship Foundation. XC (Grant 42376253) and XT (Grant 42276257) were supported by
1288 National Natural Science Foundation of China. CFD was funded by the Natural Sciences and Engineering
1289 Research Council of Canada (NSERC; RGPIN-03761-2017) and the Canada Research Chairs Program (950-
1290 231237).



1291 **References**

- 1292 Albrecht, T., R. Winkelmann & A. Levermann (2020) Glacial-cycle simulations of the Antarctic Ice Sheet with
1293 the Parallel Ice Sheet Model (PISM) – Part 2: Parameter ensemble analysis. *The Cryosphere*, 14, 633-
1294 656.
- 1295 Allen, C. (2008) A brief history of radio-echo sounding of ice. *Earthzine Monthly Newsletter*.
1296 <https://earthzine.org/a-brief-history-of-radio-echo-sounding-of-ice-2/> (last accessed 21 May 2024).
- 1297 Arcone, S. A., R. Jacobel & G. Hamilton (2012a) Unconformable stratigraphy in East Antarctica: Part I. Large
1298 firm cosets, recrystallized growth, and model evidence for intensified accumulation. *Journal of*
1299 *Glaciology*, 58, 240-252.
- 1300 Arcone, S. A., R. Jacobel & G. Hamilton (2012b) Unconformable stratigraphy in East Antarctica: Part II.
1301 Englacial cosets and recrystallized layers. *Journal of Glaciology*, 58, 253-264.
- 1302 Arenas-Pingarrón, Á., H. F. J. Corr, C. Robinson, T. A. Jordan & P. V. Brennan (2023) Polarimetric Airborne
1303 Scientific Instrument, Mark 2: An ice-sounding airborne synthetic-aperture radar for subglacial
1304 3D imagery. *IET Radar, Sonar & Navigation*, 17, 1391-1404.
- 1305 Arnold, E., C. Leuschen, F. Rodriguez-Morales, J. Li, J. Paden, R. Hale, et al. (2020) CRISIS airborne radars
1306 and platforms for ice and snow sounding. *Annals of Glaciology*, 61, 58-67.
- 1307 Ashmore, D. W., R. G. Bingham, N. Ross, M. J. Siegert, T. A. Jordan & D. W. F. Mair (2020) Englacial
1308 architecture and age-depth constraints across the West Antarctic Ice Sheet. *Geophysical Research*
1309 *Letters*, 47, e2019GL086663.
- 1310 Baggenstos, D., J. P. Severinghaus, R. Mulvaney, J. R. McConnell, M. Sigl, O. J. Maselli, et al. (2018) A
1311 horizontal ice core from Taylor Glacier, its implications for Antarctic climate history, and an improved
1312 Taylor Dome Ice Core time scale. *Paleoceanography and Paleoclimatology*, 33, 778-794.
- 1313 Beem, L. H., D. A. Young, J. S. Greenbaum, D. D. Blankenship, M. G. P. Cavitte, J. Guo, et al. (2021)
1314 Aerogeophysical characterization of Titan Dome, East Antarctica, and potential as an ice-core target.
1315 *The Cryosphere*, 15, 1719-1730.
- 1316 Bell, R. E., D. D. Blankenship, C. A. Finn, D. L. Morse, T. A. Scambos, J. M. Brozena, et al. (1998) Influence
1317 of subglacial geology on the onset of a West Antarctic ice stream from aerogeophysical observations.
1318 *Nature*, 394, 58-62.
- 1319 Bell, R. E., F. Ferraccioli, T. T. Creyts, D. Braaten, H. Corr, I. Das, et al. (2011) Widespread persistent
1320 thickening of the East Antarctic Ice Sheet by freezing from the base. *Science*, 331, 1592-1595.
- 1321 Bell, R. E., K. Tinto, I. Das, M. Wolovick, W. Chu, T. T. Creyts, et al. (2014) Deformation, warming and softening
1322 of Greenland's ice by refreezing meltwater. *Nature Geoscience*, 7, 497-502.
- 1323 Bender, M. L., B. Barnett, G. Dreyfus, J. Jouzel & D. Porcelli (2008) The contemporary degassing rate of ⁴⁰Ar
1324 from the solid Earth. *Proceedings of the National Academy of Sciences*, 105, 8232-8237.
- 1325 Bentley, C. R. (1990) The Ross Ice Shelf Geophysical and Glaciological Survey (RIGGS): Introduction and
1326 summary of measurements performed. *Antarctic Research Series, AGU*, 42, 1-20.
- 1327 Bentley, M. J., C. Ó Cofaigh, J. B. Anderson, H. Conway, B. Davies, A. G. C. Graham, et al. (2014) A
1328 community-based geological reconstruction of Antarctic Ice Sheet deglaciation since the Last Glacial
1329 Maximum. *Quaternary Science Reviews*, 100, 1-9.
- 1330 Bingham, R. G., F. Ferraccioli, E. C. King, R. D. Larter, H. D. Pritchard, A. M. Smith, et al. (2012) Inland thinning
1331 of West Antarctic Ice Sheet steered along subglacial rifts. *Nature*, 487, 468-471.
- 1332 Bingham, R. G., D. M. Rippin, N. B. Karlsson, H. F. J. Corr, F. Ferraccioli, T. A. Jordan, et al. (2015) Ice-flow
1333 structure and ice-dynamic changes in the Weddell Sea sector of West Antarctica from radar-imaged
1334 internal layering. *Journal of Geophysical Research: Earth Surface*, 120, 655-670.
- 1335 Bingham, R. G. & M. J. Siegert (2007) Radio-echo sounding over polar ice masses. *Journal of Environmental*
1336 *and Engineering Geophysics*, 12, 47-62.
- 1337 Bingham, R. G., M. J. Siegert, D. A. Young & D. D. Blankenship (2007) Organized flow from the South Pole to
1338 the Filchner-Ronne Ice Shelf: An assessment of balance velocities in interior East Antarctica using
1339 radio-echo sounding data. *Journal of Geophysical Research: Earth Surface*, 112, F03S26.
- 1340 Bingham, R. G., D. G. Vaughan, E. C. King, D. Davies, S. L. Cornford, A. M. Smith, et al. (2017) Diverse
1341 landscapes beneath Pine Island Glacier influence ice flow. *Nature Communications*, 8, 1618.
- 1342 Blankenship, D. D., D. L. Morse, C. A. Finn, R. E. Bell, M. E. Peters, S. D. Kempf, et al. 2001. Geologic controls
1343 on the initiation of rapid basal motion for West Antarctic ice streams: A geophysical perspective
1344 including new airborne radar sounding and laser altimetry results. In *The West Antarctic Ice Sheet:*
1345 *Behavior and Environment*, 105-121.
- 1346 Bodart, J. A., R. G. Bingham, D. W. Ashmore, N. B. Karlsson, A. S. Hein & D. G. Vaughan (2021) Age-depth
1347 stratigraphy of Pine Island Glacier inferred from airborne radar and ice-core chronology. *Journal of*
1348 *Geophysical Research: Earth Surface*, 126, e2020JF005927.
- 1349 Bodart, J. A., R. G. Bingham, D. A. Young, J. A. MacGregor, D. W. Ashmore, E. Quartini, et al. (2023) High
1350 mid-Holocene accumulation rates over West Antarctica inferred from a pervasive ice-penetrating radar
1351 reflector. *The Cryosphere*, 17, 1497-1512.



- 1352 Bons, P. D., T. de Riese, S. Franke, M. G. Llorens, T. Sachau, N. Stoll, et al. (2021) Comment on “Exceptionally
1353 high heat flux needed to sustain the Northeast Greenland Ice Stream” by Smith-Johnsen et al. (2020).
1354 *The Cryosphere*, 15, 2251-2254.
- 1355 Bons, P. D., D. Jansen, F. Mundel, C. C. Bauer, T. Binder, O. Eisen, et al. (2016) Converging flow and
1356 anisotropy cause large-scale folding in Greenland's ice sheet. *Nature Communications*, 7, 11427.
- 1357 Born, A. (2017) Tracer transport in an isochronal ice-sheet model. *Journal of Glaciology*, 63, 22-38.
- 1358 Born, A. & A. Robinson (2021) Modeling the Greenland englacial stratigraphy. *The Cryosphere*, 15, 4539-4556.
- 1359 Bouchet, M., A. Landais, A. Grisart, F. Parrenin, F. Prié, R. Jacob, et al. (2023) The Antarctic Ice Core
1360 Chronology 2023 (AICC2023) chronological framework and associated timescale for the European
1361 Project for Ice Coring in Antarctica (EPICA) Dome C ice core. *Climate of the Past*, 19, 2257-2286.
- 1362 Brook, E. J. & C. Buizert (2018) Antarctic and global climate history viewed from ice cores. *Nature*, 558, 200-
1363 208.
- 1364 Brook, E. J. & M. D. Kurz (1993) Surface-exposure chronology using in situ cosmogenic ³He in Antarctic quartz
1365 sandstone boulders. *Quaternary Research*, 39, 1-10.
- 1366 Burton-Johnson, A., R. Dziadek & C. Martín (2020) Geothermal heat flow in Antarctica: Current and future
1367 directions. *The Cryosphere*, 14, 3843-3873.
- 1368 Callens, D., R. Drews, E. Witrant, M. Philippe & F. Pattyn (2016) Temporally stable surface mass balance
1369 asymmetry across an ice rise derived from radar internal-reflection horizons through inverse modeling.
1370 *Journal of Glaciology*, 62, 525-534.
- 1371 Carter, S. P., D. D. Blankenship, M. E. Peters, D. A. Young, J. W. Holt & D. L. Morse (2007) Radar-based
1372 subglacial-lake classification in Antarctica. *Geochemistry, Geophysics, Geosystems*, 8, Q03016.
- 1373 Carter, S. P., D. D. Blankenship, D. A. Young & J. W. Holt (2009) Using radar-sounding data to identify the
1374 distribution and sources of subglacial water: Application to Dome C, East Antarctica. *Journal of
1375 Glaciology*, 55, 1025-1040.
- 1376 Castelletti, D., D. M. Schroeder, S. Hensley, C. Grima, G. Ng, D. Young, et al. (2017) An interferometric
1377 approach to cross-track clutter detection in two-channel VHF radar sounders. *IEEE Transactions on
1378 Geoscience and Remote Sensing*, 55, 6128-6140.
- 1379 Castelletti, D., D. M. Schroeder, T. M. Jordan & D. Young (2021) Permanent scatterers in repeat-pass airborne
1380 VHF radar sounder for layer-velocity estimation. *IEEE Geoscience and Remote Sensing Letters*, 18,
1381 1766-1770.
- 1382 Castelletti, D., D. M. Schroeder, E. Mantelli & A. Hilger (2019) Layer-optimized SAR processing and slope
1383 estimation in radar-sounder data. *Journal of Glaciology*, 65, 983-988.
- 1384 Catania, G., C. Hulbe & H. Conway (2010) Grounding-line basal melt rates determined using radar-derived
1385 internal stratigraphy. *Journal of Glaciology*, 56, 545-554.
- 1386 Catania, G. A., T. A. Scambos, H. Conway & C. F. Raymond (2006) Sequential stagnation of Kamb Ice Stream,
1387 West Antarctica. *Geophysical Research Letters*, 33, L14502.
- 1388 Cavitte, M. G. P., D. D. Blankenship, D. A. Young, D. M. Schroeder, F. Parrenin, E. Le Meur, et al. (2016)
1389 Deep radiostratigraphy of the East Antarctic plateau: Connecting the Dome C and Vostok ice-core
1390 sites. *Journal of Glaciology*, 62, 323-334.
- 1391 Cavitte, M. G. P., H. Goosse, K. Matsuoka, S. Wauthy, V. Goel, R. Dey, et al. (2023) Investigating the spatial
1392 representativeness of East Antarctic ice cores: A comparison of ice core and radar-derived surface
1393 mass balance over coastal ice rises and Dome Fuji. *The Cryosphere*, 17, 4779-4795.
- 1394 Cavitte, M. G. P., H. Goosse, S. Wauthy, T. Kausch, J.-L. Tison, B. Van Liefferinge, et al. (2022) From ice core
1395 to ground-penetrating radar: Representativeness of SMB at three ice rises along the Princess Ragnhild
1396 Coast, East Antarctica. *Journal of Glaciology*, 68, 1221-1233.
- 1397 Cavitte, M. G. P., F. Parrenin, C. Ritz, D. A. Young, B. Van Liefferinge, D. D. Blankenship, et al. (2018)
1398 Accumulation patterns around Dome C, East Antarctica, in the last 73 kyr. *The Cryosphere*, 12, 1401-
1399 1414.
- 1400 Cavitte, M. G. P., D. A. Young, R. Mulvaney, C. Ritz, J. S. Greenbaum, G. Ng, et al. (2021) A detailed
1401 radiostratigraphic data set for the central East Antarctic Plateau spanning from the Holocene to the
1402 mid-Pleistocene. *Earth System Science Data*, 13, 4759-4777.
- 1403 Christianson, K., R. W. Jacobel, H. J. Horgan, S. Anandakrishnan & R. B. Alley (2012) Subglacial Lake
1404 Whillans: Ice-penetrating radar and GPS observations of a shallow active reservoir beneath a West
1405 Antarctic ice stream. *Earth and Planetary Science Letters*, 331-332, 237-245.
- 1406 Chu, W., A. M. Hilger, R. Culberg, D. M. Schroeder, T. M. Jordan, H. Seroussi, et al. (2021) Multisystem
1407 synthesis of radar sounding observations of the Amundsen Sea Sector from the 2004–2005 field
1408 season. *Journal of Geophysical Research: Earth Surface*, 126, e2021JF006296.
- 1409 Chung, A., F. Parrenin, R. Mulvaney, L. Vittuari, M. Frezzotti, A. Zanutta, et al. (2024) Age, thinning and spatial
1410 origin of the Beyond EPICA ice from a 2.5D ice flow model. *EGUsphere*, 2024, 1-21.
- 1411 Chung, A., F. Parrenin, D. Steinhage, R. Mulvaney, C. Martín, M. G. P. Cavitte, et al. (2023) Stagnant ice and
1412 age modelling in the Dome C region, Antarctica. *The Cryosphere*, 17, 3461-3483.



- 1413 Clark, P. U., D. Archer, D. Pollard, J. D. Blum, J. A. Rial, V. Brovkin, et al. (2006) The middle Pleistocene
1414 transition: Characteristics, mechanisms, and implications for long-term changes in atmospheric pCO₂.
1415 *Quaternary Science Reviews*, 25, 3150-3184.
- 1416 Clarke, G. K. C., N. Lhomme & S. J. Marshall (2005) Tracer transport in the Greenland Ice Sheet: Three-
1417 dimensional isotopic stratigraphy. *Quaternary Science Reviews*, 24, 155-171.
- 1418 Clough, J. W. (1977) Radio-echo sounding: Reflections from internal layers in ice sheets. *Journal of Glaciology*,
1419 18, 3-14.
- 1420 Cole-Dai, J., D. G. Ferris, J. A. Kennedy, M. Sigl, J. R. McConnell, T. J. Fudge, et al. (2021) Comprehensive
1421 record of volcanic eruptions in the Holocene (11,000 years) from the WAIS Divide, Antarctica, ice core.
1422 *Journal of Geophysical Research: Atmospheres*, 126, e2020JD032855.
- 1423 Conway, H., G. Catania, C. F. Raymond, A. M. Gades, T. A. Scambos & H. Engelhardt (2002) Switch of flow
1424 direction in an Antarctic ice stream. *Nature*, 419, 465-467.
- 1425 Conway, H., B. L. Hall, G. H. Denton, A. M. Gades & E. D. Waddington (1999) Past and future grounding-line
1426 retreat of the West Antarctic Ice Sheet. *Science*, 286, 280-283.
- 1427 Cook, C. P., T. van de Fliedert, T. Williams, S. R. Hemming, M. Iwai, M. Kobayashi, et al. (2013) Dynamic
1428 behaviour of the East Antarctic Ice Sheet during Pliocene warmth. *Nature Geoscience*, 6, 765-769.
- 1429 Cornford, S. L., D. F. Martin, A. J. Payne, E. G. Ng, A. M. Le Brocq, R. M. Gladstone, et al. (2015) Century-
1430 scale simulations of the response of the West Antarctic Ice Sheet to a warming climate. *The
1431 Cryosphere*, 9, 1579-1600.
- 1432 Corr, H., F. Ferraccioli, N. Frearson, T. Jordan, C. Robinson, E. Armadillo, et al. (2007) Airborne radio-echo
1433 sounding of the Wilkes Subglacial Basin, the Transantarctic Mountains, and the Dome C region. *Terra
1434 Antarctica Reports*, 13, 55-63.
- 1435 Corr, H. F. J. & D. G. Vaughan (2008) A recent volcanic eruption beneath the West Antarctic Ice Sheet. *Nature
1436 Geoscience*, 1, 122-125.
- 1437 Craven, M., M. Higham & A. Brocklesby. 2001. Ice thicknesses and surface and bedrock elevations from the
1438 Lambert Glacier Basin traverses 1990-95. In *Research Report (Antarctic CRC)*. Antarctic CRC;
1439 Australian Antarctic Division.
- 1440 Creyts, T. T., F. Ferraccioli, R. E. Bell, M. Wolovick, H. Corr, K. C. Rose, et al. (2014) Freezing of ridges and
1441 water networks preserves the Gamburtsev Subglacial Mountains for millions of years. *Geophysical
1442 Research Letters*, 41, 8114-8122.
- 1443 Cui, X., J. S. Greenbaum, S. Lang, X. Zhao, L. Li, J. Guo, et al. (2020a) The scientific operations of Snow
1444 Eagle 601 in Antarctica in the past five austral seasons. *Remote Sensing*, 12, 2994.
- 1445 Cui, X., H. Jeofry, J. S. Greenbaum, J. Guo, L. Li, L. E. Lindzey, et al. (2020b) Bed topography of Princess
1446 Elizabeth Land in East Antarctica. *Earth System Science Data*, 12, 2765-2774.
- 1447 Cui, X. B., W. J. Du, H. Xie & B. Sun (2020c) The ice flux to the Lambert Glacier and Amery Ice Shelf along
1448 the Chinese inland traverse and implications for mass balance of the drainage basins, East Antarctica.
1449 *Polar Research*, 39, 3582.
- 1450 Dahl-Jensen, D., N. S. Gundestrup, K. Keller, S. J. Johnsen, S. P. Gogineni, C. T. Allen, et al. (1997) A search
1451 in north Greenland for a new ice-core drill site. *Journal of Glaciology*, 43, 300-306.
- 1452 Damaske, D. & M. McLean (2005) An aerogeophysical survey south of the Prince Charles Mountains, East
1453 Antarctica. *Terra Antarctica*, 12, 87-98.
- 1454 Dansgaard, W. & S. J. Johnsen (1969) A flow model and a time scale for the ice core from Camp Century,
1455 Greenland. *Journal of Glaciology*, 8, 215 - 223.
- 1456 Das, I., R. E. Bell, T. A. Scambos, M. Wolovick, T. T. Creyts, M. Studinger, et al. (2013) Influence of persistent
1457 wind scour on the surface mass balance of Antarctica. *Nature Geoscience*, 6, 367-371.
- 1458 Das, I., L. Padman, R. E. Bell, H. A. Fricker, K. J. Tinto, C. Hulbe, et al. (2020) Multidecadal basal-melt rates
1459 and structure of the Ross Ice Shelf, Antarctica, using airborne ice-penetrating radar. *Journal of
1460 Geophysical Research: Earth Surface*, 125, e2019JF005241.
- 1461 Dawson, E. J., D. M. Schroeder, W. Chu, E. Mantelli & H. Seroussi (2022) Ice mass-loss sensitivity to the
1462 Antarctic Ice Sheet basal thermal state. *Nature Communications*, 13, 4957.
- 1463 DeConto, R. M. & D. Pollard (2016) Contribution of Antarctica to past and future sea-level rise. *Nature*, 531,
1464 591-597.
- 1465 DeConto, R. M., D. Pollard, R. B. Alley, I. Velicogna, E. Gasson, N. Gomez, et al. (2021) The Paris Climate
1466 Agreement and future sea-level rise from Antarctica. *Nature*, 593, 83-89.
- 1467 Delf, R., D. M. Schroeder, A. Curtis, A. Giannopoulos & R. G. Bingham (2020) A comparison of automated
1468 approaches to extracting englacial-layer geometry from radar data across ice sheets. *Annals of
1469 Glaciology*, 61, 234-241.
- 1470 Dome Fuji Ice Core Project Members (2017) State dependence of climatic instability over the past 720,000
1471 years from Antarctic ice cores and climate modeling. *Science Advances*, 3, e1600446.
- 1472 Dong, S., X. Tang, J. Guo, L. Fu, X. Chen & B. Sun (2021) EisNet: Extracting bedrock and internal layers from
1473 radiostratigraphy of ice sheets with machine learning. *IEEE Transactions on Geoscience and Remote
1474 Sensing*, 60, 4303212.



- 1475 Dowdeswell, J. A. & S. Evans (2004) Investigations of the form and flow of ice sheets and glaciers using radio-
1476 echo sounding. *Reports on Progress in Physics*, 67, 1821-1861.
- 1477 Drewry, D. J. (1975) Terrain units in eastern Antarctica. *Nature*, 256, 194-195.
- 1478 Drewry, D. J. 1983. Antarctica: Glaciological and Geophysical Folio. Cambridge: Cambridge University Press.
- 1479 Drewry, D. J. 2023. *The Land Beneath the Ice: The Pioneering Years of Radar Exploration in Antarctica*.
1480 Princeton: Princeton University Press.
- 1481 Drewry, D. J. & D. T. Meldrum (1978) Antarctic airborne radio-echo sounding, 1977–78. *Polar Record*, 19,
1482 267-273.
- 1483 Drews, R., O. Eisen, D. Steinhage, I. Weikusat, S. Kipfstuhl & F. Wilhelms (2012) Potential mechanisms for
1484 anisotropy in ice-penetrating radar data. *Journal of Glaciology*, 58, 613-624.
- 1485 Drews, R., O. Eisen, I. Weikusat, S. Kipfstuhl, A. Lambrecht, D. Steinhage, et al. (2009) Layer disturbances
1486 and the radio-echo free zone in ice sheets. *The Cryosphere*, 3, 195-203.
- 1487 Drews, R., C. Martín, D. Steinhage & O. Eisen (2013) Characterizing the glaciological conditions at
1488 Halvfarryggen Ice Dome, Dronning Maud Land, Antarctica. *Journal of Glaciology*, 59, 9-20.
- 1489 Drews, R., K. Matsuoka, C. Martín, D. Callens, N. Bergeot & F. Pattyn (2015) Evolution of Derwael Ice Rise in
1490 Dronning Maud Land, Antarctica, over the last millennia. *Journal of Geophysical Research: Earth
1491 Surface*, 120, 564-579.
- 1492 Dutton, A., A. E. Carlson, A. J. Long, G. A. Milne, P. U. Clark, R. DeConto, et al. (2015) Sea-level rise due to
1493 polar ice-sheet mass loss during past warm periods. *Science*, 349, aaa4019.
- 1494 Eisen, O. (2008) Inference of velocity pattern from isochronous layers in firn, using an inverse method. *Journal
1495 of Glaciology*, 54, 613-630.
- 1496 Eisen, O., I. Hamann, S. Kipfstuhl, D. Steinhage & F. Wilhelms (2007) Direct evidence for continuous radar
1497 reflector originating from changes in crystal-orientation fabric. *The Cryosphere*, 1, 1-10.
- 1498 Eisen, O., C. Martín, N. Blindow, D. Steinhage & R. C. A. Hindmarsh. 2008. Manifestation of ice properties
1499 and dynamics in radar stratigraphy: Berkner Island ice saddle as a case study. In *Symposium on
1500 radioglaciology and its applications*. Madrid, Spain.
- 1501 Eisen, O., U. Nixdorf, F. Wilhelms & H. Miller (2002) Electromagnetic wave speed in polar ice: Validation of
1502 the common-midpoint technique with high-resolution dielectric-profiling and γ -density measurements.
1503 *Annals of Glaciology*, 34, 150-156.
- 1504 Eisen, O., W. Rack, U. Nixdorf & F. Wilhelms (2005) Characteristics of accumulation around the EPICA deep-
1505 drilling site in Dronning Maud Land, Antarctica. *Annals of Glaciology*, 41, 41-46.
- 1506 Eisen, O., F. Wilhelms, U. Nixdorf & H. Miller (2003) Revealing the nature of radar reflections in ice: DEP-
1507 based FDTD forward modeling. *Geophysical Research Letters*, 30, 1218.
- 1508 Eisen, O., F. Wilhelms, D. Steinhage & J. Schwander (2006) Improved method to determine radio-echo
1509 sounding reflector depths from ice-core profiles of permittivity and conductivity. *Journal of Glaciology*,
1510 52, 299-310.
- 1511 EPICA Community Members (2004) Eight glacial cycles from an Antarctic ice core. *Nature*, 429, 623-628.
- 1512 Ershadi, M. R., R. Drews, C. Martín, O. Eisen, C. Ritz, H. Corr, et al. (2022) Polarimetric radar reveals the
1513 spatial distribution of ice fabric at domes and divides in East Antarctica. *The Cryosphere*, 16, 1719-
1514 1739.
- 1515 Escutia, C., M. A. Bárcena, R. G. Lucchi, O. Romero, A. M. Ballegeer, J. J. Gonzalez, et al. (2009) Circum-
1516 Antarctic warming events between 4 and 3.5 Ma recorded in marine sediments from the Prydz Bay
1517 (ODP Leg 188) and the Antarctic Peninsula (ODP Leg 178) margins. *Global and Planetary Change*,
1518 69, 170-184.
- 1519 Evans, S. & B. M. E. Smith (1970) Radio-echo exploration of the Antarctic Ice Sheet, 1969–70. *Polar Record*,
1520 15, 336-338.
- 1521 Fahnestock, M., W. Abdalati, S. Luo & S. Gogineni (2001a) Internal-layer tracing and age-depth-accumulation
1522 relationships for the northern Greenland Ice Sheet. *Journal of Geophysical Research: Atmospheres*,
1523 106, 33789-33797.
- 1524 Fahnestock, M. A., W. Abdalati, I. R. Joughin, J. M. Brozena & P. Gogineni (2001b) High geothermal heat flow,
1525 basal melt, and the origin of rapid ice flow in central Greenland. *Science*, 294, 2338 - 2342.
- 1526 Ferraccioli, F., P. C. Jones, M. L. Curtis & P. T. Leat (2005) Subglacial imprints of early Gondwana break-up
1527 as identified from high-resolution aerogeophysical data over western Dronning Maud Land, East
1528 Antarctica. *Terra Nova*, 17, 573-579.
- 1529 Fischer, H., J. Severinghaus, E. Brook, E. Wolff, M. Albert, O. Alemany, et al. (2013) Where to find 1.5 million
1530 yr old ice for the IPICS "Oldest-Ice" ice core. *Climate of the Past*, 9, 2489-2505.
- 1531 Fogwill, C. J., C. S. M. Turney, N. R. Golledge, D. M. Etheridge, M. Rubino, D. P. Thornton, et al. (2017)
1532 Antarctic ice-sheet discharge driven by atmosphere-ocean feedbacks at the Last Glacial Termination.
1533 *Scientific Reports*, 7, 39979.
- 1534 Fox-Kemper, B., H. T. Hewitt, C. Xiao, G. Aðalgeirsdóttir, S. S. Drijfhout, T. L. Edwards, et al. 2021. Ocean,
1535 cryosphere and sea-level change. In *Climate Change 2021: The Physical Science Basis. Contribution
1536 of Working Group I to the Sixth Assessment Report of the Intergovernmental Panel on Climate Change*,
1537 eds. V. Masson-Delmotte, P. Zhai, A. Pirani, S. L. Connors, C. Péan, S. Berger, N. Caud, Y. Chen, L.



- 1538 Goldfarb, M. I. Gomis, M. Huang, K. Leitzell, E. Lonnoy, J. B. R. Matthews, T. K. Maycock, T.
1539 Waterfield, O. Yelekçi, R. Yu & B. Zhou, 1211-1362. Cambridge: Cambridge University Press.
- 1540 Franke, S., H. Eisermann, W. Jokat, G. Eagles, J. Asseng, H. Miller, et al. (2021) Preserved landscapes
1541 underneath the Antarctic Ice Sheet reveal the geomorphological history of Jutulstraumen Basin. *Earth*
1542 *Surface Processes and Landforms*, 46, 2728-2745.
- 1543 Franke, S., T. Gerber, C. Warren, D. Jansen, O. Eisen & D. Dahl-Jensen (2023) Investigating the radar
1544 response of englacial-debris-entrained basal-ice units in East Antarctica using electromagnetic
1545 forward modeling. *IEEE Transactions on Geoscience and Remote Sensing*, 61, 4301516.
- 1546 Franke, S., D. Jansen, T. Binder, J. D. Paden, N. Dörr, T. A. Gerber, et al. (2022) Airborne ultra-wideband
1547 radar sounding over the shear margins and along flow lines at the onset region of the Northeast
1548 Greenland Ice Stream. *Earth System Science Data*, 14, 763-779.
- 1549 Franke, S., M. Wolovick, R. Drews, D. Jansen, K. Matsuoka & P. D. Bons (2024) Sediment freeze-on and
1550 transport near the onset of a fast-flowing glacier in East Antarctica. *Geophysical Research Letters*, 51,
1551 e2023GL107164.
- 1552 Frémand, A. C., J. A. Bodart, T. A. Jordan, F. Ferraccioli, C. Robinson, H. F. J. Corr, et al. (2022) British
1553 Antarctic Survey's aerogeophysical data: Releasing 25 years of airborne gravity, magnetic, and radar
1554 datasets over Antarctica. *Earth System Science Data*, 14, 3379-3410.
- 1555 Frémand, A. C., P. Fretwell, J. A. Bodart, H. D. Pritchard, A. Aitken, J. L. Bamber, et al. (2023) Antarctic
1556 Bedmap data: Findable, Accessible, Interoperable, and Reusable (FAIR) sharing of 60 years of ice
1557 bed, surface, and thickness data. *Earth System Science Data*, 15, 2695-2710.
- 1558 Frezzotti, M., G. Bitelli, P. De Michelis, A. Deponti, A. Forieri, S. Gandolfi, et al. (2004) Geophysical survey at
1559 Talos Dome, East Antarctica: The search for a new deep-drilling site. *Annals of Glaciology*, 39, 423-
1560 432.
- 1561 Fudge, T. J., B. H. Hills, A. N. Horlings, N. Holschuh, J. E. Christian, L. Davidge, et al. (2023) A site for deep
1562 ice coring at West Hercules Dome: Results from ground-based geophysics and modeling. *Journal of*
1563 *Glaciology*, 69, 538-550.
- 1564 Fujita, S., P. Holmlund, I. Andersson, I. Brown, H. Enomoto, Y. Fujii, et al. (2011) Spatial and temporal
1565 variability of snow accumulation rate on the East Antarctic ice divide between Dome Fuji and EPICA
1566 DML. *The Cryosphere*, 5, 1057-1081.
- 1567 Fujita, S., H. Maeno, S. Uratsuka, T. Furukawa, S. Mae, Y. Fujii, et al. (1999) Nature of radio-echo layering in
1568 the Antarctic Ice Sheet detected by a two-frequency experiment. *Journal of Geophysical Research:*
1569 *Solid Earth*, 104, 13013-13024.
- 1570 Fujita, S., T. Matsuoka, T. Ishida, K. Matsuoka & S. Mae. 2000. A summary of the complex dielectric permittivity
1571 of ice in the megahertz range and its applications for radar sounding of polar ice sheets. In *International*
1572 *Symposium on Physics of Ice Core Records*, 185 - 212. Shikotsukohan, Hokkaido, Japan.
- 1573 Gagliardini, O., T. Zwinger, F. Gillet-Chaulet, G. Durand, L. Favier, B. de Fleurian, et al. (2013) Capabilities
1574 and performance of Elmer/Ice, a new-generation ice-sheet model. *Geoscientific Model Development*,
1575 6, 1299-1318.
- 1576 Gasson, E., R. DeConto, D. Pollard & R. H. Levy (2016) Dynamic Antarctic ice sheet during the early to mid-
1577 Miocene. *Proceedings of the National Academy of Sciences*, 113, 3459-3464.
- 1578 Gerber, T. A., D. A. Lilien, N. M. Rathmann, S. Franke, T. J. Young, F. Valero-Delgado, et al. (2023) Crystal-
1579 orientation-fabric anisotropy causes directional hardening of the Northeast Greenland Ice Stream.
1580 *Nature Communications*, 14, 2653.
- 1581 Geyer, A., A. Di Roberto, J. L. Smellie, M. Van Wyk de Vries, K. S. Panter, A. P. Martin, et al. (2023) Volcanism
1582 in Antarctica: An assessment of the present state of research and future directions. *Journal of*
1583 *Volcanology and Geothermal Research*, 444, 107941.
- 1584 Goel, V., C. Martín & K. Matsuoka (2018) Ice-rise stratigraphy reveals changes in surface mass balance over
1585 the last millennia in Dronning Maud Land. *Journal of Glaciology*, 64, 932-942.
- 1586 Goel, V., C. Martín & K. Matsuoka (2024) Evolution of ice rises in the Fimbul Ice Shelf, Dronning Maud Land,
1587 over the last millennium. *Antarctic Science*, 36, 110-124.
- 1588 Goelles, T., K. Grosfeld & G. Lohmann (2014) Semi-Lagrangian transport of oxygen isotopes in polythermal
1589 ice sheets: implementation and first results. *Geoscientific Model Development*, 7, 1395-1408.
- 1590 Goelzer, H., S. Nowicki, A. Payne, E. Larour, H. Seroussi, W. H. Lipscomb, et al. (2020) The future sea-level
1591 contribution of the Greenland Ice Sheet: A multi-model ensemble study of ISMIP6. *The Cryosphere*,
1592 14, 3071-3096.
- 1593 Gogineni, P., T. Chuah, C. Allen, K. Jezek & R. K. Moore (1998) An improved coherent radar depth sounder.
1594 *Journal of Glaciology*, 44, 659-669.
- 1595 Gollledge, N. R., E. D. Keller, N. Gomez, K. A. Naughten, J. Bernales, L. D. Trusel, et al. (2019) Global
1596 environmental consequences of twenty-first-century ice-sheet melt. *Nature*, 566, 65-72.
- 1597 Gollledge, N. R., D. E. Kowalewski, T. R. Naish, R. H. Levy, C. J. Fogwill & E. G. W. Gasson (2015) The multi-
1598 millennial Antarctic commitment to future sea-level rise. *Nature*, 526, 421-425.
- 1599 Goodge, J. W. & J. P. Severinghaus (2016) Rapid Access Ice Drill: A new tool for exploration of the deep
1600 Antarctic ice sheets and subglacial geology. *Journal of Glaciology*, 62, 1049-1064.



- 1601 Goodge, J. W., J. P. Severinghaus, J. Johnson, D. Tosi & R. Bay (2021) Deep ice drilling, bedrock coring and
1602 dust logging with the Rapid Access Ice Drill (RAID) at Minna Bluff, Antarctica. *Annals of Glaciology*,
1603 62, 324-339.
- 1604 Gow, A. J. & T. Williamson (1976) Rheological implications of the internal structure and crystal fabrics of the
1605 West Antarctic Ice Sheet as revealed by deep core drilling at Byrd Station. *Geological Society of
1606 America Bulletin*, 87, 1665-1677.
- 1607 Gudmandsen, P., E. Nilsson, M. Pallisgaard, N. Skou & F. Søndergaard (1975) New equipment for radio-echo
1608 sounding. *Antarctic Journal of the United States*, 10, 234-236.
- 1609 Gulick, S. P. S., A. E. Shevenell, A. Montelli, R. Fernandez, C. Smith, S. Warny, et al. (2017) Initiation and
1610 long-term instability of the East Antarctic Ice Sheet. *Nature*, 552, 225-229.
- 1611 Hale, R., H. Miller, S. Gogineni, J. B. Yan, F. Rodriguez-Morales, C. Leuschen, et al. 2016. Multi-channel ultra-
1612 wideband radar sounder and imager. In *2016 IEEE International Geoscience and Remote Sensing
1613 Symposium (IGARSS)*, 2112-2115.
- 1614 Hammer, C. U. (1980) Acidity of polar ice cores in relation to absolute dating, past volcanism, and radio-
1615 echoes. *Journal of Glaciology*, 25, 359-372.
- 1616 Hammer, C. U., H. B. Clausen & C. C. Langway (1997) 50,000 years of recorded global volcanism. *Climatic
1617 Change*, 35, 1-15.
- 1618 Harrison, C. H. (1973) Radio-echo sounding of horizontal layers in ice. *Journal of Glaciology*, 12, 383-397.
- 1619 Hays, J. D., J. Imbrie & N. J. Shackleton (1976) Variations in the Earth's orbit: Pacemaker of the ice ages.
1620 *Science*, 194, 1121-1132.
- 1621 Heister, A. & R. Scheiber (2018) Coherent large-beamwidth processing of radio-echo sounding data. *The
1622 Cryosphere*, 12, 2969-2979.
- 1623 Hélière, F., C.-C. Lin, H. F. J. Corr & D. G. Vaughan (2007) Radio-echo sounding of Pine Island Glacier, West
1624 Antarctica: Aperture-synthesis processing and analysis of feasibility from space. *IEEE Transactions
1625 on Geoscience and Remote Sensing*, 45, 2573-2582.
- 1626 Hempel, L., F. Thyssen, N. Gundestrup, H. B. Clausen & H. Miller (2000) A comparison of radio-echo sounding
1627 data and electrical conductivity of the GRIP Ice Core. *Journal of Glaciology*, 46, 369-374.
- 1628 Henry, A. C. J., C. Schannwell, V. Višnjić, J. Millstein, P. D. Bons, O. Eisen, et al. (2024) Predicting the
1629 three-dimensional age-depth field of an ice rise. *Authorea*, DOI:
1630 10.22541/essoar.169230234.44865946/v1.
- 1631 Higgins, J. A., A. V. Kurbatov, N. E. Spaulding, E. Brook, D. S. Introne, L. M. Chimiak, et al. (2015) Atmospheric
1632 composition 1 million years ago from blue ice in the Allan Hills, Antarctica. *Proceedings of the National
1633 Academy of Sciences*, 112, 6887-6891.
- 1634 Hillebrand, T. R., J. O. Stone, M. Koutnik, C. King, H. Conway, B. Hall, et al. (2021) Holocene thinning of
1635 Darwin and Hatherton glaciers, Antarctica, and implications for grounding-line retreat in the Ross Sea.
1636 *The Cryosphere*, 15, 3329-3354.
- 1637 Hillenbrand, C.-D., J. A. Smith, D. A. Hodell, M. Greaves, C. R. Poole, S. Kender, et al. (2017) West Antarctic
1638 Ice Sheet retreat driven by Holocene warm water incursions. *Nature*, 547, 43-48.
- 1639 Hills, B. H., K. Christianson, A. O. Hoffman, T. J. Fudge, N. Holschuh, E. C. Kahle, et al. (2022) Geophysics
1640 and thermodynamics at South Pole Lake indicate stability and a regionally thawed bed. *Geophysical
1641 Research Letters*, 49, e2021GL096218.
- 1642 Hindmarsh, R. C. A., E. C. King, R. Mulvaney, H. F. J. Corr, G. Hiess & F. Gillet-Chaulet (2011) Flow at ice-
1643 divide triple junctions: 2. Three-dimensional views of isochrone architecture from ice-penetrating radar
1644 surveys. *Journal of Geophysical Research: Earth Surface*, 116, F02024.
- 1645 Hindmarsh, R. C. A., G. J.-M. C. Leysinger Vieli & F. Parrenin (2009) A large-scale numerical model for
1646 computing isochrone geometry. *Annals of Glaciology*, 50, 130-140.
- 1647 Hindmarsh, R. C. A., G. J.-M. C. Leysinger Vieli, M. J. Raymond & G. H. Gudmundsson (2006) Draping or
1648 overriding: The effect of horizontal stress gradients on internal layer architecture in ice sheets. *Journal
1649 of Geophysical Research: Earth Surface*, 111, F02018.
- 1650 Hodgkins, R., M. J. Siegert & J. A. Dowdeswell (2000) Geophysical investigations of ice-sheet internal layering
1651 and deformation in the Dome C region of central East Antarctica. *Journal of Glaciology*, 46, 161-166.
- 1652 Holland, P. R., H. F. J. Corr, D. G. Vaughan, A. Jenkins & P. Skvarca (2009) Marine ice in Larsen Ice Shelf.
1653 *Geophysical Research Letters*, 36, L11604.
- 1654 Holschuh, N., K. Christianson & S. Anandakrishnan (2014) Power loss in dipping internal reflectors, imaged
1655 using ice-penetrating radar. *Annals of Glaciology*, 55, 49-56.
- 1656 Holschuh, N., K. Christianson, H. Conway, R. Jacobel & B. Welch (2018) Persistent tracers of historic ice flow
1657 in glacial stratigraphy near Kamb Ice Stream, West Antarctica. *The Cryosphere*, 12, 2821 - 2829.
- 1658 Holschuh, N., D. A. Lilien & K. Christianson (2019) Thermal weakening, convergent flow, and vertical heat
1659 transport in the Northeast Greenland Ice Stream shear margins. *Geophysical Research Letters*, 46,
1660 8184-8193.
- 1661 Holschuh, N., B. R. Parizek, R. B. Alley & S. Anandakrishnan (2017) Decoding ice-sheet behavior using
1662 englacial layer slopes. *Geophysical Research Letters*, 44, 5561-5570.



- 1663 Humbert, A., D. Steinhage, V. Helm, S. Beyer & T. Kleiner (2018) Missing evidence of widespread subglacial
1664 lakes at Recovery Glacier, Antarctica. *Journal of Geophysical Research: Earth Surface*, 123, 2802-
1665 2826.
- 1666 IceCube Collaboration (2013) South Pole glacial climate reconstruction from multi-borehole laser particulate
1667 stratigraphy. *Journal of Glaciology*, 59, 1117-1128.
- 1668 Jacobel, R. W., A. M. Gades, D. L. Gottschling, S. M. Hodge & D. L. Wright (1993) Interpretation of radar-
1669 detected internal layer folding in West Antarctic ice streams. *Journal of Glaciology*, 39, 528-537.
- 1670 Jacobel, R. W., T. A. Scambos, N. A. Nereson & C. F. Raymond (2000) Changes in the margin of Ice Stream
1671 C, Antarctica. *Journal of Glaciology*, 46, 102-110.
- 1672 Jacobel, R. W. & B. C. Welch (2005) A time marker at 17.5 kyr BP detected throughout West Antarctica. *Annals
1673 of Glaciology*, 41, 47-51.
- 1674 Jansen, D., S. Franke, C. C. Bauer, T. Binder, D. Dahl-Jensen, J. Eichler, et al. (2024) Shear margins in upper
1675 half of Northeast Greenland Ice Stream were established two millennia ago. *Nature Communications*,
1676 15, 1193.
- 1677 Jennings, S. J. A. & M. J. Hambrey (2021) Structures and deformation in glaciers and ice sheets. *Reviews of
1678 Geophysics*, 59, e2021RG000743.
- 1679 Jones, D. J. & M. Hendy (1985) Glaciological measurements in eastern Wilkes Land, Antarctica. *ANARE
1680 Research Notes*, 28, 164 - 73.
- 1681 Jordan, T. A., C. Martín, F. Ferraccioli, K. Matsuoka, H. Corr, R. Forsberg, et al. (2018) Anomalously high
1682 geothermal flux near the South Pole. *Scientific Reports*, 8, 16785.
- 1683 Jordan, T. M., C. Martín, A. M. Brisbourne, D. M. Schroeder & A. M. Smith (2022) Radar characterization of
1684 ice-crystal-orientation fabric and anisotropic viscosity within an Antarctic ice stream. *Journal of
1685 Geophysical Research: Earth Surface*, 127, e2022JF006673.
- 1686 Jordan, T. M., D. M. Schroeder, C. W. Elsworth & M. R. Siegfried (2020) Estimation of ice fabric within Whillans
1687 Ice Stream using polarimetric phase-sensitive radar sounding. *Annals of Glaciology*, 61, 74-83.
- 1688 Jouzel, J., V. Masson-Delmotte, O. Cattani, G. Dreyfus, S. Falourd, G. Hoffmann, et al. (2007) Orbital and
1689 millennial Antarctic climate variability over the past 800,000 years. *Science*, 317, 793-796.
- 1690 Karlsson, N. B., T. Binder, G. Eagles, V. Helm, F. Pattyn, B. Van Liefferinge, et al. (2018) Glaciological
1691 characteristics in the Dome Fuji region and new assessment for "Oldest Ice". *The Cryosphere*, 12,
1692 2413-2424.
- 1693 Karlsson, N. B., R. G. Bingham, D. M. Rippin, R. C. A. Hindmarsh, H. F. J. Corr & D. G. Vaughan (2014)
1694 Constraining past accumulation in the central Pine Island Glacier basin, West Antarctica, using radio-
1695 echo sounding. *Journal of Glaciology*, 60, 553-562.
- 1696 Karlsson, N. B., D. M. Rippin, R. G. Bingham & D. G. Vaughan (2012) A 'continuity-index' for assessing ice-
1697 sheet dynamics from radar-sounded internal layers. *Earth and Planetary Science Letters*, 335-336,
1698 88-94.
- 1699 Karlsson, N. B., D. M. Rippin, D. G. Vaughan & H. F. J. Corr (2009) The internal layering of Pine Island Glacier,
1700 West Antarctica, from airborne radar-sounding data. *Annals of Glaciology*, 50, 141-146.
- 1701 Karlsson, N. B., D. M. Schroeder, L. S. Sørensen, W. Chu, J. Dall, N. H. Andersen, et al. (2024) A newly
1702 digitized ice-penetrating radar data set acquired over the Greenland ice sheet in 1971–1979. *Earth
1703 System Science Data*, 16, 3333-3344.
- 1704 King, E. C. (2009) Flow dynamics of the Rutford Ice Stream ice-drainage basin, West Antarctica, from radar
1705 stratigraphy. *Annals of Glaciology*, 50, 42-48.
- 1706 King, E. C. (2011) Ice stream or not? Radio-echo sounding of Carlson Inlet, West Antarctica. *The Cryosphere*,
1707 5, 907-916.
- 1708 Kingslake, J., R. C. A. Hindmarsh, G. Aðalgeirsdóttir, H. Conway, H. F. J. Corr, F. Gillet-Chaulet, et al. (2014)
1709 Full-depth englacial vertical ice-sheet velocities measured using phase-sensitive radar. *Journal of
1710 Geophysical Research: Earth Surface*, 119, 2604-2618.
- 1711 Kingslake, J., C. Martín, R. J. Arthern, H. F. J. Corr & E. C. King (2016) Ice-flow reorganization in West
1712 Antarctica 2.5 kyr ago dated using radar-derived englacial flow velocities. *Geophysical Research
1713 Letters*, 43, 9103-9112.
- 1714 Kingslake, J., R. P. Scherer, T. Albrecht, J. Coenen, R. D. Powell, R. Reese, et al. (2018) Extensive retreat
1715 and re-advance of the West Antarctic Ice Sheet during the Holocene. *Nature*, 558, 430-434.
- 1716 Koch, I., R. Drews, O. Eisen, S. Franke, D. Jansen, K. Matsuoka, et al. (2023) Radar internal reflection horizons
1717 from multisystem data reflect ice dynamic and surface accumulation history along the Princess
1718 Ragnhild Coast, Dronning Maud Land, East Antarctica. *Journal of Glaciology*, Firstview
1719 <https://doi.org/10.1017/jog.2023.93>
- 1720 Konrad, H., A. E. Hogg, R. Mulvaney, R. Arthern, R. J. Tuckwell, B. Medley, et al. (2019) Observations of
1721 surface mass balance on Pine Island Glacier, West Antarctica, and the effect of strain history in fast-
1722 flowing sections. *Journal of Glaciology*, 65, 595-604.
- 1723 Koutnik, M. R., T. J. Fudge, H. Conway, E. D. Waddington, T. A. Neumann, K. M. Cuffey, et al. (2016) Holocene
1724 accumulation and ice flow near the West Antarctic Ice Sheet Divide ice-core site. *Journal of
1725 Geophysical Research: Earth Surface*, 121, 907-924.



- 1726 Kovacs, A., A. J. Gow & R. M. Morey (1995) The in-situ dielectric constant of polar firn revisited. *Cold Regions*
1727 *Science and Technology*, 23, 245-256.
- 1728 Kowalewski, S., V. Helm, E. M. Morris & O. Eisen (2021) The regional-scale surface mass balance of Pine
1729 Island Glacier, West Antarctica, over the period 2005–2014, derived from airborne radar soundings
1730 and neutron probe measurements. *The Cryosphere*, 15, 1285-1305.
- 1731 Laird, C. M., W. A. Blake, K. Matsuoka, H. Conway, C. T. Allen, C. J. Leuschen, et al. (2010) Deep ice
1732 stratigraphy and basal conditions in central West Antarctica revealed by coherent radar. *IEEE*
1733 *Geoscience and Remote Sensing Letters*, 7, 246-250.
- 1734 Le Meur, E., O. Magand, L. Arnaud, M. Fily, M. Frezzotti, M. Cavitte, et al. (2018) Spatial and temporal
1735 distributions of surface mass balance between Concordia and Vostok stations, Antarctica, from
1736 combined radar and ice-core data: First results and detailed error analysis. *The Cryosphere*, 12, 1831-
1737 1850.
- 1738 Lecavalier, B. S., L. Tarasov, G. Balco, P. Spector, C. D. Hillenbrand, C. Buizert, et al. (2023) Antarctic Ice
1739 Sheet paleo-constraint database. *Earth System Science Data*, 15, 3573-3596.
- 1740 Lee, H., H. Seo, H. Han, H. Ju & J. Lee (2021) Velocity anomaly of Campbell Glacier, East Antarctica, observed
1741 by double-differential interferometric SAR and ice-penetrating radar. *Remote Sensing*, 13, 2691.
- 1742 Legrain, E., F. Parrenin & E. Capron (2023) A gradual change is more likely to have caused the Mid-
1743 Pleistocene Transition than an abrupt event. *Communications Earth & Environment*, 4, 90.
- 1744 Lenaerts, J. T. M., B. Medley, M. R. van den Broeke & B. Wouters (2019) Observing and modeling ice-sheet
1745 surface mass balance. *Reviews of Geophysics*, 57, 376-420.
- 1746 Leysinger Vieli, G. J.-M. C., R. C. A. Hindmarsh & M. J. Siegert (2007) Three-dimensional flow influences on
1747 radar layer stratigraphy. *Annals of Glaciology*, 46, 22-28.
- 1748 Leysinger Vieli, G. J.-M. C., R. C. A. Hindmarsh, M. J. Siegert & B. Sun (2011) Time-dependence of the spatial
1749 pattern of accumulation rate in East Antarctica deduced from isochronic radar layers using a 3-D
1750 numerical ice flow model. *Journal of Geophysical Research: Earth Surface*, 116, F02018.
- 1751 Leysinger Vieli, G. J.-M. C., C. Martín, R. C. A. Hindmarsh & M. P. Lüthi (2018) Basal freeze-on generates
1752 complex ice-sheet stratigraphy. *Nature Communications*, 9, 4669.
- 1753 Leysinger Vieli, G. J.-M. C., M. J. Siegert & A. J. Payne (2004) Reconstructing ice-sheet accumulation rates
1754 at Ridge B, East Antarctica. *Annals of Glaciology*, 39, 326-330.
- 1755 Lilien, D. A., D. Steinhage, D. Taylor, F. Parrenin, C. Ritz, R. Mulvaney, et al. (2021) New radar constraints
1756 support presence of ice older than 1.5 Myr at Little Dome C. *The Cryosphere*, 15, 1881-1888.
- 1757 Lindzey, L. E., L. H. Beem, D. A. Young, E. Quartini, D. D. Blankenship, C. K. Lee, et al. (2020)
1758 Aerogeophysical characterization of an active subglacial lake system in the David Glacier catchment,
1759 Antarctica. *The Cryosphere*, 14, 2217-2233.
- 1760 Liu, W., K. Purdon, T. Stafford, J. Paden & X. Li (2016) Open Polar Server (OPS): An open-source
1761 infrastructure for the cryosphere community. *ISPRS International Journal of Geo-Information*, 5, 32.
- 1762 Luo, K., S. Liu, J. Guo, T. Wang, L. Li, X. Cui, et al. (2020) Radar-derived internal structure and basal
1763 roughness characterization along a traverse from Zhongshan Station to Dome A, East Antarctica.
1764 *Remote Sensing*, 12, 1079.
- 1765 Luo, K., X. Tang, S. Liu, J. Guo, J. S. Greenbaum, L. Li, et al. (2022) Deep radiostratigraphy constraints support
1766 the presence of persistent wind scouring behavior for more than 100 ka in the East Antarctic Ice Sheet.
1767 *IEEE Transactions on Geoscience and Remote Sensing*, 60, 4306213.
- 1768 Lythe, M. B., D. G. Vaughan & BEDMAP Consortium (2001) BEDMAP: A new ice thickness and subglacial
1769 topographic model of Antarctica. *Journal of Geophysical Research: Solid Earth*, 106, 11335-11351.
- 1770 MacGregor, J. A., L. N. Boisvert, B. Medley, A. A. Petty, J. P. Harbeck, R. E. Bell, et al. (2021) The scientific
1771 legacy of NASA's Operation IceBridge. *Reviews of Geophysics*, 59, e2020RG000712.
- 1772 MacGregor, J. A., W. T. Colgan, M. A. Fahnestock, M. Morlighem, G. A. Catania, J. D. Paden, et al. (2016)
1773 Holocene deceleration of the Greenland Ice Sheet. *Science*, 351, 590-593.
- 1774 MacGregor, J. A., M. A. Fahnestock, G. A. Catania, J. D. Paden, S. P. Gogineni, S. K. Young, et al. (2015a)
1775 Radiostratigraphy and age structure of the Greenland Ice Sheet. *Journal of Geophysical Research:*
1776 *Earth Surface*, 120, 212-241.
- 1777 MacGregor, J. A., J. L. Li, J. D. Paden, G. A. Catania, G. D. Clow, M. A. Fahnestock, et al. (2015b) Radar
1778 attenuation and temperature within the Greenland Ice Sheet. *Journal of Geophysical Research: Earth*
1779 *Surface*, 120, 983-1008.
- 1780 MacGregor, J. A., K. Matsuoka, M. R. Koutnik, E. D. Waddington, M. Studinger & D. P. Winebrenner (2009)
1781 Millennially averaged accumulation rates for the Vostok Subglacial Lake region inferred from deep
1782 internal layers. *Annals of Glaciology*, 50, 25-34.
- 1783 MacGregor, J. A., D. P. Winebrenner, H. Conway, K. Matsuoka, P. A. Mayewski & G. D. Clow (2007) Modeling
1784 englacial radar attenuation at Siple Dome, West Antarctica, using ice chemistry and temperature data.
1785 *Journal of Geophysical Research: Earth Surface*, 112, F03008.
- 1786 Mackintosh, A. N., E. Verleyen, P. E. O'Brien, D. A. White, R. S. Jones, R. McKay, et al. (2014) Retreat history
1787 of the East Antarctic Ice Sheet since the Last Glacial Maximum. *Quaternary Science Reviews*, 100,
1788 10-30.



- 1789 Martín, C. & G. H. Gudmundsson (2012) Effects of nonlinear rheology, temperature and anisotropy on the
1790 relationship between age and depth at ice divides. *The Cryosphere*, 6, 1221-1229.
- 1791 Martín, C., G. H. Gudmundsson & E. C. King (2014) Modelling of Kealey Ice Rise, Antarctica, reveals stable
1792 ice-flow conditions in East Ellsworth Land over millennia. *Journal of Glaciology*, 60, 139-146.
- 1793 Martín, C., R. C. A. Hindmarsh & F. J. Navarro (2006) Dating ice flow change near the flow divide at Roosevelt
1794 Island, Antarctica, by using a thermomechanical model to predict radar stratigraphy. *Journal of
1795 Geophysical Research: Earth Surface*, 111, F01011.
- 1796 Martín, C., R. C. A. Hindmarsh & F. J. Navarro (2009) On the effects of divide migration, along-ridge flow, and
1797 basal sliding on isochrones near an ice divide. *Journal of Geophysical Research: Earth Surface*, 114,
1798 F02006.
- 1799 Matsuoka, K., T. Furukawa, S. Fujita, H. Maeno, S. Uratsuka, R. Naruse, et al. (2003) Crystal-orientation
1800 fabrics within the Antarctic Ice Sheet revealed by a multipolarization plane and dual-frequency radar
1801 survey. *Journal of Geophysical Research: Solid Earth*, 108, 2499.
- 1802 Matsuoka, K., A. Gades, H. Conway, G. Catania & C. F. Raymond (2009) Radar signatures beneath a surface
1803 topographic lineation near the outlet of Kamb Ice Stream and Engelhardt Ice Ridge, West Antarctica.
1804 *Annals of Glaciology*, 50, 98-104.
- 1805 Matsuoka, K., R. C. A. Hindmarsh, G. Moholdt, M. J. Bentley, H. D. Pritchard, J. Brown, et al. (2015) Antarctic
1806 ice rises and rumples: Their properties and significance for ice-sheet dynamics and evolution. *Earth-
1807 Science Reviews*, 150, 724-745.
- 1808 Matsuoka, K., J. A. MacGregor & F. Pattyn (2012) Predicting radar attenuation within the Antarctic Ice Sheet.
1809 *Earth and Planetary Science Letters*, 359-360, 173-183.
- 1810 McConnell, J. R., A. Burke, N. W. Dunbar, P. Köhler, J. L. Thomas, M. M. Arienzo, et al. (2017) Synchronous
1811 volcanic eruptions and abrupt climate change ~17.7 ka plausibly linked by stratospheric ozone
1812 depletion. *Proceedings of the National Academy of Sciences*, 114, 10035-10040.
- 1813 Medhurst, T. G. (1985) Glaciological measurements in western Wilkes Land, Antarctica. *ANARE Research
1814 Notes*, 28.
- 1815 Medley, B., I. Joughin, S. B. Das, E. J. Steig, H. Conway, S. Gogineni, et al. (2013) Airborne-radar and ice-
1816 core observations of annual snow accumulation over Thwaites Glacier, West Antarctica, confirm the
1817 spatiotemporal variability of global and regional atmospheric models. *Geophysical Research Letters*,
1818 40, 3649-3654.
- 1819 Medley, B., I. Joughin, B. E. Smith, S. B. Das, E. J. Steig, H. Conway, et al. (2014) Constraining the recent
1820 mass balance of Pine Island and Thwaites glaciers, West Antarctica, with airborne observations of
1821 snow accumulation. *The Cryosphere*, 8, 1375-1392.
- 1822 Millar, D. H. M. (1981) Radio-echo layering in polar ice sheets and past volcanic activity. *Nature*, 292, 441-443.
- 1823 Millar, D. H. M. (1982) Acidity levels in ice sheets from radio echo-sounding. *Annals of Glaciology*, 3, 199-203.
- 1824 Miners, W. D., A. Hildebrand, S. Gerland, N. Blindow, D. Steinhage & E. W. Wolff (1997) Forward modeling of
1825 the internal layers in radio-echo sounding using electrical and density measurements from ice cores.
1826 *Journal of Physical Chemistry B*, 101, 6201-6204.
- 1827 Mojtabavi, S., O. Eisen, S. Franke, D. Jansen, D. Steinhage, J. Paden, et al. (2022) Origin of englacial
1828 stratigraphy at three deep ice core sites of the Greenland Ice Sheet by synthetic radar modelling.
1829 *Journal of Glaciology*, 68, 799-811.
- 1830 Moqadam, H. & O. Eisen (2024) Review of feature tracing in radio-echo sounding products of terrestrial ice
1831 sheets and planetary bodies. *EGUsphere*, 2024, egusphere-2024-1674.
- 1832 Morgan, V., T. Jacka, G. Akerman & A. Clarke (1982) Outlet glacier and mass-budget studies in Enderby,
1833 Kemp, and Mac. Robertson Lands, Antarctica. *Annals of Glaciology*, 3, 204-210.
- 1834 Morlighem, M. 2020. MEaSURES BedMachine Antarctica, Version 2. NASA National Snow and Ice Data
1835 Center Distributed Active Archive Center.
- 1836 Morse, D. L., D. D. Blankenship, E. D. Waddington & T. A. Neumann (2002) A site for deep ice coring in West
1837 Antarctica: Results from aerogeophysical surveys and thermo-kinematic modeling. *Annals of
1838 Glaciology*, 35, 36-44.
- 1839 Moss, G., V. Višnjević, O. Eisen, F. M. Oraschewski, C. Schröder, J. H. Macke, et al. (2023) Simulation-based
1840 inference of surface accumulation and basal-melt rates of an Antarctic ice shelf from isochronal layers.
1841 *ArXiv*, abs/2312.02997.
- 1842 Moussessian, A., R. L. Jordan, E. Rodriguez, A. Safaeinili, T. L. Akins, W. N. Edelstein, et al. 2000. A new
1843 coherent radar for ice sounding in Greenland. In *International Geoscience and Remote Sensing
1844 Symposium (IGARRS) Proceedings*, 484-486 vol.2.
- 1845 Muldoon, G. R., C. S. Jackson, D. A. Young & D. D. Blankenship (2018) Bayesian estimation of englacial radar
1846 chronology in Central West Antarctica. *Dynamics and Statistics of the Climate System*, 3, dzy004.
- 1847 Naish, T., R. Powell, R. Levy, G. Wilson, R. Scherer, F. Talarico, et al. (2009) Obliquity-paced Pliocene West
1848 Antarctic ice sheet oscillations. *Nature*, 458, 322-328.
- 1849 Napoleoni, F., S. Jamieson, N. Ross, M. Bentley, A. Rivera, A. Smith, et al. (2020) Subglacial lakes and
1850 hydrology across the Ellsworth Subglacial Highlands, West Antarctica. *The Cryosphere*, 14, 4507-
1851 4524.



- 1852 Narcisi, B. & J. R. Petit (2021) Englacial tephra of East Antarctica. *Geological Society, London, Memoirs*, 55,
1853 649-664.
- 1854 NEEM Community Members (2013) Eemian interglacial reconstructed from a Greenland folded ice core.
1855 *Nature*, 493, 489-494.
- 1856 Nereson, N. A., C. F. Raymond, R. W. Jacobel & E. D. Waddington (2000) The accumulation pattern across
1857 Siple Dome, West Antarctica, inferred from radar-detected internal layers. *Journal of Glaciology*, 46,
1858 75-87.
- 1859 Nereson, N. A., C. F. Raymond, E. D. Waddington & R. W. Jacobel (1998) Migration of the Siple Dome ice
1860 divide, West Antarctica. *Journal of Glaciology*, 44, 643-652.
- 1861 Neumann, T. A., H. Conway, S. F. Price, E. D. Waddington, G. A. Catania & D. L. Morse (2008) Holocene
1862 accumulation and ice-sheet dynamics in central West Antarctica. *Journal of Geophysical Research:*
1863 *Earth Surface*, 113, F02018.
- 1864 Ng, F. & H. Conway (2004) Fast-flow signature in the stagnated Kamb Ice Stream, West Antarctica. *Geology*,
1865 32, 481-484.
- 1866 Ng, F. & E. C. King (2011) Kinematic waves in polar firn stratigraphy. *Journal of Glaciology*, 57, 1119-1134.
- 1867 Nicholls, K. W., H. F. J. Corr, C. L. Stewart, L. B. Lok, P. V. Brennan & D. G. Vaughan (2015) A ground-based
1868 radar for measuring vertical strain rates and time-varying basal melt rates in ice sheets and shelves.
1869 *Journal of Glaciology*, 61, 1079-1087.
- 1870 Nixdorf, U., D. Steinhage, U. Meyer, L. Hempel, M. Jenett, P. Wachs, et al. (1999) The newly developed
1871 airborne radio-echo sounding system of the AWI as a glaciological tool. *Annals of Glaciology*, 29, 231-
1872 238.
- 1873 Nye, J. (1957) The distribution of stress and velocity in glaciers and ice sheets. *Proceedings of the Royal*
1874 *Society A: Mathematical, Physical and Engineering Sciences*, 239, 113-133.
- 1875 Obase, T., A. Abe-Ouchi, F. Saito, S. Tsutaki, S. Fujita, K. Kawamura, et al. (2023) A one-dimensional
1876 temperature and age modeling study for selecting the drill site of the oldest ice core near Dome Fuji,
1877 Antarctica. *The Cryosphere*, 17, 2543-2562.
- 1878 Oppenheimer, M., B. C. Glavovic, J. Hinkel, R. van de Wal, A. K. Magnan, A. Abd-Elgawad, et al. 2019. Sea-
1879 level rise and implications for low-lying islands, coasts and communities. In *IPCC Special Report on*
1880 *the Ocean and Cryosphere in a Changing Climate*, eds. H.-O. Pörtner, D. C. Roberts, V. Masson-
1881 Delmotte, P. Zhai, M. Tignor, E. Poloczanska, K. Mintenbeck, A. Alegria, M. Nicolai, A. Okem, J.
1882 Petzold, B. Rama & N. M. Weyer, 321-445. Cambridge: Cambridge University Press.
- 1883 Oraschewski, F. M., I. Koch, M. R. Ershadi, J. Hawkins, O. Eisen & R. Drews (2023) Layer-optimized SAR
1884 processing with a mobile phase-sensitive radar for detecting the deep englacial stratigraphy of Colle
1885 Gnifetti, Switzerland/Italy. *EGUsphere*, 2023, 1-21.
- 1886 Otosaka, I. N., A. Shepherd, E. R. Ivins, N. J. Schlegel, C. Amory, M. R. van den Broeke, et al. (2023) Mass
1887 balance of the Greenland and Antarctic ice sheets from 1992 to 2020. *Earth System Science Data*, 15,
1888 1597-1616.
- 1889 Paden, J., K. Tinto, D. Young, K. Christianson, D. Schroeder, M. Rahnmooanfar, et al. 2021. Open Polar Radar
1890 software and services to standardize radar echograms and integrate into a geospatial database. . In
1891 *AGU Fall Meeting 2021*, 2021AGUFM.C51A.08P.
- 1892 Pantou, C. (2014) Automated mapping of local layer slope and tracing of internal layers in radio echograms.
1893 *Annals of Glaciology*, 55, 71-77.
- 1894 Pantou, C. & N. B. Karlsson (2015) Automated mapping of near-bed radio-echo layer disruptions in the
1895 Greenland Ice Sheet. *Earth and Planetary Science Letters*, 432, 323-331.
- 1896 Parrenin, F., M. G. P. Cavitte, D. D. Blankenship, J. Chappellaz, H. Fischer, O. Gagliardini, et al. (2017) Is
1897 there 1.5-million-year-old ice near Dome C, Antarctica? *The Cryosphere*, 11, 2427-2437.
- 1898 Parrenin, F. & R. Hindmarsh (2007) Influence of a non-uniform velocity field on isochrone geometry along a
1899 steady flowline of an ice sheet. *Journal of Glaciology*, 53, 612-622.
- 1900 Passalacqua, O., C. Ritz, F. Parrenin, S. Urbini & M. Frezzotti (2017) Geothermal flux and basal melt rate in
1901 the Dome C region inferred from radar reflectivity and heat modelling. *The Cryosphere*, 11, 2231-2246.
- 1902 Pattyn, F. (2010) Antarctic subglacial conditions inferred from a hybrid ice-sheet/ice-stream model. *Earth and*
1903 *Planetary Science Letters*, 295, 451-461.
- 1904 Pauling, A. G., C. M. Bitz & E. J. Steig (2023) Linearity of the climate-system response to raising and lowering
1905 West Antarctic and coastal Antarctic topography. *Journal of Climate*, 36, 6195-6212.
- 1906 Peters, M. E., D. D. Blankenship, S. P. Carter, S. D. Kempf, D. A. Young & J. W. Holt (2007) Along-track
1907 focusing of airborne radar sounding data from West Antarctica for improving basal reflection analysis
1908 and layer detection. *IEEE Transactions on Geoscience and Remote Sensing*, 45, 2725-2736.
- 1909 Peters, M. E., D. D. Blankenship & D. L. Morse (2005) Analysis techniques for coherent airborne radar
1910 sounding: Application to West Antarctic ice streams. *Journal of Geophysical Research: Solid Earth*,
1911 110, B06303.
- 1912 Pettit, E. C., T. Thorsteinsson, H. P. Jacobson & E. D. Waddington (2007) The role of crystal fabric in flow near
1913 an ice divide. *Journal of Glaciology*, 53, 277-288.
- 1914 Pettit, E. C. & E. D. Waddington (2003) Ice flow at low deviatoric stress. *Journal of Glaciology*, 49, 359-369.



- 1915 Pettit, E. C., E. D. Waddington, W. D. Harrison, T. Thorsteinsson, D. Elsberg, J. Morack, et al. (2011) The
1916 crossover stress, anisotropy and the ice flow law at Siple Dome, West Antarctica. *Journal of Glaciology*,
1917 57, 39-52.
- 1918 Pittard, M. L., P. L. Whitehouse, M. J. Bentley & D. Small (2022) An ensemble of Antarctic deglacial simulations
1919 constrained by geological observations. *Quaternary Science Reviews*, 298, 107800.
- 1920 Pollard, D. & R. M. DeConto (2009) Modelling West Antarctic Ice Sheet growth and collapse through the past
1921 five million years. *Nature*, 458, 329-332.
- 1922 Popov, S. (2015) Recent Russian remote sensing investigations in Antarctica within the framework of scientific
1923 traverses. *Advances in Polar Science*, 26, 113-121.
- 1924 Popov, S. (2020) Fifty-five years of Russian radio-echo sounding investigations in Antarctica. *Annals of*
1925 *Glaciology*, 61, 14-24.
- 1926 Popov, S. (2022) Ice cover, subglacial landscape, and estimation of bottom melting of Mac. Robertson,
1927 Princess Elizabeth, Wilhelm II, and western Queen Mary Lands, East Antarctica. *Remote Sensing*, 14,
1928 241.
- 1929 Pratap, B., R. Dey, K. Matsuoka, G. Moholdt, K. Lindbäck, V. Goel, et al. (2022) Three-decade spatial patterns
1930 in surface mass balance of the Nivlisen Ice Shelf, central Dronning Maud Land, East Antarctica.
1931 *Journal of Glaciology*, 68, 174-186.
- 1932 Rahnmooifar, M., M. Yari, J. Paden, L. Koenig & O. Ibikunle (2021) Deep multi-scale learning for automatic
1933 tracking of internal layers of ice in radar data. *Journal of Glaciology*, 67, 39-48.
- 1934 Raymond, C. F. (1983) Deformation in the vicinity of ice divides. *Journal of Glaciology*, 29, 357-373.
- 1935 Reeh, N., H. Oerter & H. H. Thomsen (2002) Comparison between Greenland ice-margin and ice-core oxygen-
1936 18 records. *Annals of Glaciology*, 35, 136-144.
- 1937 Retzlaff, R., N. Lord & C. R. Bentley (1993) Airborne-radar studies: Ice Streams A, B and C, West Antarctica.
1938 *Journal of Glaciology*, 39, 495-506.
- 1939 Rieckh, T., A. Born, A. Robinson, R. Law & G. Gulle (2024) Introducing ELSA v2.0: An isochronal model for
1940 ice-sheet layer tracing. *EGUsphere*, 1-20.
- 1941 Rignot, E., J. Mouginot & B. Scheuchl. 2017. MEaSURES InSAR-Based Antarctica Ice Velocity Map, Version
1942 2. NASA National Snow and Ice Data Center Distributed Active Archive Center.
- 1943 Rignot, E., R. H. Thomas, P. Kanagaratnam, G. Casassa, E. Frederick, S. Gogineni, et al. (2004) Improved
1944 estimation of the mass balance of glaciers draining into the Amundsen Sea sector of West Antarctica
1945 from the CECS/NASA 2002 campaign. *Annals of Glaciology*, 39, 231-237.
- 1946 Rippin, D. M., J. L. Bamber, M. J. Siegert, D. G. Vaughan & H. F. J. Corr (2003a) Basal topography and ice
1947 flow in the Bailey/Slessor region of East Antarctica. *Journal of Geophysical Research: Earth Surface*,
1948 108, F16008.
- 1949 Rippin, D. M., M. J. Siegert & J. L. Bamber (2003b) The englacial stratigraphy of Wilkes Land, East Antarctica,
1950 as revealed by internal radio-echo sounding layering, and its relationship with balance velocities.
1951 *Annals of Glaciology*, 36, 189-196.
- 1952 Rippin, D. M., M. J. Siegert, J. L. Bamber, D. G. Vaughan & H. F. J. Corr (2006) Switch-off of a major enhanced
1953 ice-flow unit in East Antarctica. *Geophysical Research Letters*, 33, L15501.
- 1954 Rivera, A., J. Uribe, R. Zamora & J. Oberreuter (2015) Subglacial Lake CECs: Discovery and in situ survey of
1955 a privileged research site in West Antarctica. *Geophysical Research Letters*, 42, 3944-3953.
- 1956 Rix, J., R. Mulvaney, J. Hong & D. A. N. Ashurst (2019) Development of the British Antarctic Survey Rapid-
1957 Access Isotope Drill. *Journal of Glaciology*, 65, 288-298.
- 1958 Robin, G. d. Q., D. J. Drewry & D. T. Meldrum (1977) International studies of ice sheet and bedrock.
1959 *Philosophical Transactions of the Royal Society of London Series B - Biological Sciences*, 279, 185-
1960 196.
- 1961 Robin, G. d. Q., S. Evans & J. T. Bailey (1969) Interpretation of radio echo sounding in polar ice sheets.
1962 *Philosophical Transactions of the Royal Society of London Series A - Mathematical and Physical*
1963 *Sciences*, 265, 437-505.
- 1964 Robin, G. d. Q. & D. H. M. Millar (1982) Flow of ice sheets in the vicinity of subglacial peaks. *Annals of*
1965 *Glaciology*, 3, 290-294.
- 1966 Rodriguez-Morales, F., S. Gogineni, C. J. Leuschen, J. D. Paden, J. Li, C. C. Lewis, et al. (2013) Advanced
1967 multifrequency radar instrumentation for polar research. *IEEE Transactions on Geoscience and*
1968 *Remote Sensing*, 52, 2824-2842.
- 1969 Ross, N., H. Corr & M. Siegert (2020) Large-scale englacial folding and deep-ice stratigraphy within the West
1970 Antarctic Ice Sheet. *The Cryosphere*, 14, 2103-2114.
- 1971 Ross, N. & M. Siegert (2020) Basal melting over Subglacial Lake Ellsworth and its catchment: Insights from
1972 englacial layering. *Annals of Glaciology*, 61, 198-205.
- 1973 Ross, N., M. J. Siegert, J. Woodward, A. M. Smith, H. F. J. Corr, M. J. Bentley, et al. (2011) Holocene stability
1974 of the Amundsen-Weddell ice divide, West Antarctica. *Geology*, 39, 935-938.
- 1975 Rowell, I. F., R. Mulvaney, J. Rix, D. R. Tetzner & E. W. Wolff (2023) Viability of chemical and water isotope
1976 ratio measurements of RAID ice chippings from Antarctica. *Journal of Glaciology*, 69, 623-638.



- 1977 Sanderson, R. J., N. Ross, K. Winter, R. G. Bingham, S. L. Callard, T. A. Jordan, et al. (2024) Dated radar-
1978 stratigraphy between Dome A and South Pole, East Antarctica: Old-ice potential and ice-sheet history.
1979 *Journal of Glaciology*.
- 1980 Sanderson, R. J., K. Winter, S. L. Callard, F. Napoleoni, N. Ross, T. A. Jordan, et al. (2023) Englacial
1981 architecture of Lambert Glacier, East Antarctica. *The Cryosphere*, 17, 4853-4871.
- 1982 Scambos, T. A., R. E. Bell, R. B. Alley, S. Anandakrishnan, D. H. Bromwich, K. Brunt, et al. (2017) How much,
1983 how fast?: A science review and outlook for research on the instability of Antarctica's Thwaites Glacier
1984 in the 21st century. *Global and Planetary Change*, 153, 16-34.
- 1985 Scanlan, K. M., A. Rutishauser, D. A. Young & D. D. Blankenship (2020) Interferometric discrimination of cross-
1986 track bed clutter in ice-penetrating radar sounding data. *Annals of Glaciology*, 61, 68-73.
- 1987 Schannwell, C., R. Drews, T. A. Ehlers, O. Eisen, C. Mayer & F. Gillet-Chaulet (2019) Kinematic response of
1988 ice-rise divides to changes in ocean and atmosphere forcing. *The Cryosphere*, 13, 2673-2691.
- 1989 Schroeder, D. M., R. G. Bingham, D. D. Blankenship, K. Christianson, O. Eisen, G. E. Flowers, et al. (2020)
1990 Five decades of radioglaciology. *Annals of Glaciology*, 61, 1-13.
- 1991 Schroeder, D. M., A. L. Broome, A. Conger, A. Lynch, E. J. Mackie & A. Tarzona (2022) Radiometric analysis
1992 of digitized Z-scope records in archival radar sounding film. *Journal of Glaciology*, 68, 733-740.
- 1993 Schroeder, D. M., J. A. Dowdeswell, M. J. Siegert, R. G. Bingham, W. N. Chu, E. J. MacKie, et al. (2019)
1994 Multidecadal observations of the Antarctic Ice Sheet from restored analog radar records. *Proceedings
1995 of the National Academy of Sciences*, 116, 18867-18873.
- 1996 Schwander, J., T. F. Stocker, R. Walther & S. Marending (2023) Progress of the RADIX (Rapid Access Drilling
1997 and Ice eXtraction) fast-access drilling system. *The Cryosphere*, 17, 1151-1164.
- 1998 Seroussi, H., S. Nowicki, A. J. Payne, H. Goelzer, W. H. Lipscomb, A. Abe-Ouchi, et al. (2020) ISMIP6
1999 Antarctica: a multi-model ensemble of the Antarctic Ice Sheet evolution over the 21st century. *The
2000 Cryosphere*, 14, 3033-3070.
- 2001 Siegert, M., N. Ross, H. Corr, J. Kingslake & R. Hindmarsh (2013) Late Holocene ice-flow reconfiguration in
2002 the Weddell Sea sector of West Antarctica. *Quaternary Science Reviews*, 78, 98-107.
- 2003 Siegert, M. J. (2003) Glacial–interglacial variations in central East Antarctic ice accumulation rates. *Quaternary
2004 Science Reviews*, 22, 741-750.
- 2005 Siegert, M. J., J. C. Ellis-Evans, M. Tranter, C. Mayer, J.-R. Petit, A. Salamatin, et al. (2001a) Physical,
2006 chemical and biological processes in Lake Vostok and other Antarctic subglacial lakes. *Nature*, 414,
2007 603-609.
- 2008 Siegert, M. J., R. D. Eyers & I. E. Tabacco (2001b) Three-dimensional ice sheet structure at Dome C, central
2009 East Antarctica: Implications for the interpretation of the EPICA ice core. *Antarctic Science*, 13, 182-
2010 187.
- 2011 Siegert, M. J., R. C. A. Hindmarsh & G. S. Hamilton (2003a) Evidence for a large surface ablation zone in
2012 central East Antarctica during the last Ice Age. *Quaternary Research*, 59, 114-121.
- 2013 Siegert, M. J. & R. Hodgkins (2000) A stratigraphic link across 1100 km of the Antarctic Ice Sheet between the
2014 Vostok ice-core site and Titan Dome (near South Pole). *Geophysical Research Letters*, 27, 2133-2136.
- 2015 Siegert, M. J., R. Hodgkins & J. A. Dowdeswell (1998) A chronology for the Dome C deep ice-core site through
2016 radio-echo layer correlation with the Vostok Ice Core, Antarctica. *Geophysical Research Letters*, 25,
2017 1019-1022.
- 2018 Siegert, M. J., R. Kwok, C. Mayer & B. Hubbard (2000) Water exchange between the subglacial Lake Vostok
2019 and the overlying ice sheet. *Nature*, 403, 643-646.
- 2020 Siegert, M. J. & A. J. Payne (2004) Past rates of accumulation in central West Antarctica. *Geophysical
2021 Research Letters*, 31, L12403.
- 2022 Siegert, M. J., A. J. Payne & I. Joughin (2003b) Spatial stability of Ice Stream D and its tributaries, West
2023 Antarctica, revealed by radio-echo sounding and interferometry. *Annals of Glaciology*, 37, 377-382.
- 2024 Siegert, M. J., M. Pokar, J. A. Dowdeswell & T. Benham (2005) Radio-echo layering in West Antarctica: A
2025 spreadsheet dataset. *Earth Surface Processes and Landforms*, 30, 1583-1591.
- 2026 Siegert, M. J., B. Welch, D. Morse, A. Vieli, D. D. Blankenship, I. Joughin, et al. (2004) Ice-flow direction change
2027 in interior West Antarctica. *Science*, 305, 1948-1951.
- 2028 Sigl, M., M. Toohey, J. R. McConnell, J. Cole-Dai & M. Severi (2022) Volcanic stratospheric sulfur injections
2029 and aerosol optical depth during the Holocene (past 11,500 years) from a bipolar ice-core array. *Earth
2030 System Science Data*, 14, 3167-3196.
- 2031 Sime, L. C., R. C. A. Hindmarsh & H. Corr (2011) Automated processing to derive dip angles of englacial radar
2032 reflectors in ice sheets. *Journal of Glaciology*, 57, 260-266.
- 2033 Sime, L. C., N. B. Karlsson, J. D. Paden & S. P. Gogineni (2014) Isochronous information in a Greenland ice
2034 sheet radio echo sounding data set. *Geophysical Research Letters*, 41, 1593-1599.
- 2035 Smith, B. E., N. E. Lord & C. R. Bentley (2002) Crevasse ages on the northern margin of Ice Stream C, West
2036 Antarctica. *Annals of Glaciology*, 34, 209-216.
- 2037 Spaulding, N. E., J. A. Higgins, A. V. Kurbatov, M. L. Bender, S. A. Arcone, S. Campbell, et al. (2013) Climate
2038 archives from 90 to 250 ka in horizontal and vertical ice cores from the Allan Hills Blue Ice Area,
2039 Antarctica. *Quaternary Research*, 80, 562-574.



- 2040 Steinhage, D., S. Kipfstuhl, U. Nixdorf & H. Miller (2013) Internal structure of the ice sheet between Kohlen
2041 station and Dome Fuji, Antarctica, revealed by airborne radio-echo sounding. *Annals of Glaciology*,
2042 54, 163-167.
- 2043 Steinhage, D., U. Nixdorf, U. Meyer & H. Miller (2001) Subglacial topography and internal structure of central
2044 and western Dronning Maud Land, Antarctica, determined from airborne radio-echo sounding. *Journal*
2045 *of Applied Geophysics*, 47, 183-189.
- 2046 Sutter, J., H. Fischer & O. Eisen (2021) Investigating the internal structure of the Antarctic Ice Sheet: The utility
2047 of isochrones for spatiotemporal ice-sheet model calibration. *The Cryosphere*, 15, 3839-3860.
- 2048 Sutter, J., H. Fischer, K. Grosfeld, N. B. Karlsson, T. Kleiner, B. Van Liefferinge, et al. (2019) Modelling the
2049 Antarctic Ice Sheet across the mid-Pleistocene transition: Implications for Oldest Ice. *The Cryosphere*,
2050 13, 2023-2041.
- 2051 Svensson, A., M. Bigler, T. Blunier, H. B. Clausen, D. Dahl-Jensen, H. Fischer, et al. (2013) Direct linking of
2052 Greenland and Antarctic ice cores at the Toba eruption (74 ka BP). *Climate of the Past*, 9, 749-766.
- 2053 Swithinkbank, C. (1969) Airborne radio-echo sounding by the British Antarctic Survey. *The Geographical*
2054 *Journal*, 135, 551-553.
- 2055 Tabacco, I., C. Bianchi, J. Baskaradas, L. Cafarella, S. Umberto, A. Zirizzotti, et al. (2008) Italian RES
2056 investigation in Antarctica: The new radar system. *Terra Antarctica Reports*, 14, 213 - 216.
- 2057 Tabacco, I. E., C. Bianchi, M. Chiappini, A. Passerini, A. Zirizzotti & E. Zuccheretti (1999) Latest improvements
2058 for the echo sounding system of the Italian radar glaciological group and measurements in Antarctica.
2059 *Annali Di Geofisica*, 42, 271-276.
- 2060 Tang, X., K. Luo, S. Dong, Z. Zhang & B. Sun (2022) Quantifying basal roughness and internal-layer continuity
2061 index of ice sheets by an integrated means with radar data and deep learning. *Remote Sensing*, 14,
2062 4507.
- 2063 Tarasov, L. & W. R. Peltier (2003) Greenland glacial history, borehole constraints, and Eemian extent. *Journal*
2064 *of Geophysical Research: Solid Earth*, 108, 2143.
- 2065 Teisberg, T. O. & D. M. Schroeder. 2023. Digital tools for analog data: Reconstructing the first ice-penetrating
2066 radar surveys of Antarctica and Greenland. In *International Geoscience and Remote Sensing*
2067 *Symposium (IGARRS) Proceedings*, 44-47.
- 2068 Teisberg, T. O., D. M. Schroeder, A. L. Broome, F. Lurie & W. D. 2022. Development of a UAV-borne pulsed
2069 ice-penetrating radar system. In *IGARSS 2022 - 2022 IEEE International Geoscience and Remote*
2070 *Sensing Symposium*, 7405-7408.
- 2071 Thyssen, F. & K. Grosfeld (1988) Ekström Ice Shelf, Antarctica. *Annals of Glaciology*, 11, 180-183.
- 2072 Tinto, K. J., L. Padman, C. S. Siddoway, S. R. Springer, H. A. Fricker, I. Das, et al. (2019) Ross Ice Shelf
2073 response to climate driven by the tectonic imprint on seafloor bathymetry. *Nature Geoscience*, 12,
2074 441-449.
- 2075 Traversa, G., D. Fugazza & M. Frezzotti (2023) Megadunes in Antarctica: Migration and characterization from
2076 remote and in situ observations. *The Cryosphere*, 17, 427-444.
- 2077 Tsutaki, S., S. Fujita, K. Kawamura, A. Abe-Ouchi, K. Fukui, H. Motoyama, et al. (2022) High-resolution
2078 subglacial topography around Dome Fuji, Antarctica, based on ground-based radar surveys over 30
2079 years. *The Cryosphere*, 16, 2967-2983.
- 2080 Turchetti, S., K. Dean, S. Naylor & M. Siegert (2008) Accidents and opportunities: A history of the radio-echo
2081 sounding of Antarctica, 1958–79. *The British Journal for the History of Science*, 41, 417-444.
- 2082 Ulaby, F. & D. B. Lang. 2015. A Strategy for Active Remote Sensing Amid Increased Demand for Radio
2083 Spectrum. Washington DC: The National Academies Press.
- 2084 Urbini, S., L. Cafarella, A. Zirizzotti, I. E. Ignazio, C. Bottari, J. A. Baskaradas, et al. (2010) Radio-echo-
2085 sounding data analysis of the Shackleton Ice Shelf. *Annals of Geophysics*, 53, 79-87.
- 2086 Van Autenboer, T. & H. Declair. 1975. Jelbartisen - Trolltunga, Dronning Maud Land, Antarctica. Radio-
2087 glaciological survey data report. In *Geological Survey of Belgium*, 114.
- 2088 Van Liefferinge, B. & F. Pattyn (2013) Using ice-flow models to evaluate potential sites of million year-old ice
2089 in Antarctica. *Climate of the Past*, 9, 2335-2345.
- 2090 Van Liefferinge, B., D. Taylor, S. Tsutaki, S. Fujita, P. Gogineni, K. Kawamura, et al. (2021) Surface mass
2091 balance controlled by local surface slope in inland Antarctica: Implications for ice-sheet mass balance
2092 and Oldest Ice delineation in Dome Fuji. *Geophysical Research Letters*, 48, e2021GL094966.
- 2093 Vaughan, D. G., H. F. J. Corr, C. S. M. Doake & E. D. Waddington (1999) Distortion of isochronous layers in
2094 ice revealed by ground-penetrating radar. *Nature*, 398, 323-326.
- 2095 Višnjević, V., R. Drews, C. Schannwell, I. Koch, S. Franke, D. Jansen, et al. (2022) Predicting the steady-state
2096 isochronal stratigraphy of ice shelves using observations and modeling. *The Cryosphere*, 16, 4763-
2097 4777.
- 2098 Waddington, E. D., T. A. Neumann, M. R. Koutnik, H.-P. Marshall & D. L. Morse (2007) Inference of
2099 accumulation-rate patterns from deep layers in glaciers and ice sheets. *Journal of Glaciology*, 53, 694-
2100 712.
- 2101 WAIS Divide Project Members (2015) Precise inter-polar phasing of abrupt climate change during the last ice
2102 age. *Nature*, 520, 661-665.



- 2103 Wang, T. T., B. Sun, X. Y. Tang, X. P. Pang, X. B. Cui, J. X. Guo, et al. (2016) Spatio-temporal variability of
2104 past accumulation rates inferred from isochronous layers at Dome A, East Antarctica. *Annals of*
2105 *Glaciology*, 57, 87-93.
- 2106 Wang, Z., A. Chung, D. Steinhage, F. Parrenin, J. Freitag & O. Eisen (2023) Mapping age and basal conditions
2107 of ice in the Dome Fuji region, Antarctica, by combining radar internal-layer stratigraphy and flow
2108 modeling. *The Cryosphere*, 17, 4297-4314.
- 2109 Wearing, M. G. & J. Kingslake (2019) Holocene formation of Henry Ice Rise, West Antarctica, inferred from
2110 ice-penetrating radar. *Journal of Geophysical Research: Earth Surface*, 124, 2224-2240.
- 2111 Weertman, J. (1976) Sliding-no sliding zone effect and age determination of ice cores. *Quaternary Research*,
2112 6, 203-207.
- 2113 Welch, B. C. & R. W. Jacobel (2003) Analysis of deep-penetrating radar surveys of West Antarctica, US-ITASE
2114 2001. *Geophysical Research Letters*, 30, 1444.
- 2115 Welch, B. C. & R. W. Jacobel (2005) Bedrock topography and wind erosion sites in East Antarctica:
2116 observations from the 2002 US-ITASE traverse. *Annals of Glaciology*, 41, 92-96.
- 2117 Welch, B. C., R. W. Jacobel & S. A. Arcone (2009) First results from radar profiles collected along the US-
2118 ITASE traverse from Taylor Dome to South Pole (2006–2008). *Annals of Glaciology*, 50, 35-41.
- 2119 Wilkinson, M. D., M. Dumontier, I. J. Aalbersberg, G. Appleton, M. Axton, A. Baak, et al. (2016) The FAIR
2120 guiding principles for scientific data management and stewardship. *Scientific Data*, 3, 160018.
- 2121 Winski, D. A., T. J. Fudge, D. G. Ferris, E. C. Osterberg, J. M. Fegyveresi, J. Cole-Dai, et al. (2019) The SP19
2122 chronology for the South Pole Ice Core – Part 1: volcanic matching and annual layer counting. *Climate*
2123 *of the Past*, 15, 1793-1808.
- 2124 Winter, A., D. Steinhage, E. J. Arnold, D. D. Blankenship, M. G. P. Cavitte, H. F. J. Corr, et al. (2017)
2125 Comparison of measurements from different radio-echo sounding systems and synchronization with
2126 the ice core at Dome C, Antarctica. *The Cryosphere*, 11, 653-668.
- 2127 Winter, A., D. Steinhage, T. T. Creyts, T. Kleiner & O. Eisen (2019a) Age stratigraphy in the East Antarctic Ice
2128 Sheet inferred from radio-echo sounding horizons. *Earth System Science Data*, 11, 1069-1081.
- 2129 Winter, K., J. Woodward, S. A. Dunning, C. S. M. Turney, C. J. Fogwill, A. S. Hein, et al. (2016) Assessing the
2130 continuity of the blue-ice climate record at Patriot Hills, Horseshoe Valley, West Antarctica.
2131 *Geophysical Research Letters*, 43, 2019-2026.
- 2132 Winter, K., J. Woodward, N. Ross, S. A. Dunning, R. G. Bingham, H. F. J. Corr, et al. (2015) Airborne-radar
2133 evidence for tributary flow switching in Institute Ice Stream, West Antarctica: Implications for ice-sheet
2134 configuration and dynamics. *Journal of Geophysical Research: Earth Surface*, 120, 1611-1625.
- 2135 Winter, K., J. Woodward, N. Ross, S. A. Dunning, A. S. Hein, M. J. Westoby, et al. (2019b) Radar-detected
2136 englacial debris in the West Antarctic Ice Sheet. *Geophysical Research Letters*, 46, 10454-10462.
- 2137 Wolovick, M. J. & T. T. Creyts (2016) Overturned folds in ice sheets: Insights from a kinematic model of
2138 traveling sticky patches and comparisons with observations. *Journal of Geophysical Research: Earth*
2139 *Surface*, 121, 1065-1083.
- 2140 Wolovick, M. J., T. T. Creyts, W. R. Buck & R. E. Bell (2014) Traveling slippery patches produce thickness-
2141 scale folds in ice sheets. *Geophysical Research Letters*, 41, 8895-8901.
- 2142 Wolovick, M. J., J. C. Moore & L. Zhao (2021a) Joint inversion for surface accumulation rate and geothermal
2143 heat flow from ice-penetrating radar observations at Dome A, East Antarctica. Part I: Model description,
2144 data constraints, and inversion results. *Journal of Geophysical Research: Earth Surface*, 126,
2145 e2020JF005937.
- 2146 Wolovick, M. J., J. C. Moore & L. Zhao (2021b) Joint inversion for surface accumulation rate and geothermal
2147 heat flow from ice-penetrating radar observations at Dome A, East Antarctica. Part II: Ice-sheet state
2148 and geophysical analysis. *Journal of Geophysical Research: Earth Surface*, 126, e2020JF005936.
- 2149 Woodward, J. & E. C. King (2009) Radar surveys of the Rutford Ice Stream onset zone, West Antarctica:
2150 Indications of flow (in)stability? *Annals of Glaciology*, 50, 57-62.
- 2151 Wright, A. P., D. A. Young, J. L. Roberts, D. M. Schroeder, J. L. Bamber, J. A. Dowdeswell, et al. (2012)
2152 Evidence of a hydrological connection between the ice divide and ice-sheet margin in the Aurora
2153 Subglacial Basin, East Antarctica. *Journal of Geophysical Research: Earth Surface*, 117, F01033.
- 2154 Wrona, T., M. J. Wolovick, F. Ferraccioli, H. Corr, T. Jordan & M. J. Siegert (2018) Position and variability of
2155 complex structures in the central East Antarctic Ice Sheet. *Geological Society Special Publications*,
2156 461, 113-129.
- 2157 Xiong, S., J.-P. Muller & R. C. Carretero (2018) A new method for automatically tracing englacial layers from
2158 MCoRDS data in NW Greenland. *Remote Sensing*, 10, 43.
- 2159 Xu, B., S. Lang, X. Cui, L. Li, X. Liu, J. Guo, et al. (2022) Focused synthetic-aperture-radar processing of ice-
2160 sounding data collected over East Antarctic Ice Sheet via spatial-correlation-based algorithm using
2161 fast back projection. *IEEE Transactions on Geoscience and Remote Sensing*, 60, 5233009.
- 2162 Yan, Y., E. J. Brook, A. V. Kurbatov, J. P. Severinghaus & J. A. Higgins (2021) Ice-core evidence for
2163 atmospheric oxygen decline since the Mid-Pleistocene Transition. *Science Advances*, 7, eabj9341.



- 2164 Yari, M., O. Ibikunle, D. Varshney, T. Chowdhury, A. Sarkar, J. Paden, et al. (2021) Airborne snow-radar data
2165 simulation with deep learning and physics-driven methods. *IEEE Journal of Selected Topics in Applied*
2166 *Earth Observations and Remote Sensing*, 14, 12035-12047.
- 2167 Yilmaz, Ö. 2001. *Seismic Data Analysis: Processing, Inversion, and Interpretation of Seismic Data*. Tulsa, OK:
2168 Society of Exploration Geophysicists.
- 2169 Young, D. A., D. M. Schroeder, D. D. Blankenship, S. D. Kempf & E. Quartini (2016) The distribution of basal
2170 water between Antarctic subglacial lakes from radar sounding. *Philosophical Transactions of the Royal*
2171 *Society A: Mathematical, Physical and Engineering Sciences*, 374, 20140297.
- 2172 Young, D. A., A. P. Wright, J. L. Roberts, R. C. Warner, N. W. Young, J. S. Greenbaum, et al. (2011) A dynamic
2173 early East Antarctic Ice Sheet suggested by ice-covered fjord landscapes. *Nature*, 474, 72-75.
- 2174 Zamora, R., G. Casassa, A. Rivera, F. Ordenes, G. Neira, L. Araya, et al. 2007. Crevasse detection in glaciers
2175 of southern Chile and Antarctica by means of ground-penetrating radar. In *IAHS Assembly*. Foz do
2176 Iguacu, Brazil: IAHS Publications.
- 2177 Zeising, O., T. A. Gerber, O. Eisen, M. R. Ershadi, N. Stoll, I. Weikusat, et al. (2023) Improved estimation of
2178 the bulk ice-crystal-fabric asymmetry from polarimetric phase co-registration. *The Cryosphere*, 17,
2179 1097-1105.
- 2180 Zhao, L. Y., J. C. Moore, B. Sun, X. Y. Tang & X. R. Guo (2018) Where is the 1-million-year-old ice at Dome
2181 A? *The Cryosphere*, 12, 1651-1663.
- 2182



2183 **Appendix: Suggested standardised structure for the publication of traced IRHs across Antarctica**

2184 For publishing future radiostratigraphy datasets, we recommend scientists to follow the structure and
2185 naming convention specified in Table A1 for the first ten columns, after which additional columns may be
2186 added at the discretion of the scientists.

2187 In the metadata, we recommend that authors also provide at least the following information:

2188 (a) Name(s), version(s) and frequency of RES system(s) used.

2189 (b) Value for speed of radar wave in ice used to convert IRH depths to metres below the ice surface.

2190 (c) Value for any firn correction applied.

2191 (d) The coordinate system(s) used following the World Geodetic System 1984 datum and appropriate
2192 projection (i.e., EPSG:3031 for Antarctica).

2193 (e) If applicable, the type of radar product (e.g. waveform) on which the IRHs were traced.

2194 (f) The uncertainties associated with either the IRH age or depth based on RES system resolution and IRH
2195 picking, amongst others. Ideally, if the metadata vary throughout the dataset, then such information should
2196 be attached to each data point as additional columns to those shown in Table A1.

2197 (g) The source of age control (i.e., ice-core age scale, model).

2198 Additional information may also be added to the metadata, such as the type of processing used to extract
2199 the IRHs (if different from the processing used to trace the bed); the distance in the along-track direction
2200 along the RES transect for each data point; a flag number indicating whether the ice thickness, surface and
2201 bed elevations come directly from the along-track radar or from an interpolated gridded product, if
2202 applicable; the spatial resolution (or spacing distance between each data point); the dating method (s) used
2203 to provide an age for each IRH; and the type of software and tools used to pick the IRHs. Missing values in
2204 the float data should be set to NaN and specified in the metadata. We also recommend the use of open-
2205 access and FAIR data formats for storing the data, such as CSV or tabular data file (or netcdf if CSV or tabular
2206 data file is not suitable) where metadata can be easily embedded together with the data. Finally, we
2207 recommend scientists to publish their data in open-access repositories alongside the paper publication, with
2208 a DOI that can be linked back to the original paper. Together, these suggested protocols will ensure the
2209 longevity of the data products for future applications and enable faster retrieval thereof, particularly with
2210 regards to the large data volumes expected from automatic IRH tracking algorithms in the future.



2211 **Table A1.** Suggested standardised structure for the publication of IRH datasets associated with the
2212 AntArchitecture community effort following FAIR data standards.

2213 (For EGUsphere formatting, this 12-column table is presented across two rows.)

2214 Table rows 1-6:

Line ID or transect name	Trace timestamp (GPS time)	Longitude (decimal degrees)	Latitude (decimal degrees)	X coordinate (EPSG:3031; metres)	Y coordinate (EPSG:3031; metres)
--------------------------	----------------------------	-----------------------------	----------------------------	----------------------------------	----------------------------------

2215

2216 Table rows 7-12

IRH name	IRH (two-way travel-time through ice only)	IRH depth below ice surface (metres)	Ice thickness (metres)	Surface elevation (metres a.s.l.)	Bed elevation (metres a.s.l.)
----------	--	--------------------------------------	------------------------	-----------------------------------	-------------------------------

2217